SAINT PETERSBURG STATE UNIVERSITY

Nikita Andreevich Kazarinov

SPACE AND TIME DISCRETNESS OF DYNAMIC FRACTURE AND RELATED EFFECTS

Scientific specialty – 1.1.8. Solid mechanics

Thesis for the degree of Doctor of Physical and Mathematical Sciences

Translation from Russian

Scientific advisor:

Corr.-member of RAS,

Doctor of Science,

Professor Yuri Petrov

Saint Petersburg 2024

Contents

INTRODUCTION **3**

Relevance and development of the thesis topic 3
Goals and objectives of the study 22
Scientific novelty of the research, theoretical and practical significance of the obtained results 24
Research methods 26
Results of the work and their theoretical and practical significance 27
Approbation of results 29
Author's contribution 33
Acknowledgments 33
Support 34
Structure of the thesis 34
Main scientific results 34
Thesis defense key points 35

CHAPTER 1. ANALOGY BETWEEN THE DYNAMIC FRACTURE PROCESSES IN BRITTLE SOLIDS AND FAILURE OF A "MASS-ON-A-SPRING" SYSTEM **38**

1.1. Dynamic failure of a linear oscillator 38
1.2. The incubation time fracture model 42
1.3 Crack initiation analysis and analogy with an oscillator 44
1.4 Chapter 1 conclusions 55

CHAPTER 2. FRACTURE IN A "MASS-ON-A-SPRING" SYSTEM. DIRECT MODELLING OF THE DYNAMIC FRACTURE USING THE LINEAR OSCILLATOR MODEL **58**

2.1 Fracture in the "mass-on-a-spring" system 58
2.2 Experiments on crack initiation 62
2.3 Experiments on spallation in rods by Mikhailova et al. [3] 77
2.4 Analysis of the obtained results 81
2.5 Chapter 2 conclusions 84

CHAPTER 3. FEATURES OF DYNAMIC FRACTURE PROCESSES OBSERVED IN PERIODIC STRUCTURES **86**

3.1 Statement of the problem for a single oscillator 86
3.2 System of two oscillators 87
3.4. A chain with an arbitrary finite number of links 91
3.5 Analysis of the solutions for the chain and for an elastic rod. Gibbs effect 101
3.7 Numerical study of fracture a periodic structure in course of relaxation 105
3.8 Chapter 3 conclusions 108

CHAPTER 4. SPACE AND TIME DISCREETNESS OF THE CRACK PROPAGATION PROCESS **109**

4.1 The incubation time fracture criterion for the crack propagation problems 109
4.2 Numerical implementation of the incubation time approach for the dynamic crack propagation problems 111
4.3 Instability of SIF for moving cracks 119
4.4 Crack velocity oscillations 122
4.5 The propagation of multiple cracks with arbitrary directions. Dynamic fragmentation 126
4.6 Chapter 4 conclusions 135

CHAPTER 5. INCUBATION TIME APPROACH FOR IMPACT PROBLEMS **137**

5.1 The incubation time approach for numerical simulations of impact fracture 137
5.2 Application of artificial neural networks to predict strength of perforated targets 147
5.3 Chapter 5 conclusions 166

CONCLUSIONS **168**

REFERENCES **172**

Introduction

Relevance and development of the thesis topic

The analogy between the fracture models of continuous media and the fracture of discrete systems is of fundamental importance, since it allows one to understand the behavior of materials and structures at both macroscopic and microscopic scales. Finding such analogies is important for a number of reasons. By drawing parallels between continuous media (such as solids) and discrete systems (such as oscillators, networks of particles or atoms), scientists and engineers can develop a common understanding of the fundamental principles that determine the strength and fracture toughness of materials. The unified framework provides possibility to apply all concepts and methodologies at different scales and systems.

The history of identifying patterns and dependencies in critical processes shows that concepts and principles obtained in one area can be transferred to another area. For example, knowledge gained from studying the fracture mechanics of discrete systems, such as networks of interconnected particles, can be applied to understand of the behavior of continuous materials such as metals or ceramics. This transferability allows researchers to use knowledge and methods developed in one field to make progress in another areas.

In addition to this by viewing the behavior of materials and structures through the lens of both continuous and discrete models, researchers can identify new patterns and phenomena that may not be obvious when considering only one point of view. This holistic approach facilitates the discovery of new mechanisms and relationships that determine strength and fracture toughness, leading to advances in materials design and more precise engineering predictions of structural load-bearing capacity.

Analogies between continuous and discrete systems play a particularly important role in computational modeling and numerical experiments. Methods developed for the discrete systems modeling, such as molecular dynamics or discrete element methods, can be adapted and applied based on the identified analogies to model the behavior of continuous materials at different length and time scales. This allows researchers to predict and understand the response of materials and structures under different loading conditions and in different environments.

Thus, in essence, the fundamental nature of the analogies between continuum and discrete system models lies in their ability to provide a common basis for understanding, communicating concepts, discovering new patterns, and facilitating computer simulations that are needed to advance our knowledge of the behavior of materials and to improve their design, as well performance of engineering systems.

When quasi-static fracture problems are discussed, the strength of a material with defects such as cracks is often associated with the value of the stress intensity factor (SIF) K_I (mode I load is considered in the work) measured at the moment of fracture: according to the well-known Irvin failure criterion, a crack initiates if K_I reaches a certain critical value K_{Ic}, which is interpreted as a material property. This failure criterion works well for problems with quasi-static loads, however, with increasing loading rates, the critical value of the SIF also increases, which requires the introduction of a new critical value of the SIF for each loading rate [1]. However, even this modification of the Irwin criterion cannot be used to study cases of fracture when the local stress field at the fracture point has already exceeded its maximum values and has reached a stage of noticeable decrease [2-4]. This fundamental fracture effect is poorly understood and cannot be explained within the framework of classical approaches.

For convenience, the term fracture delay is introduced: if, under given boundary and initial conditions, fracture at the vicinity of the crack tip occurs after the peak of the local tensile force field has passed (this can be expressed, for example, in terms of

the current value of the stress intensity factor), then the fracture delay is considered to take place. The time elapsed from the peak of local tensile stress to the moment of macroscopic rupture of the material will characterize the magnitude of the fracture delay. The first Chapter of the thesis shows that this phenomenon is a fundamental feature of the dynamic fracture process, which manifests itself in threshold situations and is associated with the presence of incubation processes occurring at the microscopic level and taking up certain time preceding the macroscopic rupture. The thesis explores this phenomenon using a fracture model based on the concept of incubation time. It is worth noting that the authors of the work on crack initiation due to short pulses [5] proposed an approach called the “minimum fracture time criterion”, which theoretically admits the fracture delay phenomenon, but the proposed approach lacks universality, since the minimum time parameter, as well as the value of the critical stress intensity cannot be considered as material parameters.

Additionally, a simple “mass-on-a-spring” model was used to show that the dynamic fracture process can exhibit inertial behavior when high rate or short-pulse loading is considered in Chapter 1 The linear oscillator model is used to study failure delay conditions for systems with inertia and to show that dynamic crack initiation has features similar to linear oscillator failure. It is shown that a sample with a crack can behave like an oscillator when loaded with short pulses, and thus it is possible to construct an analogy between a crack and some virtual oscillator. Inertial models based on the linear oscillator model have been widely used to study and simulate dynamic failure (see, for example, [6, 7, 8]). Moreover, linear oscillator-based models can provide some insight into very complex features of dynamic crack propagation, such as the dependence of the SIF value on crack velocity [9]. More complex discrete models (for example, chains and lattice of springs [10,11]) are actively used to study dynamic fracture and dynamic propagation of cracks.

The concept and term of crack inertia has been used in the literature for some time when moving cracks are considered, however the term inertia is either used to classify the mode of crack motion [12] or is discussed formally due to the presence of

crack acceleration value in the energy balance equations [13]. The authors of the mentioned works concentrate their efforts on the effect of fluctuations in crack speed and on the problem of limiting crack speed, while the phenomenon of fracture delay remains beyond the attention of the authors. It is worth mentioning here that both the issue of crack speed limitation and the effect of crack speed fluctuations can be studied using the incubation time approach [14,15].

The simplest short-pulse load – a rectangular force pulse – was studied in the first Chapter. The choice of such a simple load provides possibility to study two fundamental scenarios for the crack initiation in detail. The first is the threshold case, when the minimal loads necessary to cause failure are applied to the system. For example, for a fixed load pulse amplitude, the minimum load duration is determined. The opposite case is the system overload, when excessive loads are applied. Threshold cases appear to reveal fundamental fracture effects, but are difficult to implement experimentally. In contrast, the overload cases are less difficult to implement in practice.

The study of the dynamic fracture using simple fracture models such as spring oscillators is critical to practical understanding of the laws governing the fracture of solids due to dynamic loads for many reasons. Firstly, simple models such as spring oscillators clearly demonstrate the fundamental principles underlying dynamic fracture. By simplifying complex phenomena down to more manageable systems, engineers can use simple "oscillatory" language to better understand the physics and mechanics underlying shock wave propagation and material failure. Secondly, systems of dynamic oscillators can provide insight into wave propagation through structural media. Understanding how waves behave in a simplified system can help the engineers to understand waves' interactions, reflections, and energy dissipation, which is necessary to predict the behavior of shock waves in real materials. Third, simple models allow engineers to perform parameter sensitivity analysis to evaluate the influence of various factors on the fracture behavior. By systematically varying parameters that correspond to effective material properties and initial conditions,

engineers can identify the key factors influencing dynamic rupture and design materials and structures that can resist or mitigate the dynamic fracture effects. Fourth, simple models serve as valuable tools for validation of more complex numerical simulations and experimental results. For example, engineers can use simplified analytical solutions of spring oscillators to test the accuracy of numerical models and experimental data, ensuring that predictions match the observed phenomena. Fifth, simple models are an effective educational tool for teaching students and young engineers the basic principles of the dynamic fracture of continuum. Starting with basic concepts and gradually increasing their sophistication can help to provide a solid foundation for understanding the complex process of failure of solids under extreme loads. Sixth, information obtained from studying simple failure models can be used to design and optimize materials and structures to improve their resistance to damage under high rate loading conditions. Engineers can use this knowledge to develop innovative materials, protective barriers and structural reinforcements that mitigate the effects of dynamic failure in a variety of industrial applications such as aerospace, mining and civil engineering.

Thus, studying dynamic fracture using simple models such as spring oscillators is necessary to gain a deeper understanding (from the engineer's perspective) of the laws governing failure of solids under extreme conditions. These models provide insight into wave propagation, parameter sensitivity, validation of more complex numerical models and design optimization, ultimately leading to the development of durable materials and structures that can withstand extreme dynamic loads.

Dynamic fracture of media and structures can be the result of various types of loads applied to a material or structure, including static loads [16,17]. However, explicit dynamic loading can reveal specific effects associated with the strength of the material.

One of the main effects characterizing the dynamic fracture of materials is associated with a high loading rate, when a rapidly growing stress field is created in the material, leading to fracture. When the stress field growth rate is relatively small,

the material exhibits static strength properties, and static strength theories such as Irwin's crack instability criterion for cracked specimens [18] or the ultimate stress criterion for materials without defects are applicable. However, at high strain/stress rates, the material exhibits increased strength, and failure occurs at higher stress levels, which requires the introduction of separate critical parameters for each strain/stress rate. For example, in the case of samples with cracks, the ultimate stress intensity factor K_{Ic} value is replaced by its dynamic counterpart – dynamic fracture toughness K_{IC}^{d}, which, as shown in literature, can depend on the loading rate [1]. Thus, the strength of a material should be studied for a range of strain rates or rates of change in stress fields, providing possibility to construct a dynamic strength curve, which consists of two characteristic parts (branches) – a static (or low rate) branch and a dynamic branch with significantly higher strength parameters [19,20]. These types of curves are commonly interpreted as a material property, but when proper dynamic failure models are applied, the curve is actually computable. Note that the described phenomenon is also observed for plastic materials – the values of the yield strength increase with increasing stress/strain rate, which requires the introduction of dynamic parameters of the yield strength [21,22].

The fracture delay effect, which manifests itself when materials and structures are loaded with short pulses, is less common in the literature. When short dynamic loads (short impulse loads) are applied to a material, failure may occur after the stresses have exceeded their maximum values, which means failure is delayed. Experimental confirmation of this effect can be found both in experiments with samples with cracks (the crack initiation under pulse loading) [2,4] and on samples without initial defects [3,23].

Theoretical study and prediction of the above-mentioned and other effects associated with dynamic fracture (for example, issues of limiting crack speed and crack speed oscillations, the issue of the dependence of the current stress intensity factor on crack speed [16,24,25]) poses a serious challenge for theorists. Static failure criteria are naturally modified for use in the case of dynamic loading – critical static values are

replaced by their higher dynamic counterparts or even complex functionals [26]. These models are usually difficult to calibrate since they require a set of complex experiments. Another approach involves an explicit introduction of stress/strain rates into the expressions for material strength. The most prominent representative of this family of models is the Johnson-Holmquist 2 (JH2) model, which is widely used in practice to simulate fracture in the impact events [27].

A completely different way of processing the dynamic fracture phenomena is based on integral fracture criteria. Here one can mention Nikiforovsky's condition [28,29], as well as Tuler's and Butcher's failure criteria [30]. The failure criterion based on the concept of incubation time (incubation time criterion) [31] also has an integral form; the integration interval over time is determined by the characteristic relaxation time is called the incubation time, which should be interpreted as a material parameter. The incubation time criterion in its most complete form also contains the integration of stresses with respect to spatial coordinate, which emphasizes the nonlocality of this approach.

The second Chapter examines the dynamic fracture effects using the "mass-on-a-spring" model, which has certainly been used to study fracture before (see, for example, [32-34]). To study dynamic fracture and crack propagation, more complex discrete models are actively used, for example, chains of oscillators and lattices for studying dynamic crack propagation [10,35,36]. Models based on the concept of adhesion zone, enriched with inertia [37] should also be mentioned here – the approach used in the second Chapter is vaguely reminiscent of the method used in [37]. Moreover, interesting combinations of well-developed numerical approaches and ideas based on failure of the "mass-on-a-spring" system have recently appeared in the literature (see, for example, work [38] devoted to modifications of the SPH numerical approach (Smoothed Particle hydrodynamics). Models similar to the "mass-on-a-spring" system are also used in engineering and even biomedical problems [39,40]. It is worth noting the use of springs in the analytical and very valuable experimental analysis of how boundary conditions affect crack resistance in different types of

specimens [41]. Chapter 2 also discusses the failure of a linear oscillator under short pulse loading conditions, as well as failure due to a linearly increasing force. These problems provide possibility to study two effects of the dynamic fracture – the fracture delay and increase in the system's strength at higher loading rates. Next, the considered "mass-on-a-spring" model is calibrated to describe experimental results on crack initiation and spallation. The similarities between failure in a "mass-on-a-spring" system and the results obtained using a failure model based on the concept of incubation time are also discussed. In contrast to the first Chapter of the thesis, the second Chapter presents a simpler approach, which is based on an allocation of a certain volume in the body, which serves as the mass of the oscillator, and the oscillator spring stiffness is determined from considerations of the applicability of the oscillator model for the static cases.

Studying the characteristics of the dynamic fracture occurring in periodic structures, such as chains of oscillators, subjected to rapid dynamic loading, provides valuable information about the behavior of materials and structures under extreme loads. These characteristics provide fundamental information about the dependencies and peculiarities of the dynamic fracture process, which are essential for assessing the load-bearing capacity of structures and systems with a periodic discrete structure. The oscillator chains provide a simplified but representative model of periodic structures. This simplicity facilitates a deeper understanding of the physics underlying dynamic fracture. Analysis of the dynamic fracture of such structures allows researchers to obtain analytical or approximate solutions that reflect the main aspects of their behavior.

Moreover, the oscillator chains make it possible to study the propagation and interaction of waves in periodic media. As waves propagate through a structure, interactions between adjacent oscillators influence the overall response, including the initiation and propagation of cracks or defects. Understanding these interactions sheds light on how energy is transferred and dissipated in course of the dynamic fracture.

Observations and analysis of the dynamic fracture in the oscillator chains can lead to the discovery of scaling laws and universal behavior. These scaling laws describe how failure properties depend on system size, loading rate, or other relevant parameters. This versatility allows researchers to generalize insights from simple models to more complex systems and apply them across different length and time scales. It also opens up the possibility of testing theoretical models, since, for example, chains of oscillators can serve as a tool for testing theoretical models and computational methods used to simulate the dynamic fracture observed in periodic structures. Comparing analytical predictions with numerical simulations or experimental data helps to verify the accuracy and reliability of the theoretical approaches, allowing them to be applied to real-world problems.

The study of periodic oscillating systems is important for the design of sustainable materials and structures. By understanding how periodic structures influence failure behavior, engineers can tailor material architectures to improve resistance to dynamic loads, improve energy absorption, and mitigate catastrophic failure.

In essence, studying the characteristics of dynamic failure using the oscillator chain models and special periodic model structural elements discussed below offers a valuable basis for understanding the fundamental principles governing the failure of periodic structures. Using the simplicity, analytical solutions, and clear patterns provided by these models, it is possible to enhance our understanding of the dynamic failure phenomena and to develop strategies which would improve the strength and performance of materials and structures exposed to extreme environments.

Most of the structures around us are subjected to static load and the material of these systems has uneven strength due to various defects, impurities etc. As shown in the work, the failure of a statically loaded system with obvious periodicity reveals dynamic effects, which appear to be determined by the discreteness of the structure. In other words, the sudden removal of a static load which caused uniform subcritical

deformation of each element of the system, can possibly lead to subsequent dynamic failure of the entire system.

In the third Chapter of the thesis, a discrete analogue of an elastic rod is considered – a chain of identical linear oscillators with one fixed end. A special effect that is not observed in a continuum system is investigated. If at the initial moment of time the chain was uniformly stretched, and the distance between the masses was close to a critical value, then at one of the subsequent moments of time, when the system freely oscillates, the deformation of one of the links will exceed the initial value, which can lead to a failure. Thus, a pre-stretched chain of linear oscillators can collapse when the static load is suddenly removed. This effect is observed for a chain of arbitrary length, but is absent in a continuous medium.

A linear oscillator is a highly simplified model of many processes. In particular, consideration of a chain of oscillators has been used by some authors [42-44] to clarify the issue of the influence of the discrete structure of solids on their mechanical properties. In [42] the author considered the travelling longitudinal wave passing through a chain of oscillators, and in work [43] dynamic fracture of a chain was considered, however, in both cases an infinite chain was studied. Some works [44,45] considered finite chains, however, the authors did not study the fracture issues. The book [46] examines many aspects of the chains' oscillations and also contains studies of limiting transitions to continuum equations. The classic monograph devoted to the propagation of waves in discrete media is the work [47]. An approach to heat conduction problems based on chains is given in [48].

The third Chapter of the thesis also presents numerical analysis of samples with a peculiar geometry, which demonstrates that the studied effect can be found in real structures. According to the calculations, the special design of the samples makes it possible to observe an excess of the initial stresses by 20% for a long time after sudden unloading (for example, after the failure of one of the weakened structural elements).

The crack propagation problems are a separate area of the dynamic fracture mechanics with its own well-established approaches. Some of them are based on further development and deep modification of Irwin's failure condition, others use the ideas of the cohesion zone [49]. Recent research in this area provides valuable information on crack propagation in heterogeneous materials with electromechanical properties [50]. New promising numerical approaches [51,52] are also worth mentioning. Dynamic crack propagation was considered an area of purely fundamental research, but modern numerical models, material models and experimental methods help to successfully solve complex engineering and construction problems as well [53,54]. However, it should be noted that these material models are often material specific (see, for example, the Riedel-Hiermaier-Thom (RHT) model [54,55]) and contain a fairly long list of parameters that need to be determined to perform the numerical simulation.

Dynamic crack propagation is one of the most challenging areas of the dynamic fracture mechanics, as numerous effects observed in this area require a proper theoretical explanation. Both fundamental and practical aspects of the propagating crack phenomenon are of significant importance, since, on the one hand, studies of a moving crack make it possible to identify the fundamental laws of the fracture mechanics [56], and on the other hand, problems of dynamic crack initiation and propagation arise in the engineering practice. Despite the fact that the uncontrolled dynamic crack propagation is considered as a hazardous phenomenon in some cases [57,58], crack initiation may be desirable, for example in the oil and gas industry [59].

In the second half of the 20th century, various analytical results in the field of moving cracks were obtained. In the works by Broberg [60,61], Kostrov [62], Freund [63-66], Slepyan [10,42,43], Achenbach and Bazant [67], Achenbach and Dunaevsky [68] one can find analytical formulas characterizing the field stresses near the tip of a moving crack, considerations for energy release, and theoretical predictions for the value of the ultimate crack velocity.

Most of the classical experimental works on dynamic crack propagation presenting significant effects of dynamic fracture were carried out in the last decades of the 20th century: Ravi-Chandar and Knauss [1,69-71], Feinberg et al. [16], Kobayashi and Dalli [72,73], Dalli [74], Kaltoff et al. [75], Rozakis et al. [76], Zender and Rozakis [77], Maigret and Rittel [78]. It was found that some dependencies and parameters characterizing the crack propagation process exhibit unstable behavior. The following phenomena may be mentioned here: crack speed oscillations, the discrepancy between theoretical and experimentally observed limiting crack speeds [16], instability of the stress intensity factor (SIF) values for crack initiation (Kalthoff and Shockey [2]), effects associated with a change in fracture mode [79], dependence of the stress intensity factor on the crack speed ($K_I - \dot{a}$ dependence) [25, 26]. Some of the mentioned effects were considered in [15] (oscillations of the crack velocity), [80] (unstable behavior of the SIF at the start of a crack).

According to one of the most common approaches to problems of the dynamic crack propagation (the first loading mode is considered), the concept of a critical stress intensity factor value (K_{Ic}) is extended to the dynamic case. Classic failure criterion proposed by Irwin $K_I = K_{IC}$ [18], is transformed into the crack initiation condition for the case of dynamic loading, which reads as $K_I^d(t, P(t), a_0) = K_{Ic}^d\left(\dot{K}_I^d(t)\right)$ [26], where $P(t)$ is the generalized loading function, a_0 is the initial crack length, and the right side is the critical value for a particular material, which also depends on the rate of the local stress field change. This approach provides the following equation of the crack tip motion $K_I^d(t, P(t), a(t), \dot{a}(t)') = K_{ID}\big(\dot{a}(t)\big)$, where the right-hand side is a crack velocity-dependent functional, which is assumed to be a material property to be determined from experiments. As can be seen from this brief description, the model implies existence of a unique (for a particular material) dependence of the stress intensity factor on the crack propagation speed and this dependence is considered to be a material property. The existence and uniqueness of this dependence was confirmed in a number of experimental works by Owen et al. [81], Rosakis et al. [76], Dally [74]. However, when testing samples of various shapes, non-unique $K_I - \dot{a}$ dependencies

were observed [82]. In these tests, the specimens were loaded either using a wedge or tensile testing machines. Single edge notched (SEN), double cantilever beam (DCB) and compact tension (CT) specimens produce different curves $K_I - \dot{a}$ for a particular material, especially in high crack velocity regimes. The dependence of the $K_I - \dot{a}$ dependence on the shape of the samples was also discussed in [73,83].

Ravi-Chandar and Knauss found that this relationship depends on the loading conditions [70]. In [70], the samples were loaded using short pressure pulses generated by an electromagnetic loading device. In this case, the stress intensity factor varied significantly for a crack that propagated at a constant speed. Thus, the existence of a single curve $K_I - \dot{a}$ was doubted. The influence of the velocity effects was also discussed in [84], where the authors argue that the acceleration and deceleration regions of a crack form different curves $K_I - \dot{a}$.

Determination of the $K_I - \dot{a}$ curve is a complex experimental task, since it is necessary to record and analyze the complete evolution of the crack, as well as the stress-strain state near the crack. As shown in [25], the characteristics of the $K_I - \dot{a}$ curve can vary depending on the experimental method used for the determination. Despite all the discussions surrounding this relationship, it is a widely used tool for characterization of the dynamic fracture of materials (for example, results on crack propagation in graphene are given in [85]).

Accounting for the discreteness of both spatial and time scales gives a more realistic idea of the dynamic fracture of solids. Fracture processes in materials, as a rule, occur in discrete spatial elements and over finite periods of time [86,87]. Ignoring this discreteness can lead to overly simplified models that do not reflect the true behavior of cracks as they propagate through the material.

Cracks generally propagate through materials through discrete events such as the initiation, growth, and coalescence of microcracks. These events occur in certain representative volumes and develop over finite time intervals being influenced by material properties, stress states and microstructural features. Modeling spatial and

time discreteness allows one to describe more accurately the dynamics of crack propagation, including the initiation of new cracks and their interaction with existing ones.

It is known that the microstructure of a material plays an important role in determining its fracture behavior. Discrete features such as grain boundaries, dislocations, and defects influence crack initiation and propagation. By incorporating spatial and time discreteness into the fracture models, the influence of microstructural features on crack propagation can be better captured and fracture patterns in real materials can be more accurately predicted.

Scale effects are also worth noticing. Fracture processes exhibit scale-dependent behavior in which spatial and time discreteness becomes more pronounced at smaller length and time scales. Models that account for this discreteness can capture large-scale effects such as size-dependent fracture toughness and the transition from continuous to discrete behavior. Understanding and accounting for these scale effects are necessary to predict fracture behavior at different scales of space and time.

Thus, accounting for space and time discreteness of the fracture process is important for accurate description of the dynamic crack propagation in materials. By accounting for the discrete events and their evolution in space and time at multiple scales, models can provide more realistic predictions of crack behavior, leading to improved understanding, design and optimization of materials and structures subjected to extreme dynamic loading.

The fourth Chapter of the thesis provides a numerical analysis of the effects accompanying the dynamic propagation of cracks. The analysis is based on the incubation time criterion, which provides possibility to account for the spatial and time discreteness of the dynamic fracture processes. The crack velocity oscillations and unstable behavior of the current stress intensity factor are among the studied effects.

In addition to this the fourth Chapter presents a numerical approach to problems with an arbitrary crack propagation trajectory. The developed calculation scheme was

used to analyze the characteristics of fragmentation when impactors penetrate barriers. The calculation scheme is based on the incubation time fracture criterion and the finite element method in a two-dimensional formulation. The developed scheme makes it possible to study the characteristics of fragmentation processes due to the projectile penetration – the size distribution of fragments, the dependence of the total number of fragments on the impactor speed. The obtained dependences qualitatively resemble experimental data on fragmentation in brittle media [88].

The characteristics of dynamic fragmentation are the subject of research by several scientific groups both in Russia and worldwide. Classic experimental and theoretical works in this area include the studies of D.E. Grady and his colleagues [89]. In Russia, studies of fragmentation processes are carried out in groups by O.B. Naimark [90,91] and at Tomsk State University [92].

A more detailed study of the dynamic fracture processes caused by impact is presented in the fifth Chapter of the thesis. The impact fracture of materials is of great importance for engineering applications, since this phenomenon is widespread: the development of military protective systems (bulletproof vests, vehicle armor, etc.), the automotive industry (crash safety), aviation (bird strikes, space debris threats, solid particle erosion of turbine blades [193-199]) and so on.

Experiments on impact fracture of materials are very labor-intensive, since they require high-speed recording systems and precise synchronization of equipment. Moreover, such experiments can be quite expensive since the samples are disposable. Numerical modeling can serve as a tool to optimize experimental research and design of structures and materials thanks to the ever-increasing computing capabilities of modern machines [201,202]. Nowadays a wide variety of numerical approaches to dynamic fracture problems are presented in the literature, which include the finite element method enriched with the adhesion zone models (classical works by Needleman [49]), particle hydrodynamics methods [93,94], and the discrete particle approach [95], meshless Galerkin methods [96], peridynamics [97,98]. However, in addition to choosing a numerical scheme, an appropriate fracture model should be

used, since materials can exhibit complex behavior under intense dynamic loading: an increase in strength with increasing strain rate [99,100], features associated with dynamic crack propagation [24,101].

In one of the most common approaches to dynamic fracture modeling, strain or stress rate dependencies are explicitly introduced into the material models. The constitutive Johnson-Cook model [102,103] is a prominent representative of this approach and is one of the most commonly used material models in the field of impact engineering, dynamic fracture and deformation. This model has been successfully applied in a large number of studies, however it contains a relatively large set of parameters that must be determined using fairly complex procedures [104,105], and not all of these parameters have a clear physical interpretation. In general, strain rate-dependent fracture models are based on a relatively large set of parameters and functional relationships requiring complex experimental evaluation.

A relatively effective approach to solving engineering problems is based on the introduction of special dimensionless parameters [106,107], which describe the behavior of a structure subjected to dynamic loading. These values are determined using parameters characterizing the load, sample geometry and mechanical properties of the material. These dimensionless parameters make it possible to evaluate the response of a structure to a dynamic load and compare the characteristics of the structure under various test conditions (shape and dimensions of the object, load parameters, material parameters).

Another group of the dynamic fracture criteria is based on the time characteristics of the fracture process. In the fifth Chapter the incubation time-based fracture model [31,80,108] was used to numerically simulate the PMMA (Polymethylmethacrylate) plate penetration experiments [109] conducted as part of the study. During these tests, a decrease in projectile speed due to interaction with the target was recorded. Experiments were carried out on samples with three thicknesses, and the incubation time model, which includes a single time parameter, was able to provide good agreement between experiments and numerical simulations for all three

sample geometries and a wide range of initial impactor velocities. The value of the incubation time for the PMMA has been assessed in previous works using spall fracture experiments.

PMMA was used in the studies presented since can be considered as a reference material for the dynamic fracture studies. This material has remarkable properties that are valuable for fundamental fracture research: PMMA is transparent and birefringent, and thus caustic stress analysis and photoelastic methods are applicable, in addition to this, PMMA can be regarded as brittle material. PMMA has been used in numerous studies on dynamic crack propagation [15,16], impact [110,111], spallation [112,113], and its strength parameters and behavior are well known. On the other hand, PMMA is widely used for various engineering applications [114], and the presented results (both experimental and numerical) can be useful for practical needs.

As mentioned before, the modelling of the dynamic fracture due to impact is a computationally demanding task. In addition to requirements to the processing power the impact problems can also exhibit computational difficulties associated with excessive distortion of the finite element mesh and unstable behavior of the contact algorithms [115–117]. Such computational challenges are quite expected in the impact problems due to the high rates of stress change in the contact zone.

A method developed to address the mentioned problems is discussed in the work. The proposed approach is based on application of artificial neural networks (ANN) which have been trained on a set of numerical results. The approach is demonstrated on model problem describing a projectile penetrating a target with a discrete structure – a perforated plate.

The work discusses application of the ANNs for rapid numerical assessment of the strength of perforated PMMA targets [118]. The ANN models were trained using sets of numerical results obtained for a problem of the PMMA plates impact using a dynamic FEM combined with the incubation time failure criterion. The developed approach makes it possible to estimate the strength of a specific target configuration

without complex FEM calculations that require significant computing resources. A simple static problem of a perforated plate deformation is discussed before solving the impact problem, and preferred ANN architectures are presented for both problems.

In general application of machine learning methods to engineering problems and mechanical problems is being intensively studied by a significant number of research groups around the world. Considerable progress has been made in combining the ANNs with numerical methods used in fluid dynamics. Here one can mention works on the use of deep reinforcement learning for shape optimization and control [119,120]. ANNs are also used to quickly obtain solutions to the fluid dynamics problems, which typically require significant computational resources [121].

ANNs are actively introduced into the field of solid mechanics, being especially effective for the design of composites and predicting their mechanical properties [122-124]. Currently, deep learning methods are also being actively studied for topology optimization problems [125]. Moreover, machine learning-based approaches are used to efficiently design complex materials such as metamaterials and nanomaterials with unconventional specific mechanical properties [126,127].

Many of the above-mentioned works combine machine learning methods with classical numerical methods such as finite difference or finite element methods: neural networks are trained using numerically obtained data sets and are then able to predict outcomes for as-yet-unsolved problems. This approach seems particularly promising for solving problems that require significant computational resources. Assessing the strength of a material under impact loading is a typical example of such problems, since it is necessary to state and to solve the problem in a dynamic formulation, using dynamic fracture models and contact algorithms. A number of works can be mentioned here [128-131], including the prediction and optimization of the impact strength of laminates and the use of machine learning methods to accelerate dynamic finite element calculations [132] – autoencoders trained on data sets generated by FEM are used to estimate strength of pipes and to significantly speed up calculations and to ensure high accuracy. A number of works [133,134] have shown that ANNs are

effective for predicting time series resulting from impact tests, for example, the dependence of force on time obtained by modeling the dynamic failure of pipes and honeycomb structures under impact conditions. The ANNs trained on FEM results can also be used to predict the reliability of complex manufacturing processes such as riveting [135].

ANNs are also used for comprehensive material characterization, such as estimating the JH-2 damage model parameters [27] from the experimental results [136]. Moreover, the ANNs trained on the experimental results can be used as material models that describe complex material behavior under different loading rates and temperature conditions [137]. Plasticity modeling using ANNs is a growing area of research showing high potential for handling relatively standard cases [138] as well as complex effects such as necking failure and yield stress decline phenomena [139,140].

Thus, the ANNs are currently actively used to optimize properties (for example, see the use of reinforcement learning methods for designing composites [141]), accelerating calculations both by replacing direct calculations with a trained neural network [132], and by implementation of efficient ANN-based material models that are trained either on experimental data or on computational results [142]. In addition, one can mention cases where the ANNs trained on sets of experimental results are used to facilitate further experimental studies by giving insight into possible experimental results [143,144].

The ANNs are used to quickly assess the strength of the PMMA plates with a discrete structure (perforation). The ANNs are trained using datasets generated by FEM, and thus the ANNs are considered as a fast alternative to a full finite element analysis. A possible method for handling computationally complex cases where the finite element mesh is significantly distorted is also proposed. The developed approach makes it possible to estimate the strength of a specific target configuration without complex calculations using FEM, which require significant computing resources. Moreover, the ANNs are shown to be able to predict results for configurations that cannot be processed using the developed FEM code due to numerical instabilities and

errors: the trained neural network uses information from successful calculations to produce results for problematic cases. It is worth noting that the dynamic fracture of perforated samples has attracted the attention of researchers from the crack trajectories point of view [145,146]. In addition to this, the interaction of a propagating crack with microcracks is also intensively studied [147] as well as fracture of metamaterials [200].

Goals and objectives of the study

The main objectives of the research are: the development of discrete approaches to the problems and effects of dynamic fracture of continuous media, the analysis of the dynamic fracture of media with a discrete periodic structure, the analysis of the discrete nature of the instabilities of the dynamic fracture process, as well as the adaptation of the incubation time approach for the analysis of fracture in impact problems and development of new approaches to numerical problems encountered in these problems.

In order to achieve the objectives of the study, the following problems were set:

To study the analogy between the dynamic fracture processes taking place when the crack starts to move due to dynamic pulse load and failure of the “mass-on-a-spring” system. To Associate the fracture process with an oscillator with a certain natural frequency.

To develop a relatively simple engineering approach to problems of the dynamic fracture, which would allow one to analyze the main effects of the dynamic fracture: an increase in the strength of the system with growth of the loading/strain rate and the effect of the fracture delay, manifesting itself when the fracture takes place a stage of decreasing local stress fields. The proposed approach is based on the study of a discrete system failure – a linear oscillator. The parameters of their oscillator are selected in order to adequately describe available experimental data.

To investigate the dynamic fracture of periodic mechanical discrete systems using the example of linear oscillator chains with an arbitrary finite number of links. In order to accomplish this task, it is necessary to find an analytical solution to the problem of the movement of masses in a chain of linear oscillators with an arbitrary finite number of links, particular load as well as initial and boundary conditions.

To conduct a numerical analysis of strength in a system with a discrete structure in order to study the effect of secondary failure which can follow the system unloading. Provide recommendations for a possible experimental study of the fracture effects identified using the oscillator chains.

To investigate effects that manifest instabilities of the dynamic crack propagation processes and can be associated with the discrete nature of the dynamic fracture. To develop a numerical scheme for the analysis of the moving cracks, based on the incubation time fracture criterion – a model that implies spatial and time discreteness of the fracture processes. To modify the developed numerical scheme in order to make it applicable for analysis of cracks with arbitrary trajectories and this way for the study of the dynamic fragmentation processes taking place in brittle bodies under impact loading.

To develop a numerical method for the analysis of fracture under impact loading conditions, to conduct simulations of experiments penetration of barriers by projectiles. Particular attention should be paid to the threshold values of the impactor velocity. To propose an approach that allows one to circumvent the main difficulties associated with the dynamic fracture modeling in impact problems – the complex and demanding calculations, long calculation times, unstable operation of the numerical schemes.

Scientific novelty of the research, theoretical and practical significance of the obtained results

Most of the problems formulated and set within the framework of the work are solved for the first time, and the methods used to solve the problems are also unique and cannot be found in literature.

The analogy between the dynamic fracture processes and failure of discrete systems with inertia (in this case, a linear oscillator) is discussed for the first time. Moreover, consideration of rectangular loading pulses made it possible to determine the natural frequency of the oscillator, which is identified with the fracture process accompanying the crack initiation. This result was obtained only in the works of the author and the co-authors.

As noted in the first paragraph of the introductory Chapter, a linear oscillator has previously been used to model dynamic fracture, but the main advantage of the approach presented in this work is the physical and mechanical meaning of the model parameters, as well as the minimization of the number of parameters that one needs to define for the model to operate. In fact, we managed to reduce this number to one parameter, which is responsible for the size of the region of the material responsible for the formation of the oscillator mass. Moreover, for the first time, the oscillator model was used to study the dynamic fracture effects – the fracture delay and the system strength increase with a growing loading/stress rate.

The effect of secondary system failure, observed in discrete periodic structures and discussed in the third Chapter of the thesis, was first studied by a team of researchers, which includes the author of the thesis. Moreover, for the first time it is shown that the discussed effect can be expected in real systems and samples with a discrete periodic structure, which opens up a wide field of activity for experimenters.

The approach used in the fourth Chapter of the work is based on the incubation time approach, which implies spatial and time discretization of the fracture process.

Integration of this approach into a calculation scheme based on the finite element method made it possible for the first time to study two points of view on the dependence of the current value of the stress intensity factor on the crack speed. Calculations have shown that this dependence can indeed be constructed for relatively low crack velocities and slow loading, but for intense and rapid loading and high crack velocities, the scatter of SIF values does not allow constructing an unambiguous dependence. The duality of the SIF–crack velocity relationship was obtained for the first time. It is also worth noting the first implementation of the dynamic method of virtual crack propagation within the framework of a commercial FEM software. The computational scheme for analyzing dynamic fragmentation presented in the fourth Chapter has a unique structure: the finite element method is supplemented with graph theory algorithms, which makes it possible to analyze the fragmentation of the studied object at each time step of the solution.

The three-dimensional calculation scheme presented in the fifth Chapter is the first three-dimensional numerical implementation of the criterion based on the concept of incubation time. It is worth noting that the implemented calculation scheme is based on a commercial FEM software, which can facilitate the introduction of the developed approach into the engineering practice. Chapter 5 also proposes for the first time a method which could help to overcome the numerical difficulties that often accompany modeling of fracture under impact conditions. The approach is based on the use of artificial neural networks (ANN) for the problems whose formulation results in the unstable behavior of contact interaction and excessive distortion of elements due to high stresses and strain rates. The proposed approach will not provide an exact solution to the problem, but will allow one to obtain an estimate of the solution without changes in the formulation of the problem and without changing the settings of the numerical solution algorithms. This method of overcoming numerical difficulties encountered in the impact problems has been proposed for the first time.

Research methods

The problems formulated within the framework of the study are solved analytically, numerically and experimentally. The first three Chapters of the thesis, which are devoted to the study of fracture in discrete systems, mainly use an analytical approach. In particular, exact formulas for the movement of a mass on a spring under pulse and linearly increasing loads made it possible to analytically study the effect of the fracture delay and to demonstrate an increase in the strength of the system with a growing loading rate. At the same time, when calibrating the linear oscillator model, numerical methods for solving ordinary differential equations were used to describe the experimental data due to the complexity of the functions describing the system load. The problem of oscillations of a chain of linear oscillators was also solved completely analytically.

The work widely uses the finite element method (FEM) to analyze the strength of structures. In particular, FEM was used to demonstrate the effect of secondary fracture in samples with a periodic structure. FEM made it possible to design the approximate shape of samples for possible experimental study of this effect. The results of the fourth Chapter of the thesis were almost completely obtained using FEM – the dynamic crack propagation was simulated using a FEM-based numerical approach and the incubation time fracture criterion. In this case, the dynamic solver of a commercial software is used to determine the strain and stress fields in the sample; the fracture criterion is implemented using an external program. An external program was created to calculate the current value of the stress intensity criterion, based on the method of virtual crack extension. The analysis of a barrier fragmentation was carried out using a sophisticated calculation scheme for analyzing the dynamic propagation of cracks. In a modified version of the scheme, the cracks can propagate in any direction and several cracks can be studied simultaneously. The analysis of the properties of fragments was carried out using graph theory methods – fragments are regarded as subgraphs of the graph of elements of a mesh.

A more complex three-dimensional calculation scheme has been developed for the impact problem analysis (Chapter 5). The fracture criterion (the incubation time criterion) in this case is implemented as a new material for the commercial FEM software package with an explicit time integration scheme. The obtained numerical results were compared with the results of experiments conducted as part of the study.

The numerical analysis of the impact problem was supplemented with a module based on artificial neural networks (ANN). The ANN is trained on a set of already solved problems and thus a solution to a similar problem can be quickly obtained. In addition to this the module can be used to obtain approximate solutions for problems that are difficult to solve using a full calculation due to numerical instabilities, for example, excessive distortion of mesh elements. The module's performance was demonstrated using the samples with a discrete structure – the perforated plates. Firstly, sets of solution of the impact problems with various perforation schemes are obtained and then the ANNs are trained using these data sets. The trained ANN is capable of predicting the answer for a new sample with a new perforation scheme. The ANNs are also applied to problems in which the perforation scheme led to excessive distortion of the mesh and premature termination of the calculation.

Results of the work and their theoretical and practical significance

The work uncovers an analogy between the dynamic fracture process taking place at the crack onset and the linear oscillator failure, which is important for a deeper understanding of the features of the dynamic fracture occurring in brittle bodies. The possibility to attribute some inertia to the fracture process allows one to clearly explain the key effects of the dynamic fracture – an increase in the strength of the system with increasing loading speed and a fracture delay. The problem of a crack initiation as a result of rectangular pulse loads applied to the crack faces was solved used the incubation time fracture criterion. This made it possible to identify the dynamic fracture process with a certain linear oscillator with a particular natural frequency, which can serve as the basis for an experimental search for resonance phenomena in

the crack initiation problems. It is also worth noting that the optimal rectangular pulses from the point of view of the force impulse were determined. This result can be useful from a practical point of view for problems in which fracture is a favorable outcome (for example, problems encountered in the mining industry).

An applied model for fracture analysis based on a linear oscillator has been constructed. The stiffness and critical deformation of the oscillator spring are determined from considerations of the static strength of the studied material, while the mass is responsible for the dynamic fracture effects can either be selected based on compliance with experimental data, or the mass can be defined as the mass of a certain volume of the studied material involved into the fracture process. On the one hand, this approach, demonstrates clearly that the effects observed in course of the dynamic fracture are natural, and on the other hand, the developed approach allows one to quickly analyze the structure strength under dynamic loads.

Studying fracture and failure of periodic structures due sudden unloading is important both theoretically and practically. The effect of a secondary fracture has been demonstrated using a chain of linear oscillators – if in a uniformly stretched chain one of the links breaks, a secondary rupture can occur. In the continuum problem, such effect cannot be not observed, which makes it possible to set problems on the limiting transition from a discrete system to the rod problem, as well as to examine questions about the applicability of continuum models for describing real materials and media. The numerical analysis carried out in the third Chapter will make it possible to design samples for experimental verification of the studied effect and to possibly develop a new method of loading a material with short pulses, which can be possibly used to analyze the fracture delay effect.

The work developed a number of numerical approaches to problems of dynamic fracture and dynamic crack propagation. The constructed numerical schemes are based on the finite element method and the incubation time fracture criterion. They are designed to solve two-dimensional problems of the propagation of straight main cracks and multiple cracks with an arbitrary direction, as well as to solve three-dimensional

fracture problems defect-free media (for example, in problems of penetration of barriers by projectiles). Some of the calculation schemes are equipped with additional functions: solving the problem of propagation of a main crack can be accompanied by calculating the current value of the stress intensity factor using the method of virtual crack extension; a fragmentation analysis method based on graph theory has been also proposed. All the developed numerical schemes can be used in practice to calculate the strength of structures. The calculation schemes are based on commercial software packages, which can facilitate their implementation in engineering practice.

The work also proposes a numerical approach based on artificial neural networks (ANN), which allows one to quickly obtain solutions to demanding problems, as well as to solve problems which are hard to process with classic numerical schemes due to instabilities. Performance of the proposed approach is demonstrated using the impact problem involving barriers with a discrete structure – plates with perforation. The performance of various ANN architectures has been studied, and it has been shown that the mechanical formulation of the problem can greatly influence the choice of the preferred ANN architecture. This result has high practical significance for developers of computational software systems and environments.

The credibility of the results is ensured by the correspondence of theoretical calculations with the experimental data presented in the scientific literature, as well as the reproducibility of the results obtained in the work.

Approbation of results

The main results of the work were presented at the following conferences:

1. International conference Current problems in mechanics, St. Petersburg 2018
2. International conference Current problems in mechanics, St. Petersburg 2019
3. International conference Current problems in mechanics, St. Petersburg 2021

4. International Conference 6th International Conference on Crack Paths, Verona 2018

5. International conference 7th International Conference on Crack Paths, online conference, 2021

6. International Conference European Conference on Fracture 21, Catania, 2016

7. International conference European Conference on Fracture 22, Belgrade, 2018

8. International conference First Virtual European Conference on Fracture, online conference, 2020

9. International Conference European Conference on Fracture 23, Funchal, Madeira, 2022.

10. International Conference 14th International Conference on Fracture, Rhodes, Greece, 2017

11. International Conference 11th International Symposium on Plasticity and Impact Mechanics, Delhi, 2016

12. International Conference 10th European Solid Mechanics Conference, Bologna, 2018

13. International Conference XII All-Russian Congress on Fundamental Problems of Theoretical and Applied Mechanics, Ufa, 2019

14. International Conference XIII All-Russian Congress on Fundamental Problems of Theoretical and Applied Mechanics, St. Petersburg, 2023

15. LXVII International Conference Current problems of strength of APP-2024, Ekaterinburg, 2024

The research results were published in the following 20 papers (WoS/SCOPUS); 9 papers published in Q1 CJR/SJR journals:

1. N.A. Kazarinov, V.A. Bratov, Yu.V. Petrov, Simulation of dynamic crack propagation under quasi-static loading, Doklady Physics 59(2), 2014, 99-102 (author's contribution 50%)

2. I. Smirnov, N. Kazarinov,Y. Petrov, Experimental observation and numerical modeling of unstable behaviour of a fast crack velocity, Theoretical and Applied Fracture Mechanics 101, 2019, 53-58 (author's contribution 30%)

3. Yu.V. Petrov, A.A. Gruzdkov, N.A. Kazarinov, Features of the dynamic fracture of one-dimensional linear chains, Doklady Physics 53(11) ,2008, 595-599 (author's contribution 50%)

4. N.A. Kazarinov, S.A. Smirnov, Y.V. Petrov, Revisiting mass-on-spring model to address key dynamic fracture effects, Theoretical and Applied Fracture Mechanics 132, 2024, 104470 (author's contribution 80%)

5. N.A. Kazarinov, Y.V. Petrov, A.V. Cherkasov, Instability effects of the dynamic crack propagation process, Engineering Fracture Mechanics 242(1), 2021, 107438 (author's contribution 70%)

6. N.A. Kazarinov V.A. Bratov, Dynamic fracture of ceramic plates due to impact loading. Numerical investigation, Materials physics and mechanics 4(42), 2019, 389-395 (author's contribution 80%)

7. N.A. Kazarinov, V.A. Bratov, N.F. Morozov, Y.V. Petrov, V.V. Balandin, M.A. Iqbal, N.K. Gupta, Experimental and numerical analysis of PMMA impact fracture, International Journal of Impact Engineering 143, 2020, 103597 (author's contribution 60%)

8. N. Kazarinov, A. Khvorov, Predicting impact strength of perforated targets using artificial neural networks trained on FEM-generated datasets, Defense Technology 32, 2024, 32-44 (author's contribution 70%)

9. N. Kazarinov, Yu. Petrov, A. Utkin, Fracture delay effect: analogy between crack initiation due to short pulse loads and mass-spring system failure, International Journal of Impact Engineering 175, 2023, 104513 (author's contribution 60%)

10. M.O. Ignatiev, Y.V. Petrov, N.A Kazarinov, Simulation of Dynamic Crack Initiation Based on the Peridynamic Numerical Model and the Incubation Time Criterion, Technical Physics 66(3), 2021, 422-425 (author's contribution 50%)

11. M.O. Ignatiev, Y.V. Petrov, N.A. Kazarinov, E. Oterkus, Peridynamic formulation of the mean stress and incubation time fracture criteria and its correspondence to the classical Griffith's approach, Continuum Mechanics and Thermodynamics 35(4), 2023, 1523-1534 (author's contribution 40%)

12. N.A. Kazarinov, Y.V. Petrov, A.V. Cherkasov, Spatial and Temporal Discreetness as a Crucial Property of the Dynamic Fracture Process, Mechanics of Solids 55(5), 2020, 673-678 (author's contribution 70%)

13. N.A. Kazarinov, V.A. Bratov, Yu.V. Petrov, G.D. Fedorovsky, Evaluation of fracture incubation time from quasistatic tensile strength experiment, Materials Physics and Mechanics 19(1), 2014, 16-24 (author's contribution 50%)

14. Y.V. Petrov, A.V Cherkasov, N.A. Kazarinov, Instability of critical characteristics of crack propagation, Acta Mechanica 232(5), 2021, 1997-2003 (author's contribution 70%)

15. N.A. Kazarinov, Y.V. Petrov, V.A. Bratov, V.Yu. Slesarenko, Numerical investigation of stress intensity factor - crack velocity relation for a dynamically propagating crack, Materials Physics and Mechanics 29(1), 2016, 39-42 (author's contribution 70%)

16. N.A. Kazarinov, A.D. Evstifeev, Y.V. Petrov, S.A. Atroshenko, R.R. Valiev, The Effect of Grain Refinement on Solid Particle Erosion of Grade 5 Ti Alloy, Journal of Materials Engineering and Performance 27(6), 2018, 3054-3059 (author's contribution 40%)

17. N.A. Kazarinov, A.D. Evstifeev, Y.V. Petrov, S.A. Atroshenko, V.A. Lashkov, R.Z. Valiev, A.S. Bondarenko, Surface Roughness Investigation of Ultrafine-Grained Aluminum Alloy Subjected to High-Speed Erosion, Journal of Materials Engineering and Performance 25(9), 2016, 3573-3579 (author's contribution 40%)

18. A. Evstifeev, N. Kazarinov, Y. Petrov, L. Witek, A. Bednarz, Experimental and theoretical analysis of solid particle erosion of a steel compressor blade based on incubation time concept, Engineering Failure Analysis 87, 2018, 15-21 (author's contribution 40%)

19. R.Z. Valiev, E.A. Prokofiev, N.A. Kazarinov, G.I. Raab, T.B. Minasov, J. Stráský, Developing nanostructured Ti alloys for innovative implantable medical devices, Materials 13(4), 967 (author's contribution 60%)

20. N. Kazarinov, A. Stotskiy, A. Polyakov, R.Z. Valiev, N. Enikeev, Finite Element Modeling for Virtual Design to Miniaturize Medical Implants Manufactured of Nanostructured Titanium with Enhanced Mechanical Performance, Materials 15(21), 2022, 7417 (author's contribution 60%)

Author's contribution

The thesis materials are a generalization of the author's work on the research topic and reflect his personal contribution to the development of this topic. All results presented in the thesis were obtained either by the author himself or with his direct participation.

Acknowledgments

The author expresses sincere gratitude to the scientific consultant Professor Yuri Viktorovich Petrov for research leadership, mentoring and motivation to write the work. The author is also grateful to colleagues and co-authors V.A. Bratov, A.A. Gruzdkov, A.A. Utkin, S.B. Filippov, G.A. Volkov. for their support and numerous

discussions. The author is grateful to I.V. Smirnov, V.V. Balandin. And V.V. Balandin junior for the experimental results. The author also thanks his school mathematics teacher Grigory Zalmanovich Mednikov.

Support

The research was carried out with the support of the Ministry of Science and Higher Education of the Russian Federation within the framework of a megagrant (agreement No. 075-15-2022-1114 dated June 30, 2022). The author is also grateful to RSF (grants 22-11-00091 and 22-71-10019)

Structure of the thesis

The thesis consists of an introduction, five Chapters, a conclusion, and a list of references. The work is presented on 191 pages, contains 66 figures and 10 tables. The reference list contains 202 sources.

Main scientific results

- An analogy between the processes of dynamic fracture and the failure of a linear oscillator has been discovered and investigated [148].

- A dynamic fracture model based on a linear oscillator has been constructed. The model was used to describe experimental results and to study key dynamic fracture effects [34].

- The effects of unstable behavior of parameters characterizing the crack propagation process, in particular, crack velocity oscillations and variation of the stress intensity factor values have been studied. The stress intensity factor – crack velocity relation was shown to be defined by the type of the applied load [14,15,86,183,184,186,188-190].

- A numerical study of dynamic fragmentation processes under shock loading has been carried out. Numerical results describe qualitatively the experimentally observed dynamic fragmentation [88].

- New numerical and experimental approaches to analysis of strength of materials under quasi-static, cyclic and dynamic types of loads have been developed [86,109,183,184,193,195,199,201,202].

- The effect of fracture in periodic structures in case of sudden unloading has been discovered and studied [17].

- A method to accelerate calculations and to overcome numerical instabilities in impact problems of breaking through obstacles. The method is based on artificial neural networks [118].

Thesis defense key points

The analogy between fracture in the “mass-on-a-spring” system and the dynamic start of a crack has been discovered and studied. The use of the incubation time fracture criterion to analyze the start of cracks under loading with rectangular pulses made it possible to associate a linear oscillator with a certain natural frequency with the fracture process. Thus, it is shown that the process of the dynamic fracture exhibits inertial properties and characteristic times that cause the instability effects observed when classic fracture models are applied to problem with high rates of loading and high stress rates. The application of the fracture models containing characteristic times implies the introduction of the time scale to the fracture process study.

A dynamic fracture model based on the “mass-on-a-spring” system is proposed, which makes it possible to describe and predict the key effects of the dynamic fracture, which cannot be processed using classic critical value-based approaches (the fracture delay and the increase of the system strength when the loading rate/stress rate grows). The study provides a simple engineering interpretation of the complex and unstable

behavior of critical fracture characteristics that cause problems with traditional approaches.

An effect associated with fracture taking place in a system with a periodic structure after the unloading has been discovered: it has been proven that unloading waves initiated even by a quasi-static rupture can cause secondary fracture of a in multicomponent periodic structures. The effect is shown using the example of a chain of linear oscillators. For this system equations of mass motion were obtained and analytically solved. The numerical analysis has been carried out indicating the possibility of experimental confirmation of the studied effect using specially designed material samples.

A numerical scheme based on the finite element method and the incubation time criterion has been developed to analyze the dynamic propagation of straight cracks. A numerical analysis of the effects that cause discussions among specialists, such as K. Ravich-Chandar, V. Knauss, A. Rosakis, J. Dally has been carried out: the strong scatter in the values of the stress intensity factor observed in experiments under intense loading of samples and high rates of crack movement, as well as oscillations of the crack velocity. These effects are explained for the first time from the point of view of the incubation time, which implies spatial and time discretization of the fracture process.

A two-dimensional numerical scheme has been developed for modeling the fragmentation of brittle bodies under impact loading, which makes it possible to simulate the propagation of multiple cracks in an arbitrary direction. The numerical scheme is based on the finite element method, incubation time criterion and graph theory methods. It is shown that in order to simulate the main effects of fragmentation, it is not necessary to introduce complex rheological models based on a large number of defining parameters and functions of the material. For ceramic materials, the dependences of the number of fragments on their size, as well as on the speed of the projectile hitting the obstacle, have been obtained. The nature of the numerically

obtained dependences is qualitatively confirmed by the experimentally observed results.

A numerical approach for modeling fracture in impact problems has been proposed. The developed three-dimensional computational scheme is based on the finite element method in a three-dimensional formulation and the incubation time fracture criterion. This calculation scheme makes it possible to determine the threshold speeds of the projectile. The experiments on penetration of the PMMA (polymethilmethacrylate) plates have been simulated and the threshold speed of the impactor for the studied samples has been determined, and the accordance of the model with the experiments has been shown.

A new approach based on artificial neural networks (ANNs) has been proposed, making it possible to significantly speed up the solution process for the dynamic fracture problems, as well as to possibly overcome the computational difficulties inherent in this class of problems (excessive deformation of elements, unstable performance of the contact algorithms). An ANN-based algorithm has been developed that allows one to analyze the fracture process in media and materials with a discrete structure – the perforated plates. The algorithm makes it possible to obtain a solution to the problem without carrying out a full calculation, as well as to obtain a solution for computationally difficult cases.

Chapter 1. Analogy between the dynamic fracture processes in brittle solids and failure of a "mass-on-a-spring" system

The incubation time fracture criterion (ITFC) is used to analytically investigate dynamic crack initiation under short pulse loads. Particular attention is paid to the phenomenon of delayed fracture – a fundamental fracture effect which can be observed in experiments with short pulse loads. The effect can be described in the following way: the material failure occurs after local stresses reached their maximum values, meaning that the fracture takes place at a drop stage of the load and thus delay is present. It is shown that the fracture delay effect manifests itself when minimal required critical loads are applied to the system. Such loads are called threshold loads being a key tool for experimental investigation of the dynamic fracture effects. It is found that the experimentally registered fracture delay can be clearly explained within the incubation time framework. The conditions for the delay are found, threshold load parameters are evaluated and the corresponding analytical formulas are given. Additionally, a simple analogy based on a mass-spring model is discussed. Analytical formulas available for the oscillator model are used to find some non-obvious similarities between the crack instability under short pulse loads and the oscillator failure when analogous loads are applied.

1.1. Dynamic failure of a linear oscillator

Let's consider mass m on an elastic spring with stiffness c and force $f(t)$ applied to the mass. The mass deflection is described by function $x(t)$, which satisfies the following balance equation, initial conditions and a critical deflection failure condition:

$$\begin{aligned} & m\frac{d^2x}{dt^2} + cx = f(t) \\ & x(0) = \dot{x}(0) = 0 \\ & x(t) \geq x_c \Leftrightarrow \text{разрушение} \end{aligned} \qquad (1.1).$$

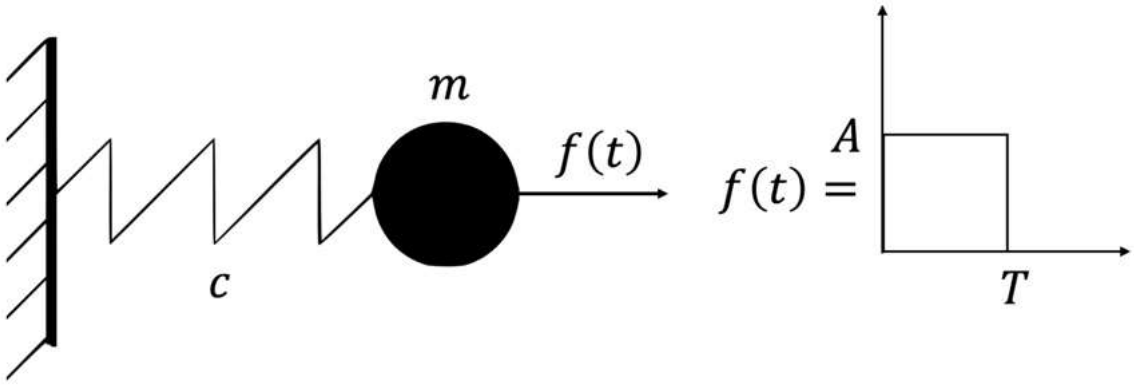

Fig. 1.1. Oscillator and loading pulse.

Problem (1.1) can be solved for a rectangular force pulse, when $f(t) = A[H(t) - H(t-T)]$, where A and T are the pulse amplitude and duration correspondingly and $H(t)$ is Heaviside step function. The solution of problem (1) is the following:

$$x(t) = \begin{cases} \frac{A}{c}(1 - \cos(\omega t)),\ t \le T \\ \frac{A}{c}\left(\cos\left(\omega(t-T)\right) - \cos(\omega t)\right),\ t > T \end{cases} \quad (1.2),$$

where $\omega = \sqrt{c/m}$ is the oscillator natural frequency. If the system failure is considered and fracture time is denoted by t^*, equation $x(t^*) = x_c$ can be used to build dependence of the pulse duration T on the fracture time t^* for a fixed pulse amplitude. If fracture time exceeds pulse duration ($t^* > T$), fracture delay takes place because fracture takes place right when the tearing force drops to zero (or prior to this moment) ($t^* \le T$) and there is no delay we can calculate minimal possible fracture time t^*_{min}:

$$t^*_{min} = T_{zero\ delay} = \frac{1}{\omega} arccos\left(1 - \frac{f_c}{A}\right) \quad (1.3)$$

In (1.3) and further $f_c = cx_c$ is critical static force for the oscillator. All pulses with durations longer than $T(t^*_{min})$ result in the exact same fracture time t^*_{min} yielding a vertical line on the $T(t^*)$ graph (figure 1.2).

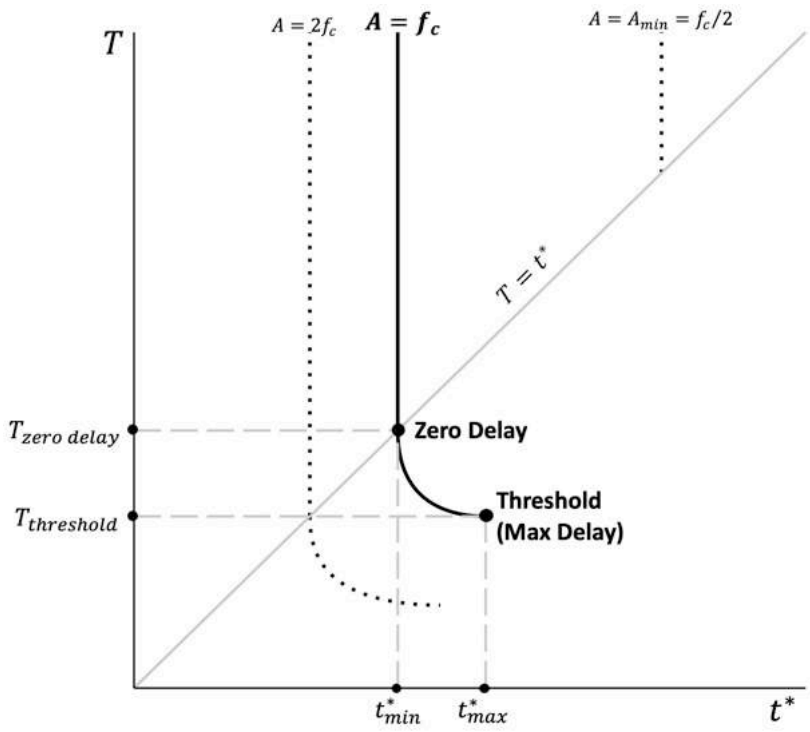

Fig. 1.2. Dependence of pulse amplitude on fracture time for pulsed causing oscillator failure with fixed amplitudes.

The fracture with a delay can be studied if $t > T$ case from (1.2) is considered. For this case solution of the equation $x(t^*) = x_c$ yields the following $T(t^*)$ dependence:

$$T = -\frac{1}{\omega} arccos\left(\frac{f_c}{A} + cos(\omega t^*)\right) + t^* \qquad (1.4).$$

Analyzing (1.4) one can evaluate minimal pulse duration for a given amplitude $T_{threshold}$, which corresponds to a maximal fracture time t^*_{max} indicating maximal fracture delay:

$$t^*_{max} = \frac{1}{\omega}\left(\pi - arccos\left(\frac{f_c}{2A}\right)\right) \qquad (1.5a),$$

$$T_{threshold} = \frac{1}{\omega}\left(\pi - 2arccos\left(\frac{f_c}{2A}\right)\right) \qquad (1.5b).$$

Formulas (1.5a,b) impose natural limitation on the pulse amplitude A due to restrictions on the $arccos$ argument which should belong the $[-1,1]$ range. Thus, in order to cause the system failure, the tearing force pulse amplitude should be equal or exceed half of static critical force (a static force which would break the spring if static problem was considered): $A \geq f_c/2$. If minimal pulse amplitude $A = f_c/2$ is considered, points t^*_{min} and t^*_{max} merge and no fracture delay can be observed and hence the $T(t^*)$ degenerates into a single vertical line. On the contrary, larger amplitudes result in longer possible fracture delay times. These variants of the $T(t^*)$ dependence are shown with dotted lines in figure 1.2.

Formula (1.3) can be used to construct a dependence of the tearing pulse duration on the pulse amplitude for the two limiting cases: for the zero-delay case $t^* = T$ should be substituted into (1.4) and if maximal fracture delay is considered (5b) should be used in order to study the threshold case. The corresponding $T(A)$ dependencies are shown in figure 3a. The graph shows a minimal admissible pulse amplitude and shorter pulses require higher amplitudes to cause the system failure – threshold loads. Note that the oscillator failure effectively occurs for pulses that lie between the two lines since we suppose that the loading stops when the system fails – the points "drop" to the zero delay $T(A)$ curve, which describes the system overloading case.

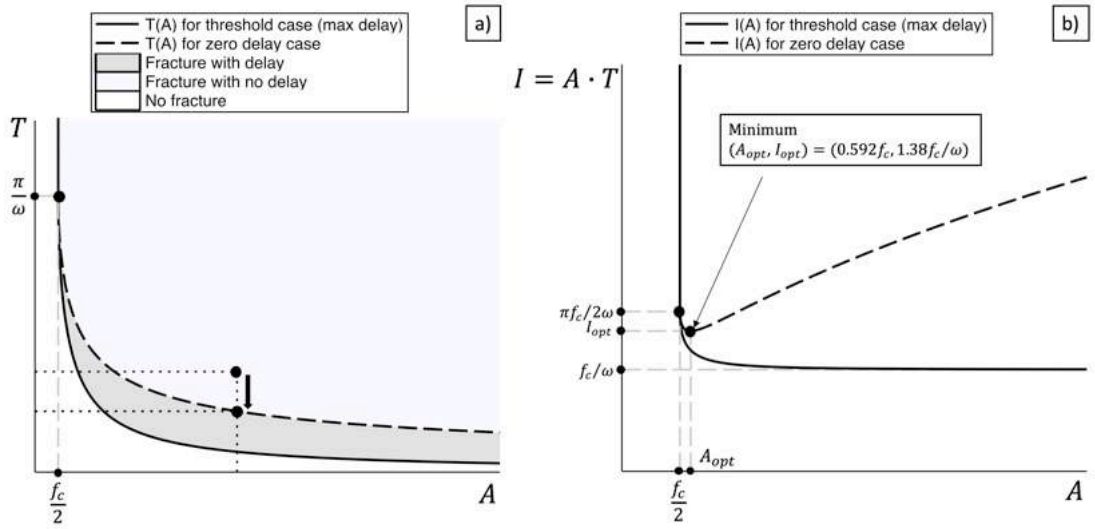

Fig. 1.3. Dependencies of loading pulse duration (a) and load impulse (b) on amplitude for pulses that cause fracture with and without delay.

Finally, we can use the obtained $T(A)$ curves to investigate impulse $I = A \cdot T(A)$ for the loads which result in the system failure. The corresponding $I(A)$ curves are shown in figure 1.3b. The zero delay $I(A)$ dependence appear to have a minimum point $(A_{opt}, I_{opt}) = (0.592 f_c, 1.38 f_c/\omega)$ providing optimal (in terms of impulse) regime for the oscillator failure when no fracture delay is considered and the system is overloaded. Thus, in order to break the oscillator optimally in terms of the load impulse and without the fracture delay (which is practically the simplest way to cause fracture, since one has to apply the force pulse and wait until the system fails) the system should be loaded with a pulse with a $0.592 f_c$ amplitude. Obviously, if fracture with a delay is considered, one should use very short pulses with high amplitudes in order to minimize the impulse of the tearing force.

This way, it was shown that the oscillator can exhibit the fracture delay effect when short tearing pulses are applied. Parameters of the critical pulses belong to particular intervals depending on which regime is considered: threshold loading or the overloading of the system. Moreover, there is a minimum value for the tearing pulse amplitude for pulses that cause the system failure and this minimal amplitude equals half of the static critical force f_c. In addition to this one can calculate an optimal (in terms of the load impulse) amplitude for a pulse which causes the oscillator failure without a delay.

1.2. The incubation time fracture model

The incubation time fracture criterion was originally proposed in works [31,80,108]. The model implies that macroscopic fracture event requires specific time – the incubation time – to develop from microscopic fracture processes such as microcracking and defect movement and coalescence. The incubation time is regarded as a material parameter to be evaluated from available dynamic fracture experiments for a given material.

According to the ITFC the fracture at point x and fracture time t^* is controlled by the following inequality:

$$\frac{1}{\tau}\int\limits_{t^*-\tau}^{t^*}\frac{1}{d}\int\limits_{x-d}^{x}\sigma(x',t')dx'dt' \geq \sigma_c \qquad (1.6),$$

where $\sigma(x,t)$ is a time-dependent tearing stress, σ_c is ultimate stress for the studied material and τ stands for the incubation time. Criterion (1.6) also contains linear size parameter d, which was firstly introduced in [149,150]. This parameter is treated as the fracture process zone size, coinciding with the minimal distance the crack tip can travel. The linear size d can be calculated using the formula $d = 2K_{Ic}^2/\pi\sigma_c^2$, where where K_{Ic} is the critical stress intensity factor for the studied material. The incubation time τ is considered to be a material property which should be evaluated experimentally. It is independent of other parameters and the best way to measure it experimentally is to conduct a test, where one knows the fracture zone location x, fracture time t^* and stress history at points of interest $\sigma(x,t)$. This way, one simply needs to substitute the stress history into the integral condition and to find the τ, which provides the equality in the formula (1.6). The stress history can be measured experimentally (the best option, which is attainable in spallation tests) or can be taken from numerical or even analytical analysis. Another way is to operate with threshold loads, which can sometimes provide possibility to calculate τ without knowing fracture time t^*. The fracture criterion (1.6) can be simplified to perform analysis of crack growth initiation due to dynamic loads when bodies with cracks are considered:

$$\frac{1}{\tau}\int\limits_{t^*-\tau}^{t^*}K(t')dt' \geq K_{Ic} \qquad (1.7).$$

For relatively slow loads criterion (1.7) is equivalent to Irwin's criterion $K_I \geq K_{Ic}$ [18] but cannot be used to simulate the crack propagation process due to possible lack of stress intensity factor dominance in case of moving cracks [151].

1.3 Crack initiation analysis and analogy with an oscillator

All the dependencies in this section will be constructed and demonstrated for experiments on crack initiation due to pulse loading from works [2,5]. Firstly, we will provide a detailed description of the incubation time model application and consequent association with the oscillator model for the results from [5] where steel samples were tested. Then experiments on plexiglass from [2] will be analyzed analogously, but in a briefer manner.

In fact, we will follow steps we made for the oscillator model described in the first section: to construct the $T(t^*)$ dependence for some given load pulse amplitude A in order to clearly show the fracture delay effect, then we will find the zone in the $T - A$ plane where critical pulses belong and finally we will calculate optimal load pulse parameters which will help us to associate some virtual oscillator with the considered crack initiation problem.

Experiments on crack initiation due to pressure pulses in 4340 steel sample from work [5]

In [5] experiments on crack initiation in 4340 steel samples due to rectangular pressure pulses are described. The authors provide data on pulses with threshold amplitudes (minimal amplitude for a given pulse duration leading to crack instability) for three pulse durations – 18 μs, 40 μs and 80 μs (figures 6 and 7 in [5]) for cracks with different initial lengths. In this study we are interested in relatively long cracks so that semi-infinite approximation could be considered applicable and corresponding formulas for the SIF would be available.

Consider an elastic plane with a semi-infinite cut $y = 0, x \leq 0$ (figure 1.4). If the material behavior is considered to be elastic, the deformed state is defined by the following system of equations:

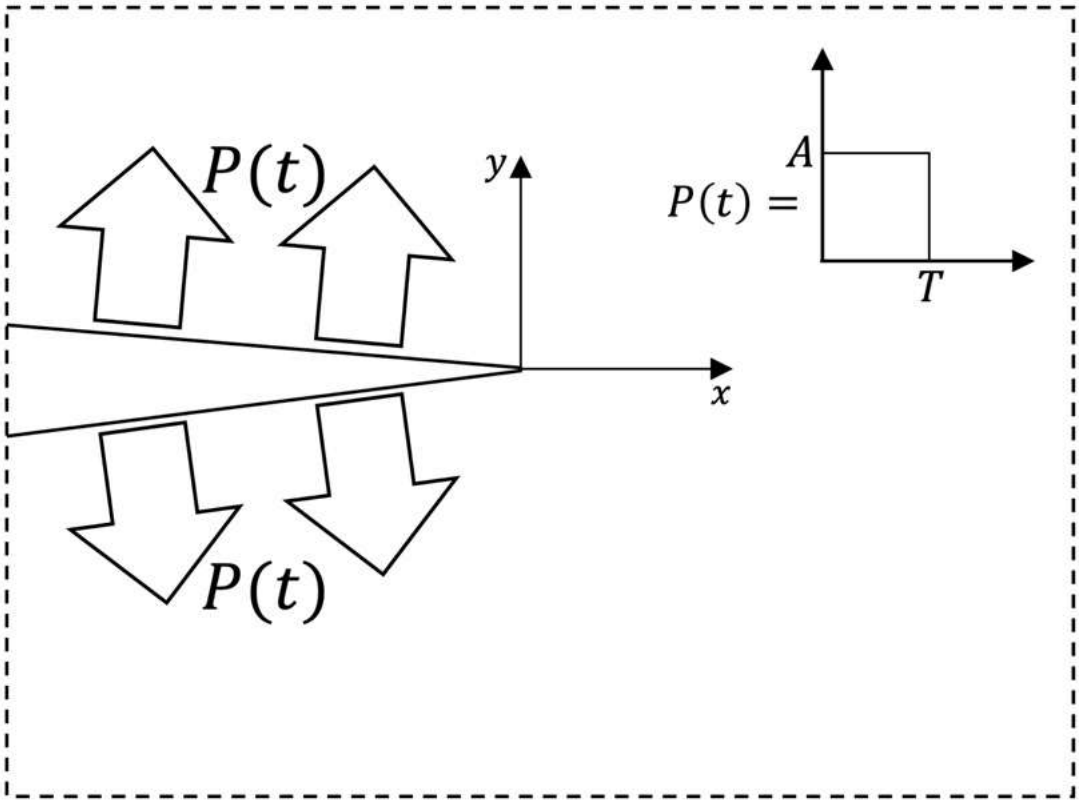

Рис. 1.4. Crack initiation problem scheme. The sample is unbounded and crack is semi-infinite.

$$\frac{\partial^2\varphi}{\partial x^2}+\frac{\partial^2\varphi}{\partial y^2}=\frac{1}{c_1^2}\frac{\partial^2\varphi}{\partial t^2}$$
$$\frac{\partial^2\psi}{\partial x^2}+\frac{\partial^2\psi}{\partial y^2}=\frac{1}{c_2^2}\frac{\partial^2\psi}{\partial t^2} \quad (1.8),$$

where φ and ψ are the Helmholz decomposition potentials, c_1 and c_2 are dilatational and transversal elastic wave velocities. Horizontal and vertical displacements (u, v) can be obtained according to formulas

$$u=\frac{\partial\varphi}{\partial x}+\frac{\partial\psi}{\partial y}, v=\frac{\partial\varphi}{\partial y}-\frac{\partial\psi}{\partial x} \quad (1.9).$$

The crack faces are supposed to be loaded with a time-dependent normal pressure $P(t)$ and the plane is stress-free for $t<0$. Thus, the following boundary conditions and initial conditions are applied:

$$\sigma_{xy}\big|_{\substack{y=\pm 0,\\ x<0}} = 0$$
$$\sigma_{y}\big|_{\substack{y=\pm 0,\\ x<0}} = P(t) \qquad (1.10).$$
$$\varphi|_{t<0} = \psi|_{t<0} = 0$$

If the step load $P(t) = A \cdot H(t)$ is considered, the stress intensity factor is given by formula [65]

$$K^H(t) = A \cdot \alpha \cdot \sqrt{t}, \alpha = \frac{4c_2\sqrt{c_1^2 - c_2^2}}{c_1\sqrt{\pi c_1}} \qquad (1.11).$$

If arbitrary load $F(t)$ is applied to the crack faces, the expression for the corresponding SIF dependence $K^F(t)$ is calculated using convolution:

$$K^F(t) = \int_0^t K^H(s) \cdot F'(t-s)ds \qquad (1.12).$$

This way formula (1.12) can be used to evaluate the $K(t)$ function for a rectangular pulse load $P(t) = A\big(H(t) - H(t-T)\big)$ with amplitude A and pulse duration T:

$$K(t) = A \cdot \alpha \cdot \left(\sqrt{t} - \sqrt{t-T}\right) \qquad (1.13)$$

In (1.13) and in the rest of the formulas in the paper the roots are supposed to be multiplied by a Heaviside function with the same argument. Now we can substitute (1.13) into criterion (1.7) (supposing that in (1.7) equality takes place) in order to investigate the crack initiation. Direct definite integral evaluation using the antiderivative formula for the square root ($\int \sqrt{x}dx = 2/3 \cdot x^{3/2}$) yields expression (1.14), which connects fracture time t^*, pulse duration T and load amplitude A and thus can be used to construct the $T(t^*)$ dependence for a fixed pulse amplitude.

$$\frac{2A\alpha}{3\tau K_{Ic}}\left((t^*)^{3/2} - (t^*-T)^{3/2} - (t^*-\tau)^{3/2} + (t^*-T-\tau)^{3/2}\right) = 1 \qquad (1.14)$$

If the zero-delay case ($t^* \leq T$) is considered, meaning that fracture takes place before the stress intensity factor reaches its maximum (see figure 1.5), the second and the fourth terms of (1.14) disappear (due to multiplication by the Heaviside function) and t^*_{min} value can be found numerically from the simplified equation. Note that for the case when $t^* < \tau$ (1.14) is obviously further simplified providing explicit formula for the t^*_{min}. The t^*_{min} value corresponds to a vertical line in the $T(t^*)$ dependence (figure 1.6).

The 4340 steel material properties used in the analysis are listed in table 1.1. Note that the incubation time value $\tau = 7\mu s$ provides the best fit of the experimental curves by a theoretical threshold $T(A)$ curve (figure 1.7).

Material property	**Value**
Critical stress intensity factor, K_{Ic} $MPa\sqrt{m}$	47
Longitudinal wave velocity, $c_1, m/s$	6000
Transversal wave velocity, $c_2, m/s$	3240
Incubation time, τ, s	7e-6

Table 1.1. 4340 steel material properties used in the calculations.

In order to investigate possible fracture delay, we should consider $t^* > T$ case and search for a threshold minimal pulse duration $T_{threshold}$ for a given fixed amplitude A which corresponds to a maximal fracture time t^*_{max} and thus to a maximal fracture delay. Obviously, at a point t^*_{max} the $T(t^*)$ dependence has minimum. Since this is a threshold case, the $t = t^*_{max}$ value can be found as a root of the following equation which arises from (1.7):

$$\max_t \int_{t-\tau}^{t} K(t')dt' = \tau K_{Ic} \qquad (1.15)$$

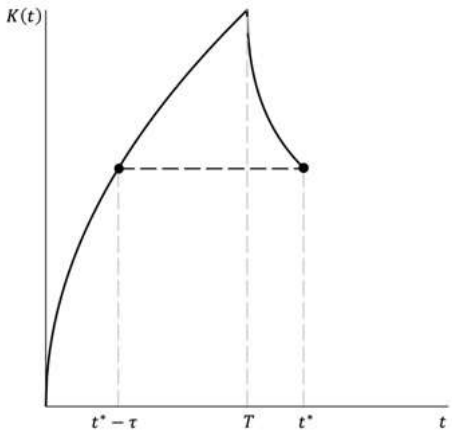

Fig. 1.5. Stress intensity factor for a pulse load applied to the crack faces.

The maximum condition can be evaluated if integral in (1.15) is differentiated with respect to t. This way, we deduce that $K(\ t^*_{max} - \tau) = K(\ t^*_{max})$. If we consider shape of the $K(t)$ function (see figure 5), we can conclude that $t^*_{max} - \tau < T < t^*_{max}$ and that fracture takes place after the $K(t)$ has passed its maximum and $dK(t)/dt < 0$. Thus, if expression for the t^*_{max} is sought for, formula (1.14) should be used without the fourth term since it vanishes due to multiplication by a Heaviside function:

$$\frac{2A\alpha}{3\tau K_{Ic}}\left((t^*)^{3/2} - (t^* - T)^{3/2} - (t^* - \tau)^{3/2}\right) = 1 \qquad (1.16)$$

Now we can use (1.16) to implicitly calculate minimum of the $T(t^*)$ function. A known formula for minimum of implicit function yields the following equation:

$$\sqrt{t} - \sqrt{t - T} = \sqrt{t - \tau} \qquad (1.17).$$

Expression (1.17) can be transformed to quadratic equation with respect to t^* and one of its roots gives a formula for the t^*_{max} we are looking for:

$$t^*_{max} = \frac{1}{3}\left(T + \tau + 2\sqrt{T^2 + \tau T + \tau^2}\right) \qquad (1.18)$$

Figure 1.6 shows the $T(t^*)$ dependence for the 4340 steel and the loading pulse amplitude $A = 500\ MPa$ (added by two supplementary amplitude values). Calculated values for the key points of the curve are also provided. The dependence looks almost

identical to the $T(t^*)$ curve for the oscillator (figure 1.2). Note that lowering of the amplitude A leads to a decrease of the t^*_{max} value and $t^*_{max} \to t^*_{min}$. However, these points never coincide, since there is no minimal pulse amplitude if the semi-infinite crack approximation is used for the analysis: even vanishingly small pulse amplitudes will result in fracture if the load duration is long enough for the load signal to arrive from distant points of the crack faces. This fact is also clear from the shape of the $K(t)$ function (figure 1.5): the stress intensity factor increases until the load ends and thus the pulse duration T can be selected to be long enough so that the fracture condition could be always met.

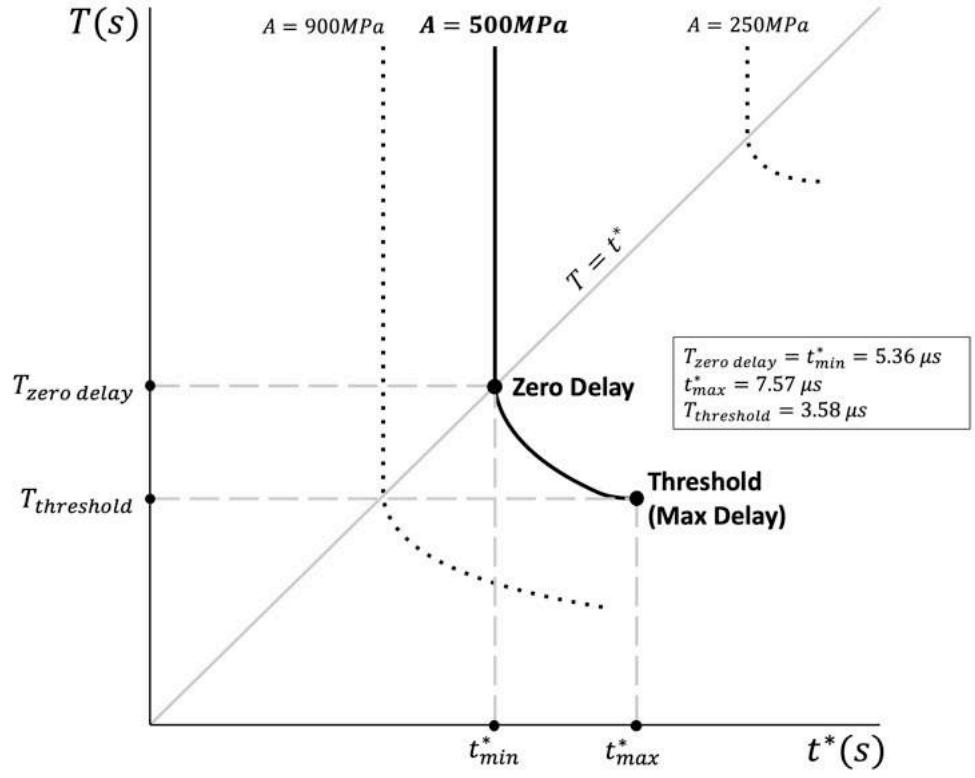

Fig. 1.6. Dependence of load duration on fracture time for 4340 steel [5] material and pulse amplitude 500 MPa.

Now, we can substitute t^*_{max} from (1.18) into (1.14) to obtain an equation that relates load pulse amplitude A and load duration T for the case of a maximal delay – a threshold case, when for a given pulse amplitude we obtain minimal admissible pulse duration causing crack movement. Another $T(A)$ relation can be built for the zero-delay (overloading case) fracture substituting $t^* = T$ into formula (1.14). Both these

dependencies have been constructed using implicit plotting tools (figure 1.7) for the 4340 steel and the threshold $T(A)$ curve is used to fit experimental points and thus to evaluate the incubation time value τ as parameter providing the best fit of the experimental data. Analogously to the oscillator model (see figure 1.3a) the crack initiation is possible for loads which belong to a zone bounded by the constructed $T(A)$ curves for zero delay and maximal delay cases. However, there is no minimal admissible pulse amplitude for the considered problem and thus, the vertical axis is an asymptote for both $T(A)$ curves, while the oscillator model provides a minimal pulse amplitude $f_c/2$. This should be expected since we consider a problem with a semi-infinite loaded crack and if the problem for a bounded sample was solved (e.g. using numerical methods to obtain the $K(t)$ function), it would be possible to calculate minimal load pulse amplitude leading to the crack onset. In figure 1.7 experimental points are taken from [5]. Note that all of them lie in a range of values that do not admit observable fracture delay – the studied load pulses are too long and the samples are obviously overloaded. In order to obtain visible fracture delay effect, much shorter pulses with higher amplitudes should be used (see grey zone between the two $T(A)$ curves in figure 1.7).

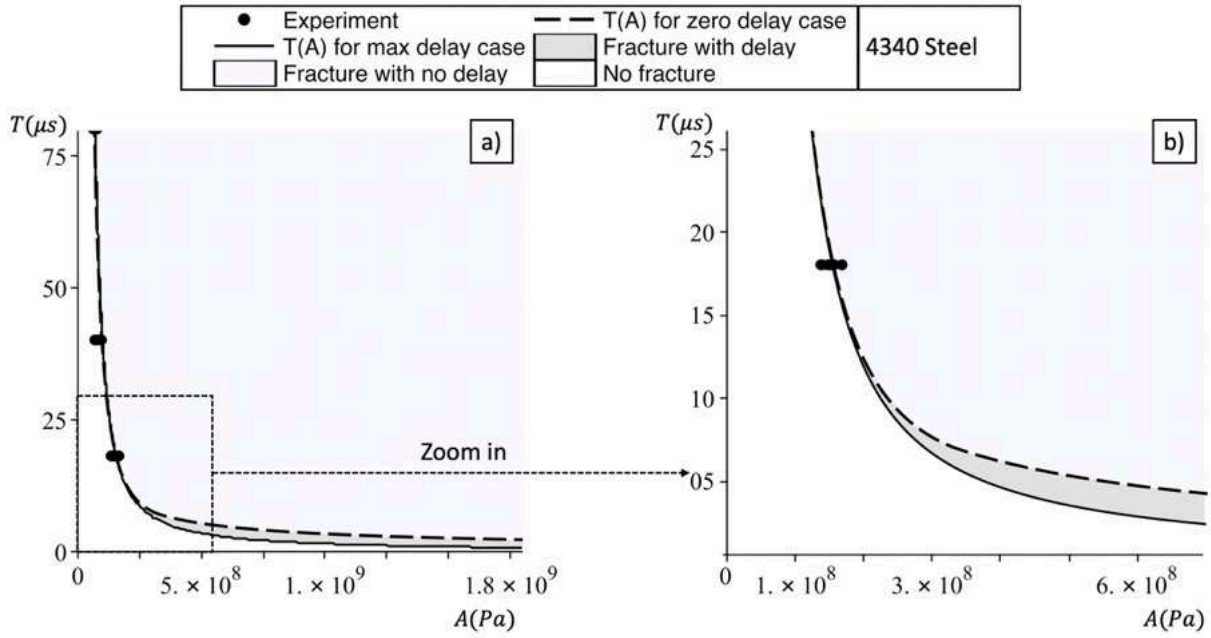

Fig. 1.7. Dependencies of loading pulse duration on pulse amplitude. Region describing pulses causing fracture marked with grey. Calculations made for experiments on 4340 steel described in [5].

Finally, we are able to calculate the load impulse $I(A) = A \cdot T(A)$ for the two studied cases (zero delay and maximum delay). These two $I(A)$ curves are shown in figure 8a and the upper curve has an obvious minimum corresponding to an optimal in terms of impulse load pulse when fracture with zero delay is considered. Note that this regime is the simplest to implement practically since the load with the optimal amplitude should be kept until the fracture occurs. This minimum can be calculated numerically for the given material (4340 steel): $\left(A_{opt}^{crack}, I_{opt}^{crack}\right) = (2.93\ MPa, 30.48\ Pa \cdot s)$.

As seen from the constructed graphs, the crack loaded with short pulses exhibits a very similar behavior to an oscillator in terms of fracture. It can be said that the fracture process (crack initiation in our case) has inertia and cannot occur instantly and thus we can associate a virtual oscillator with a particular cracked material. In this study it is impossible to calculate independently the virtual oscillator mass and stiffness since for the considered statement of the crack problem there is no minimal admissible load

pulse amplitude. However, it is possible to evaluate the eigen frequency of the virtual oscillator using expressions for the minimum of the $I(A)$ dependence for the zero-delay case.

As shown in section 1.2, this minimum for the oscillator model is calculated according to formula $\left(A_{opt}^{osc},\ I_{opt}^{osc}\right) = (0.592 f_c, 1.38 f_c/\omega)$. Thus, if we suppose that

$$\left(A_{opt}^{osc},\ I_{opt}^{osc}\right) = (0.592 f_c, 1.38 f_c/\omega) = \\ = (2.93, 30.48) = (A_{opt}^{crack},\ I_{opt}^{crack}) \quad (1.19),$$

we can calculate the eigen frequency of the virtual oscillator $\omega = 288.4\ kHz$. As it was mentioned above, in order to evaluate the virtual oscillator mass and spring stiffness, a problem with a bounded sample should be considered and minimal pulse amplitude formula would then be used as an addition to equation (1.19) providing possibility to evaluate the virtual oscillator mass and stiffness separately.

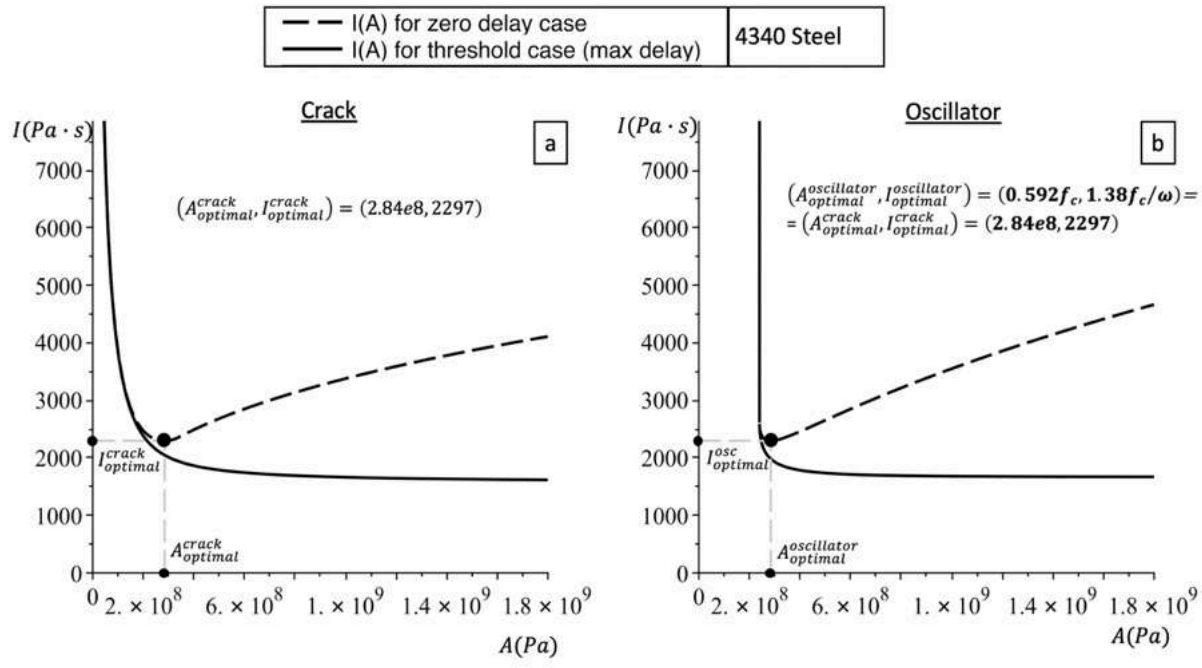

Fig. 1.8. Dependencies of load impulse on load amplitude for a crack in 4340 steel [5] and for a calibrated oscillator. Minima of the zero delay curves for the both problems are indicated.

It should be mentioned that the constructed analogy utilizes the fact that for the considered crack problem the local stress field drop starts right after the end of the loading pulse ($t = T$, see figure 1.5) and thus the whole cracked sample behaves similarly to some oscillator loaded with a rectangular tearing force.

Processing of experiments on polycarbonate from [2]

Here we will fully repeat the analysis from the previous subsection omitting all the deductions and providing final results and graphs. In [2] polycarbonate samples with penny-shaped cracks were loaded with rectangular pressure pulses with duration 2.8 μs. The authors were interested in threshold amplitudes for various diameters of the initial cracks. It is worth noticing that in this particular work authors report that fracture delay took place, however they describe this effect in slightly different terms indicating that fracture occurs at a decreasing stage of the $K(t)$ function. Despite the fact that in [2] penny-shaped cracks are discussed, we consider the above described semi-infinite crack approximation applicable since the considered pulse duration is remarkably short and the authors of [2] report the threshold pulse amplitude for relatively large cracks. The polycarbonate properties used for the calculations are listed in table 1.2.

Material property	**Value**
Critical stress intensity factor, K_{Ic} $MPa\sqrt{m}$	3.08
Longitudinal wave velocity, $c_1, m/s$	2264
Transversal wave velocity, $c_2, m/s$	1250
Incubation time, τ, s	5e-6 – from fitting of experimental points by the threshold $T(A)$ curve.

Table 1.2. Polycarbonate material properties used in the calculations

Figure 1.9 shows the $A(T)$ dependencies and the $A(T)$ for the threshold (maximal delay) case was used to calculate the incubation time value for the studied polycarbonate material. In the discussed experiments the load duration was short enough so that the fracture delay could be observed.

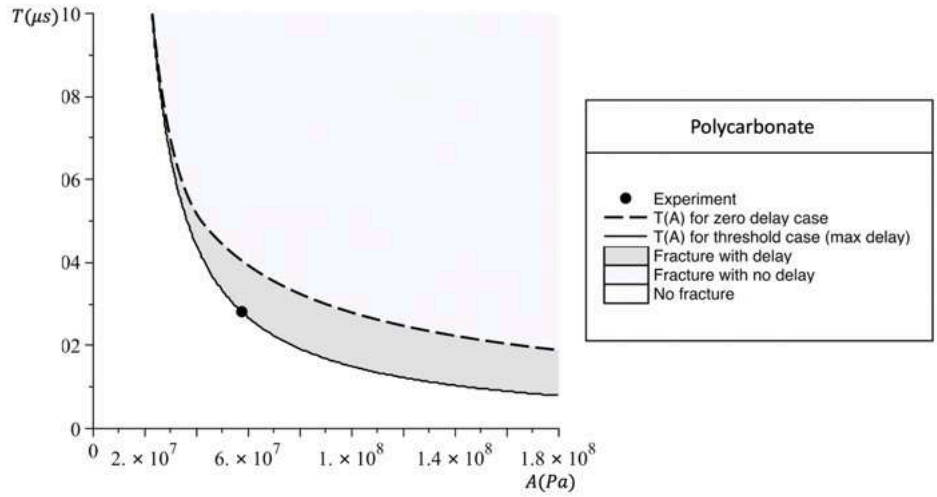

Fig. 1.9. Dependencies of loading pulse duration on pulse amplitude for polycarbonate samples [2].

The obtained $A(T)$ for polycarbonate dependencies can be used to evaluate the load impulse versus load amplitude dependencies $I(A) = A \cdot T(A)$ for both zero delay and maximal delay scenarios. These dependencies are shown in figure 1.10. Again, the zero delay $I(A)$ curve has a minimum which provides an optimal load in terms of required impulse minimization. This minimum can be used to evaluate eigen frequency of the associated virtual oscillator: $\omega = 403.8\ kHz$.

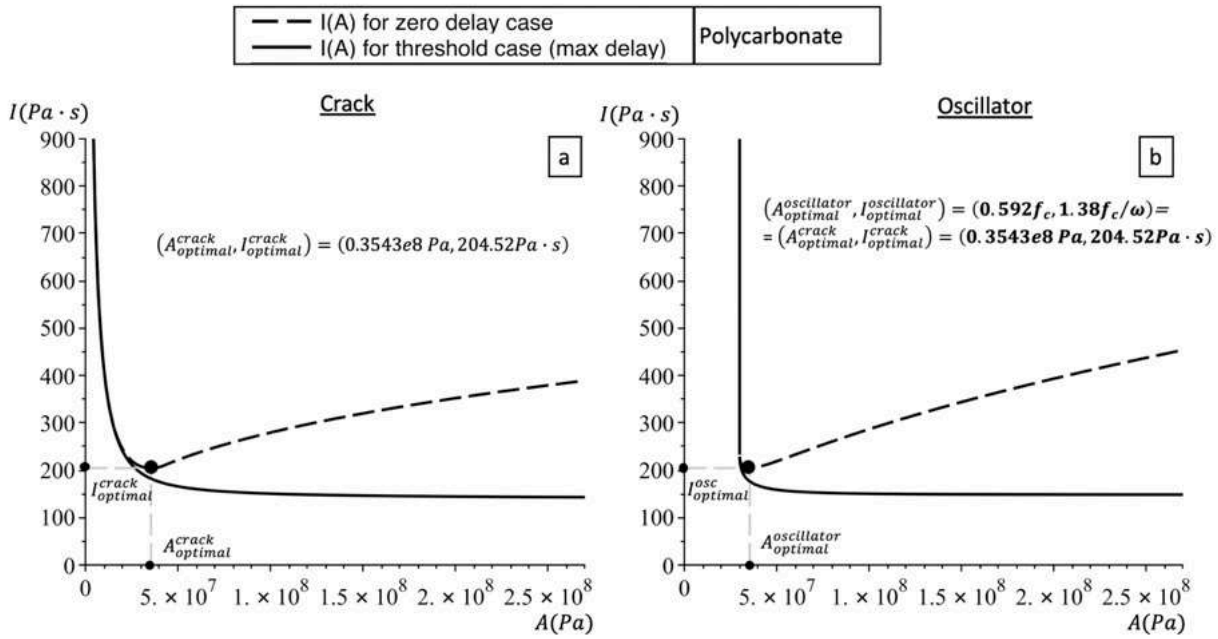

Fig. 1.10. Dependencies of load impulse on load amplitude for a crack in polycarbonate samples [2] and for a calibrated oscillator. Minima of the zero delay curves for the both problems are indicated.

1.4 Chapter 1 conclusions

The following conclusions can be driven from the conducted research. Firstly, it is shown that the incubation time model is able to predict the fracture delay phenomenon in the crack initiation problem. This phenomenon can take place when material is loaded with short pulses and fracture occurs after the local stresses passed their peak values. The widespread SIF-based models usually are unable to catch this effect, but the ITFC introduces a new material parameter, the incubation time, which accounts for preparatory microscopic processes which lead to macroscopic fracture. These processes need time to develop and thus macroscopic fracture can take place after the local stress maximum is passed. The incubation time represents a characteristic time associated with these processes and should be regarded as a material property. The ITFC can be applied in practical applications where short pulse loads are to be investigated (e.g. design of protective systems using CAD/CAE approaches).

We also show the fracture delay effect can be observed when a linear oscillator failure is considered when the system is loaded with short pulses. This lets one conclude that the fracture process can exhibit inertial features making it possible to attribute some virtual oscillator to a media with a crack. In fact, one can think of an imaginary sample with a "black box" indicating either a crack or an oscillator with appropriate parameters and load it with a stress pulse (see graphical abstract). Both variants of this sample will be almost indistinguishable if fracture is considered. This analogy opens the way for simple engineering interpretation of numerous fracture dynamics phenomena associated with brittle crack initiation and propagation processes.

In addition to this we demonstrate that there is an optimal (in terms of the load impulse) loading regime which leads to fracture – threshold pulses (lower curves in figures 1.8, 1.10) provide minimal load impulse. This way, if fracture is favorable (e.g. in rock grinding), the best strategy is to load the system with a properly calculated short load which ends before the system fails. However, even if one loads the system until it fails, there is an optimal pulse minimizing the load impulse. This optimal pulse was found for both considered systems – a linear oscillator and a crack when the system overloading case is considered. This made it possible to attribute a virtual oscillator to the crack problem which behaves in a similar manner when loaded with short pulses. For this particular problem it is impossible to calculate uniquely values of the oscillator mass and stiffness, however the eigen frequency of the virtual oscillator was provided. This limitation can be overcome if a more realistic problem with a bounded cracked sample is studied. However, we deliberately avoid discussion about mechanical value which is described by the constructed virtual oscillator, since it is a complicated and yet unsolved question. This value should probably describe the material damage, but here our goal is to show that the fracture process inertia is a natural consequence of microscopic fracture processes which precede crack initiation and which can be accounted for using the ITFC.

It can also be concluded that for the dynamic fracture studies it is essential to investigate threshold cases in which the most important time effects appear that do not fit into the classical concepts of strength and crack resistance – the concepts that rely on local ultimate stress and/or critical intensity factor parameters. In the present work these cases are described by maximum delay curves of the load characteristics dependencies (lower curves in figures 1.3,1.7,1.8,1.9,1.10). These loads provided minimal sufficient load helping to reveal fracture delay – a fundamental fracture effect. On the contrary, overloading (upper curves in figures 1.3,1.7,1.8,1.9,1.10) hides effects (fracture delay in this particular case) from the observer. These excessive loads are much easier to implement experimentally compared to the threshold loads, which appear to be optimal for fracture initiation at least in terms of the load impulse minimization. However, even generally non-optimal excessive loads appear to have optimal amplitude and duration values. The abovementioned results reveal the fundamental feature of the ITFC: it is able to operate correctly with these important threshold loads. It distinguishes the ITFC from classic quasistatic SIF based criteria and their generalized extrapolations onto dynamics.

More information can be found in [33,34,148].

Chapter 2. Fracture in a "mass-on-a-spring" system. Direct modelling of the dynamic fracture using the linear oscillator model

The second Chapter considers failure of a linear oscillator (a “mass-on-a-spring” system) and the corresponding simple engineering approach to dynamic fracture of solids. In addition to the results obtained in Chapter 1 (the effect of the fracture delay in the "mass-on-a-spring" system when loaded with short pulses of force has been investigated), the linear oscillator failure due to linearly increasing load is investigated and it is shown that the effect of increasing the strength of the system with increasing loading speed can be investigated using the linear oscillator. Thus, the inertia of the considered system makes it possible to investigate key effects of the dynamic fracture. The conducted studies have clearly demonstrated the inapplicability of standard strength models of continuous media when dynamic loads are considered. Additionally, the second Chapter presents the results of calibration of the linear oscillator model. The model has been used to describe experiments on crack initiation under dynamic loading, as well as on spallation in rods. The model shows good results, despite its simplicity and the strength of the assumptions made in course of the modeling.

2.1 Fracture in the “mass-on-a-spring” system

Here we will investigate movement and failure of a linear oscillator subjected to different load types. In all cases we will use analytical solution of the following problem:

Rectangular pulse load

Repeating some of the results of the first Chapter, we present the formulation of the fracture problem for the linear oscillator, as well as the main results obtained for the pulse loading.

Let's consider the following problem of a linear oscillator failure. The mass movement is described by a second order ordinary differential equation:

$$\begin{aligned} &m\ddot{x} + cx = f(t) \\ &x(0) = \dot{x}(0) = 0 \end{aligned} \quad (2.1),$$

where m and c are mass the spring stiffness correspondingly. We will use the critical mass deflection (x_c) fracture condition:

$$x(t) \geq x_c \Leftrightarrow \text{разрушение} \quad (2.2).$$

Condition (2.2) means that for a static case (no inertia term in (2.1)) force equaling $f_c = cx_c$ will be critical leading to the spring break.

The initial value problem (1) can be explicitly solved using Duhamel's integral:

$$x(t) = \frac{1}{m\omega}\int_0^t f(s)\sin\big(\omega(t-s)\big)\,ds \quad (2.3),$$

where $\omega = \sqrt{c/m}$ is the oscillator natural frequency. For relatively simple loading cases integration in (2.3) yields analytical formulas for the mass deflection function $x(t)$. These formulas can be used to investigate the load parameters resulting into the system failure.

Here are some results for the pulse loads from the first Chapter are presented. For example, the following formula describes the dependence of the critical pulse duration T on the fracture time t^* and amplitude A

$$T = -\frac{1}{\omega}arccos\left(\frac{f_c}{A} + cos(\omega t^*)\right) + t^* \quad (2.4).$$

Formula (2.4) can be used to demonstrate the fracture delay effect and to show that the minimal critical amplitude value equals half of the static critical force – $f_c/2$. It has been shown that parameters of the critical loading pulses (rectangular ones)

belong to some specific zone in the $(T - A)$ plane since the fracture can take place with a delay meaning that the system breaks after the load has ended. (see figure 1.3 in Chapter 1).

Linearly raising load

Multiple experimental works show that if a high-rate load is applied to a material, stresses measured at the fracture time can considerably exceed the material's static critical stress. This effect can be also seen when the oscillator failure is considered.

Let's consider the case when the loading force in (2.1) grows with a constant rate α, thus $f(t) = \alpha t$. Then, solution of the problem (2.1) according to (2.3) is the following:

$$x(t) = \frac{\alpha}{c}\left(t - \frac{1}{\omega}sin(\omega t)\right), \omega = \sqrt{c/m} \quad (2.5).$$

If the fracture time is denoted as t^*, the load force value acting at the fracture time is $f^* = \alpha t^*$. The f^* is regarded as the system strength. Then the fracture condition (2.2) can be written in two forms for convenience:

$$\omega t^* - sin(\omega t^*) = k;\ k = \frac{f_c \omega}{\alpha} \quad (2.6a)$$

$$\frac{f^*}{f_c} - 1 = \left(\frac{1}{k}\right) sin(\omega t^*) = \left(\frac{1}{k}\right) sin\left(\frac{\omega f^*}{\alpha}\right) \quad (2.6b)$$

Expressions (2.6a,b) can be used to investigate dependence of the system strength f^* on the loading rate α. As discussed above, f_c is the static critical force causing the spring break if a static problem is considered. This value is an analogue of the ultimate static stress for a brittle material. Let's consider the case when $k \ll 1$. This case refers to a dynamic fracture regime: according to (2.6a) $\omega t^* \approx sin(\omega t^*)$ and this way from (2.6b) $\frac{f^*}{f_c} - 1 \gg 1$. This can only happen if $\frac{f^*}{f_c} \gg 1$ meaning that the load at the break time t^* exceeds considerably the critical static force. In the dynamic fracture

mechanics of solid bodies this phenomenon is known as a dynamic branch of the material strength curve. If the opposite $k \gg 1$ case is considered, (2.6b) yields $\frac{f^*}{f_c} - 1 \approx 0$, since $sin(\omega t^*)$ is bounded. Thus, static fracture regime is present for this case, which is an analogue of a static branch of the strength curve. This way coefficient k (2.6a) determines the fracture regime of the system subjected to a given rising load.

Expression (2.6b) can be used to actually build the strength curve ($f^*(\alpha)$ curve) using implicit plotting. Let's consider two systems with the following parameters: ω_i and $f_{ci}, i = 1,2$. These parameters can be chosen so that system 1 is stronger than system 2 for slow loads ($f_{c1} > f_{c2}$), but for higher loading rates the situation is inverted meaning that the strength-rate curves intersect and system 2 becomes stronger than the system 1. Figure 2.1 shows such case for specially chosen parameters of the oscillators. This is a well-known phenomenon observed in experiments on real construction materials [152]. The intersection of the strength-rate curves takes place due to the fact that the system 2 starts to operate in dynamic regime earlier than the system 1: a particular load rate α corresponds to a static branch of the $f^*(\alpha)$ curve for the system 1, while activating dynamic regime for the second system. As seen from the graphs, there is a clear transitional regime with oscillations which occur due to behavior of the $x(t)$ function for particular loading rate values. For low loading rates ("static branch") the mass follows the load with almost no oscillations yielding static branch of the $f^*(\alpha)$ curve. While the loading rate increases the $x(t)$ oscillations become more pronounced and the strength curve enters the transitional oscillatory phase. For the highest α values the fracture condition (2.2) holds within the first oscillation of the $x(t)$ function generating the dynamic branch of the $f^*(\alpha)$ strength curve.

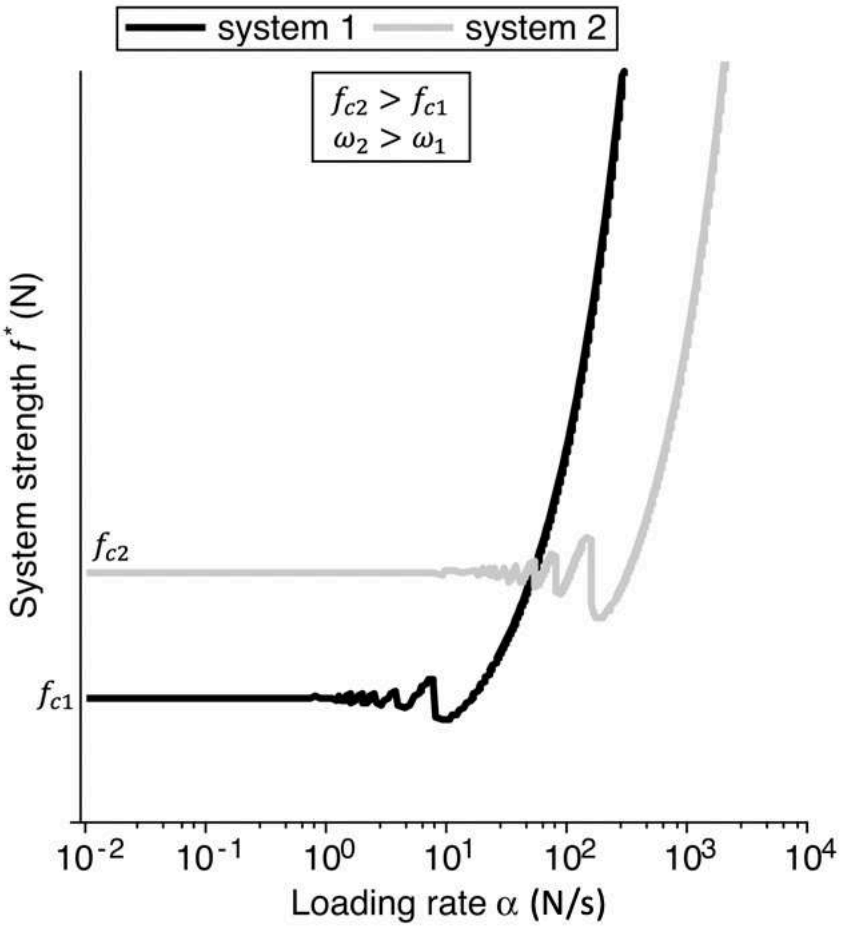

Fig. 2.1. Intersecting strength – rate curves built for the oscillators with different parameters.

2.2 Experiments on crack initiation

As it is discussed above, the linear oscillator model can reveal some fundamental dynamic fracture effects if short pulse and high-rate loads are considered. In this section the oscillator parameters (mass m, spring stiffness c and critical mass deflection) will be evaluated to model some known experimental results on dynamic fracture. Ideally the oscillator parameters will be calculated using some other problem data reducing number of adjustment parameters.

Firstly, dynamic crack initiation due to loading with various rates and due to short pulse loads will be considered and the spallation experiment will finalize this section.

Crack initiation due to dynamic loading

The general concept of the oscillator model application to the crack initiation problems is the following: the crack starts to propagate if a virtual oscillator breaks according to critical spring elongation criterion. The virtual oscillator is put in the vicinity of the crack tip and its parameters are calculated from the supposed crack elongation Δl and the material data. The oscillator load is calculated from analytical formulas for the stress field near the crack tip for the corresponding crack problem.

Consider a semi-infinite crack $x \le 0, y = 0$ which is loaded with a step function $AH(t)$, where $H(t)$ is a Heaviside function and A is the load amplitude. The load is supposed to be applied to the crack faces and the problem is set and solved in two-dimensional plain strain formulation. Full expression for the resulting stress acting on the crack trajectory $\sigma_{yy}^{AH\_faces}(x, y = 0, t) = \sigma_{yy}^{AH\_faces}(x, t)$ are provided in several works (e.g. see [65,155,156]), however this formula while being exact is complicated for further manipulations and calculations. Thus, a two-term approximation is used in this study to simplify the calculations while keeping acceptable accuracy of the stress field calculations. A procedure for the approximation evaluation is given in [154] and here the final result is used:

$$\sigma_{yy}^{AH(t)_{faces}}(x,t) = A \cdot \left(\frac{M\sqrt{t}}{\sqrt{x}} - \frac{N\sqrt{x}}{\sqrt{t}} - 1 \right) \cdot H(x - c_1 t)$$

$$M = \frac{2\sqrt{2}\sqrt{c_1}\gamma\sqrt{1-\gamma^2}}{\pi}; N = \frac{\sqrt{2}\gamma\sqrt{1-\gamma^2}(2R_1\gamma_R + \gamma_R - 2)}{\pi\gamma_R\sqrt{c_1}} \quad (2.7).$$

$$R_1 = \frac{1}{\pi}\int_{-1/\gamma}^{-1} \arctan\left(\frac{4\gamma^3 s^2\sqrt{s^2-1}\cdot\sqrt{1-\gamma^2 s^2}}{(1-2\gamma^2 s^2)^2} \right) ds$$

$$\gamma = \frac{c_2}{c_1};\ \gamma_R = \frac{c_R}{c_1}$$

In (2.7) and in the corresponding footnote c_1 and c_2 are the longitudinal and transverse wave speeds, c_R is the Rayleigh wave speed and $H(t)$ is the Heaviside step function.

Formula (2.7) is used to derive Green's function – a solution that corresponds to loading the crack faces with a Delta function $\delta(t)$:

$$\sigma_{yy}^{\delta(t)\_faces}(x,t) = G(x,t) = \frac{\partial \sigma_{yy}^{H}(x,t)}{\partial t} \cdot H(x - c_1 t) \quad (2.8),$$

which can be further applied to evaluate stress $\sigma_{yy}^{P(t)\_faces}(x,t)$ for arbitrary load $P(t)$ applied to the crack faces:

$$\sigma_{yy}^{P(t)\_faces}(x,t) = \int_0^t P(t)_{faces} \cdot G(x, t-s) ds \quad (2.9).$$

Formula (2.9) will be further used to evaluate tearing stresses for each of the considered crack initiation problems.

The oscillator model

$$m\ddot{U} + cU = f(t) \quad (2.10)$$
$$U(0) = \dot{U}(0) = 0$$
$$U \geq U_c \Leftrightarrow fracture$$

is calibrated by consecutive evaluation of parameters m, c, U_c and load $f(t)$ (figure 2.2). For each parameter the corresponding evaluation procedure and suppositions are provided.

1) Firstly, *the oscillator mass* m is defined. Two squares with a side Δl are virtually cut from a sample in the vicinity of the crack tip (see figure 3a). These squares have mass

$$m = \rho \Delta l^2 \quad (2.11).$$

and are supposed to be linked by a virtual spring with stiffness c. The spring elongation is $2U(t)$. Parameter Δl is regarded as a key fitting parameter and ideally the rest of the model parameters should be expressed in terms of Δl and other standard material data. It should be noted that higher Δl values result into larger oscillator mass which obviously increases inertia of the

2) *Applied load.* The loading force $f(t)$ applied to the mass of the virtual oscillator is calculated by integration of the analytical formula for transient stress $\sigma_{yy}^{P(t)\_faces}(x,t)$ (3.4) acting on the crack continuation

$$f(t) = \int_0^{\Delta l} \sigma_{yy}^{P(t)\_faces}(x',t)\, dx' \qquad (2.12).$$

3) *The oscillator spring stiffness c and critical mass deflection* U_c. In order to evaluate these parameters, the following supposition is made: the Irwin's fracture criterion ($K_I \geq K_{Ic}$) is applicable for the crack initiation due to static load and the oscillator model should perform correctly in the static load regime as well. Thus, the critical static force value f_c applied (in a static sense) to the virtual oscillator should result into both the mass coordinate reaching its critical value U_c and into the SIF reaching its ultimate static value K_{Ic}. This way, the f_c value can be evaluated via spatial integration of the SIF-based approximation for static stresses near the crack

$$f_c = \int_0^{\Delta l} \frac{K_{Ic}}{\sqrt{2\pi x'}}\, dx' \qquad (2.13).$$

On the other hand, it is supposed that when the critical static load is applied the crack length increases by Δl and the resulting stress intensity factor value K_I^{new} does not differ much from K_{Ic} and this way crack opening $2U_c$ corresponding to the critical static case can be calculated at a point at Δl distance counting from the new crack tip location (see figure 2.2b for clarification). The U_c value is calculated using the SIF-based approximation formulas for the displacement field and is afterwards regarded as

a critical mass deflection causing the virtual oscillator failure. Thus, the following expression is used for the U_c evaluation:

$$U_c = \frac{K_{Ic}(1+k)\sqrt{\Delta l}}{2G\sqrt{2\pi}} \qquad (2.14).$$

Expression (2.14) contains shear module $G = E/2(1+\nu)$ and parameter $k = 3-4\nu$, where E and ν are Young's module and Poisson's ratio correspondingly.

Finally, the virtual spring stiffness c is to be evaluated using the critical static force f_c and critical mass deflection U_c:

$$c = \frac{af_c}{U_c} \qquad (2.15).$$

Note that (2.15) contains an additional fitting parameter a. Ideally the whole model is calibrated using only one parameter – the zone size Δl and $a = 1$, however assumptions made for the spring stiffness calculations are rather strong and some additional fitting is to be expected. For example, the SIF value will of course drop when the crack length will increase by Δl and generally speaking selection of the Δl value defines the crack elongation at least at the initial stage, which can possibly lead to discrepancies with the experimental observations. On the other hand, it will be shown that for one of the studied problems $a = 1$ provides good results, while another problem can be processed with $a = 0.85$.

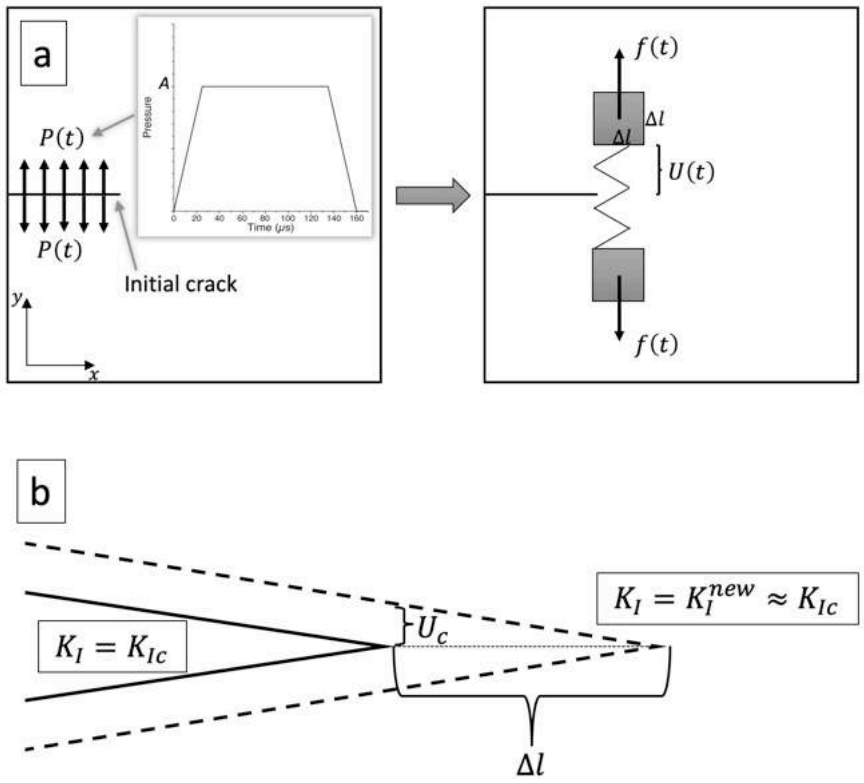

Fig. 2.2. The virtual oscillator model scheme (the load $P(t)$ is shown from work [1]) (a) and scheme for evaluation of the critical spring elongation U_c (b).

<u>High-rate loading. Experiments by Ravi-Chandar and Knauss [1]</u>

In a well-known work [1] the following experiments are reported: Homalite-100 specimens with an initial crack were loaded with trapezoid pulses applied to the crack faces. The authors varied amplitude of the loading pulse A keeping identical time of load rising (25 μs) and thus different loading rates were tested (the loading rate range was $\left[2.1e4\,\frac{MPa}{sec},\ 6.2e5\,\frac{MPa}{sec}\right]$. The starting stress intensity factor (SIF) value K_{ID} was found to be strongly dependent on the loading rate: for relatively slow load application the K_{ID} value was almost equal to the static critical SIF K_{Ic}, while for high-rate loads the starting SIF appeared to be considerably higher than the K_{Ic} value. This result is shown in figure 4 in [1], which depicts dependence of the starting SIF value on the crack initiation time $K_{ID}(t^*)$. The samples were large enough to eliminate effects related to the wave reflection from the sample edges.

For simulation of the experiments described in [1] the following loading function was used:

$$P(t)_{faces} = \begin{cases} \frac{A}{T}t, t < T \\ A, t \geq T \end{cases} \quad (2.16).$$

In (3.11) T is the load rise time and A is the load amplitude. In [1] the rise time had a fixed $T = 25\mu s$ value and thus the amplitude A variation provided different loading rates fitting into the above-mentioned range. Substitution of (2.16) into (2.9) lets us calculate the corresponding tearing stress:

$$\sigma_{yy}^{[4]}(x,t,A) = \begin{cases} 0, \ t < \frac{x}{c_1} \\ \frac{A\left(2M\sqrt{x}(c_1 t)^{3/2} - 6Nx\sqrt{x}\sqrt{t}c_1^{3/2} + 3Nxc_1^2 t - 3Mxc_1 t + 3Nx^2 c_1 + Mx^2\right)}{3c_1^{3/2}xT}, \ \frac{x}{c_1} \leq t \leq \frac{x}{c_1} + T \\ \frac{A\left(2\sqrt{x}(c_1)^{3/2}\left((Mt^{3/2} - 3Nx\sqrt{t})\sqrt{t-T} + (t-T)(MT - Mt + 4Nx)\right) - 3xT\sqrt{t-T}(M - Nc_1)\right)}{3c_1^{3/2}Tx\sqrt{t-T}}, \ \frac{x}{c_1} + T < t \end{cases} \quad (2.17).$$

Formula (2.17) is then used to evaluate force applied to the virtual oscillator using (2.12):

$$f(t,A) = \int_0^{\Delta l} \sigma_{yy}^{[1]}(x,t,A)(x',t)\,dx' \quad (2.18).$$

The used Homalite-100 material data and the calculated oscillator model parameters are collected in table 2.1.

Parameter name and units	**Value**
Young's modulus, E (Pa)	3900e6
Poisson's ratio, ν	0.35
Density, ρ (kg/m^3)	1230
Longitudinal wave velocity, c_1 (m/s)	2057
Shear wave velocity, c_2 (m/s)	1176
Rayleigh wave velocity, c_R (m/s)	1081
Ultimate stress intensity factor, K_{Ic} (MPa$\sqrt{m}$)	0.48

Zone size, Δl (m)	**0.00463**
Oscillator mass, m (kg)	0.2636
Oscillator spring stiffness, c (N/m)	2.2222e9 or 1.8888e9 (modified $\alpha = 0.85$ in (3.10)
Oscillator spring critical deformation, U_c, m	0.1172e-4

Table 2.1. Homalite-100 material data used for the oscillator model calibration and the model parameters.

Our goal is to construct the $K_{ID}(t^*)$ dependence using the described oscillator model. After parameters of the system (2.10) are evaluated, the $U(t)$ function is found numerically for each loading rate (or for each amplitude A) and fracture time t^* is evaluated from equation $U(t^*) = U_c$. The obtained t^* is substituted into the formula for the stress intensity factor for the given load [80]:

$$K_I(t) = \frac{2A\Phi\left(t^{3/2}H(t)-(t-T)^{3/2}H(t-T)\right)}{3T},\ \Phi = \frac{4c_2\sqrt{c_1^2-c_2^2}}{c_1\sqrt{\pi c_1}} \qquad (2.19)$$

Firstly, we found the Δl value which provides the best fit to experimental data using weighted least square method. The found value $\Delta l = 4.63\ mm$ appeared to be surprisingly close to the sample thickness value ($4.8\ mm$) indicated in [1]. The experimental data fitting with no additional parameters ($a = 1$ in (2.15)) is shown in figure 2.3a. The dynamic branch of the $K_{ID}(t^*)$ dependence can be obtained immediately and even the model with a standard spring stiffness value manages to capture one of the key results of the experimental study [1]: for higher load amplitudes (and thus higher loading rates the crack initiation time is smaller and the corresponding starting SIF value exceeds considerably the static ultimate SIF K_{Ic} and visa-versa: for relatively slow loading the starting SIF value equals K_{Ic}. However, the static branch (the one which is characterized by low loading rates and higher fracture times) requires lowering of the oscillator stiffness and thus the weighted least square fitting was performed for the parameter a providing $a = 0.85$ value. Results for $\Delta l = 4.63\ mm$

and $a = 0.85$ are shown in figure 2.3b. In figures 2.3a,b each point corresponds to a particular load amplitude A from (2.16) and thus to a particular loading rate.

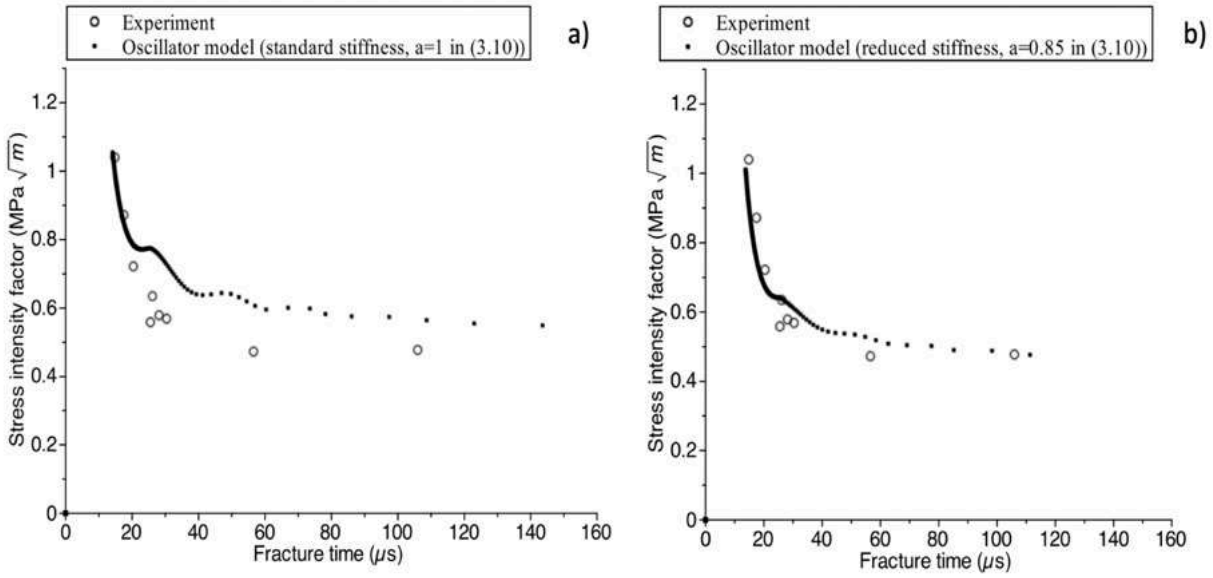

Fig. 2.3. Dependence of a starting SIF value on the fracture time: experimental points approximated by the oscillator model with standard (a) and reduced (b) stiffness.

Short pulse loading and fracture delay

In this section experiments on crack initiation in PMMA samples due to short pressure pulses applied to the crack faces are discussed. Details of experiments can be found in [4]. The pressure pulse is considered to be properly described by formula (2.20) (Figure 2.4):

$$P(t)_{faces}^{[4]} = P_0 exp\left(-\frac{2t}{T_1}\right) sin^2\left(2\pi\frac{t}{T}\right) \qquad (2.20),$$

where $T = 5.5\ \mu s$ and $T_1 \sim 4\ \mu s$. For the given T and T_1 values the applied pressure reaches its maximum value P_m at time $t_m^{load} = 1.186\ \mu s$:

$$t_m = \frac{T}{2\pi} arctan\left(\frac{2\pi T_1}{T}\right)$$
$$P_m = P(t_m)_{faces}^{[4]} \qquad (2.21).$$

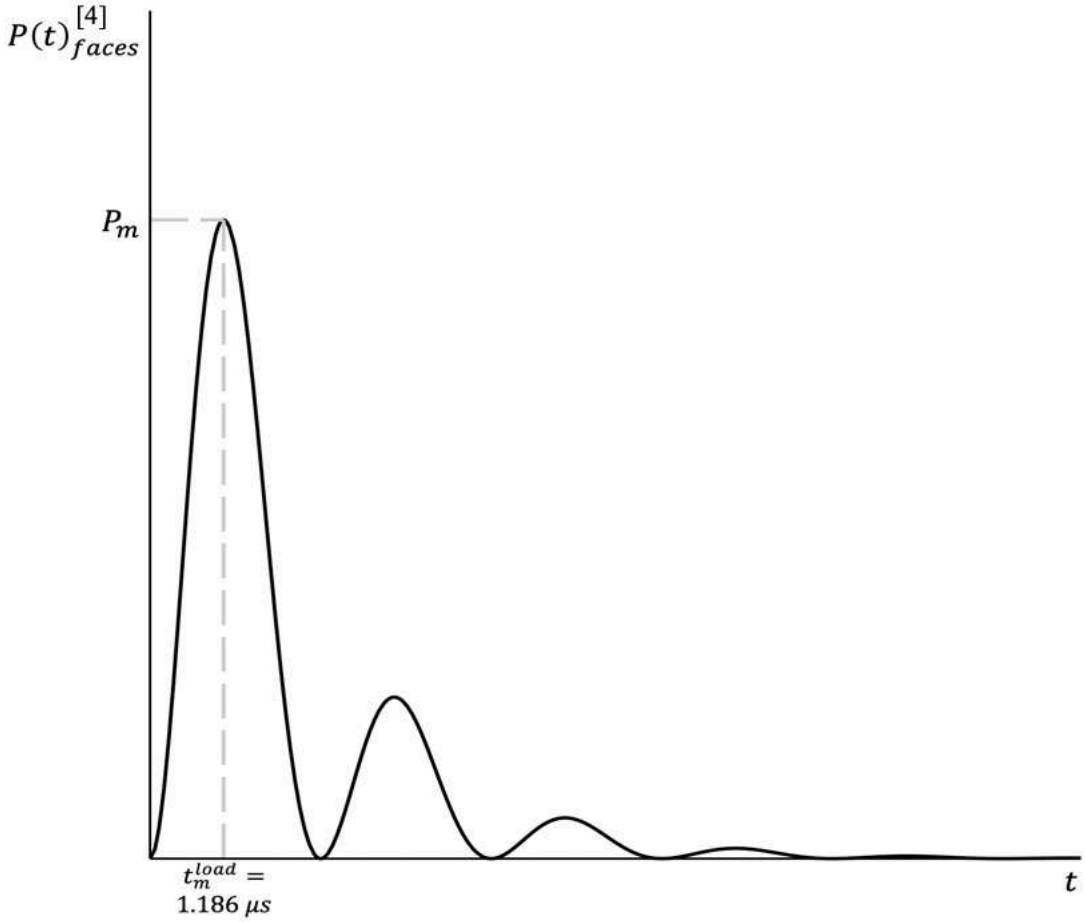

Fig. 2.4. Pressure applied to the crack faces versus time from work [4]. Load duration parameters: $T = 5.5\ \mu s$ and $T_1 = 4\ \mu s$.

The corresponding SIF formula can be evaluated using fundamental solution $K^{\delta}(t) = \alpha/2\sqrt{t}\,, \alpha = 4c_2\sqrt{c_1^2 - c_2^2}/c_1\sqrt{\pi c_1}$ for the $P(t) = \delta(t)$:

$$K(t) = \frac{\alpha}{2}\int_0^t \sqrt{s}\, P(t-s)_{faces}^{[4]} ds \qquad (2.22).$$

According to numerical calculations using (2.22) the $K(t)$ function reaches its maximum at point $t_m^K = 1.675\ \mu s$. Thus, it is clear from the provided experimental data that the crack onset takes place far after the local stress field (characterized by $K(t)$) and the load reach their maxima and this way, the fracture delay is observed.

The virtual oscillator model is applied here in a similar to the previous section way: a square with size Δl is virtually cut in the vicinity of the crack forming the virtual

oscillator mass according to (2.11). The rest of the virtual oscillator parameters and the loading force are calculated according to formulas (2.11)-(2.15). Note, that the load function (2.20) has a much more complicated expression and thus no analytical formulas for stress acting on the crack continuation are available. In this case we select the Δl parameter to be almost equal to the sample thickness – 9.7 mm (the actual sample thickness in [4] was 10 mm). This value provides good fit to the experimental points. In work [4] the load amplitude P_m is reported to vary in a 140 – 320 MPa range and for each amplitude value fracture time is found.

We studied two loading regimes applying the virtual oscillator model:

1) The first regime corresponds to the loading used in [4]: load amplitude P_m is varied in a 72 – 320 MPa range and the load time characteristics are fixed $T = 5.5\ \mu s$ and $T_1 = 4\ \mu s$. Note, that in [4] the load was in a 140 – 320 MPa range and 72 MPa was evaluated as a threshold value for $T = 5.5\ \mu s$ and $T_1 = 4\ \mu s$ time parameters.

2) In the second regime the load duration is stretched while the amplitude is kept to be of a threshold type: T and T_1 are proportionally ($T_1 = T/1.375$) increased and for each T value minimal load amplitude P_m which causes failure is found (see figure 2.5 for clarification of threshold/non-threshold (overloaded) fracture regimes). When $T \to \infty$ the threshold P_m value is expected to tend to P_m^{static} – a critical static pressure which causes the crack instability according to Irwin's condition $K_I = K_{Ic}$.

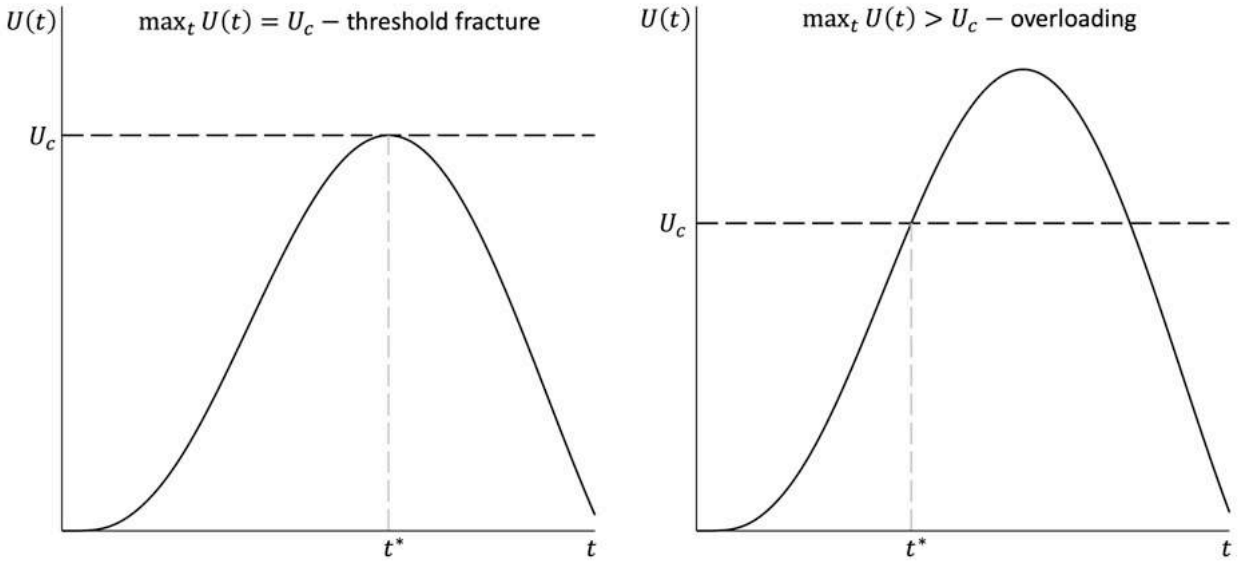

Fig. 2.5. Fracture of a threshold (left) and above-threshold (right) types.

The modelling results within the first loading regime are shown in figure 2.6a. Note that lower fracture times (and higher load amplitudes) are well-described by the oscillator model, however discrepancy is found for the P_m values which are close to lower bound of the studied range. On the other hand, the oscillator model is able to catch the fracture delay effect: fracture takes place after load and local stress field (expressed both in terms of SIF $K(t)$ and force applied to the virtual mass $f(t)$) have passed their maxima. Normalized $K(t)$ and $f(t)$ functions for $T = 5.5\ \mu s$ are plotted in figure 2.6b with indicated maxima points. Material parameters and corresponding oscillator parameters are shown in table 2.2.

Parameter name and units	**Value**
Young's modulus, E (Pa)	3300e6
Poisson's ratio, ν	0.35
Density, ρ (kg/m^3)	1230
Longitudinal wave velocity, c_1 (m/s)	2057
Shear wave velocity, c_2 (m/s)	1176
Rayleigh wave velocity, c_R (m/s)	967
Ultimate stress intensity factor, K_{Ic} (MPa$\sqrt{m}$)	1.47
Zone size, Δl (m)	**0.0097**

Oscillator mass, m (kg)	0.1157
Oscillator spring stiffness, c (N/m)	1.8803e9
Oscillator spring critical deformation, U_c, m	0.6143e-4

Table 2.2. PMMA material data used for the oscillator model calibration and the model parameters.

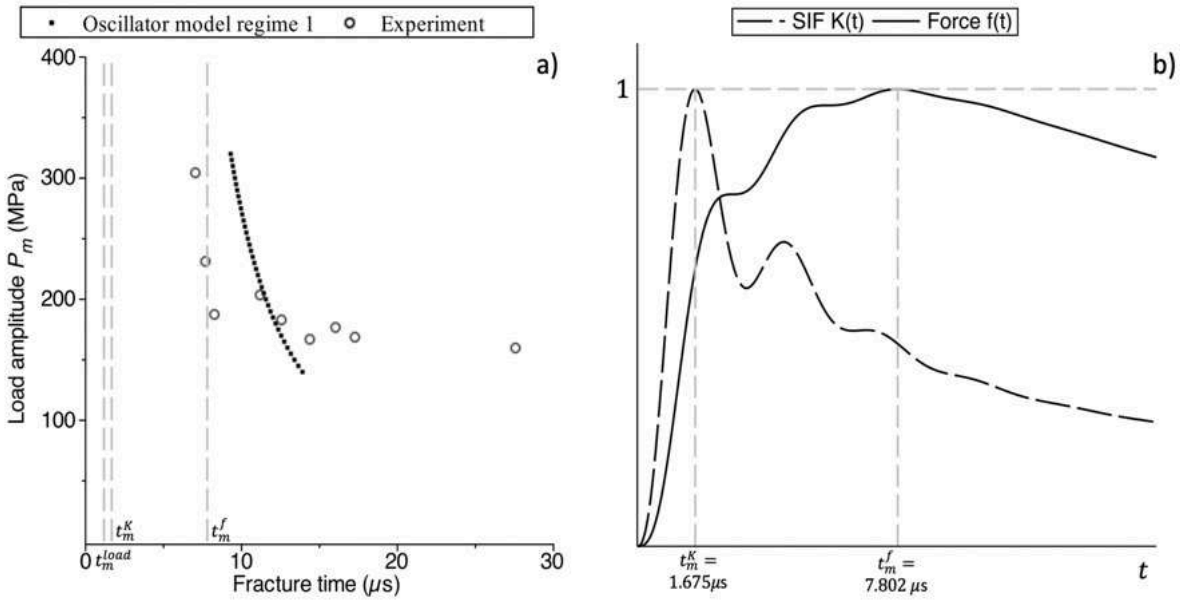

Fig. 2.6 (a): Dependence of the load function maximum on the fracture time for the loads from experimental work [4]. The maximum points of the force function t_m^f and the SIF function t_m^K for $T = 5.5\ \mu s$ and $T_1 = 4\ \mu s$ are indicated on (a) and (b) showing the fracture delay effect taking place both experimentally and according the virtual oscillator model. In (b) functions are normalized.

When second loading regime is studied and the P_m values are further decreased and the fracture times increase accordingly. The value $P_m = 72.9\ MPa$ was found to be threshold for $T = 5.5\ \mu s$ and $T_1 = 4\ \mu s$. Further increase of the load duration and thus drop of the P_m values provide transition to static strength of the system. The modelling results for the two regimes are collected in figure 2.7. The figure also shows a purely static P_m^{static} value which was calculated using finite element method. It is worth noticing that the experimental points appear to belong to dynamic fracture

regime according to the proposed approach and the static branch of the $P_m - t^*$ curve is a prediction.

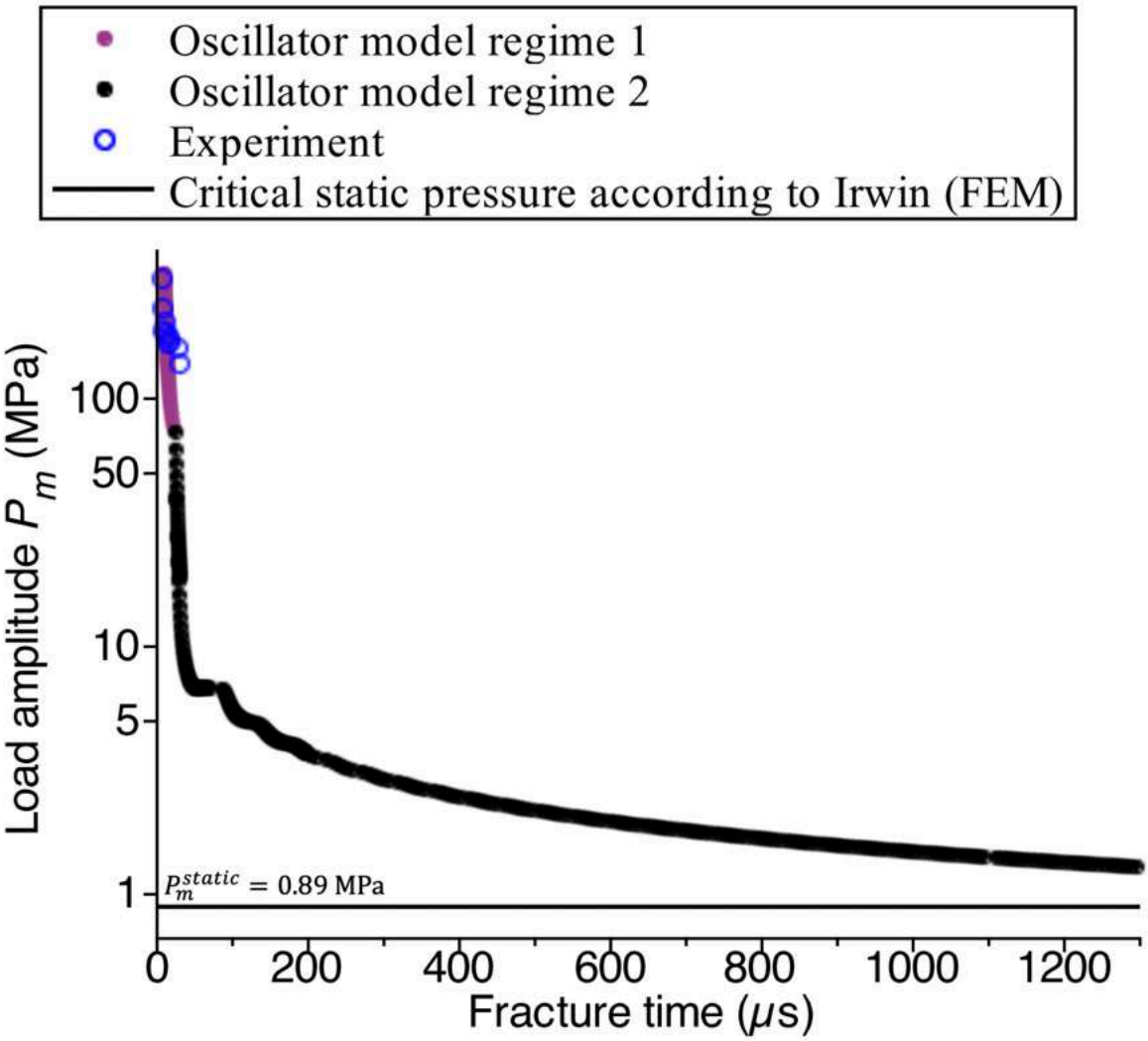

Fig. 2.7. All load regimes combined. Note that for the 1st regime the load duration is not altered – $T = 5.5\ \mu s$ and $T_1 = 4\ \mu s$. In the 2nd regime the load duration is increased while the P_m value is kept minimal for the fracture to occur (threshold value). Note a smooth transition from a dynamic fracture regime to the static strength.

In order to calculate critical static pressure P_m^{static} leading to fracture according to criterion $K_I = K_{Ic}$ when applied to the crack faces, finite element calculations were performed using ANSYS software. A symmetry condition was used (only top half of

the specimen was simulated) and a uniform rectangular mesh was used after appropriate mesh sensitivity studies. The stress intensity factor value was calculated using J-integral. In figure 2.8 one can see the meshed sample with loads and boundary conditions together with the solution – a σ_{yy} stress field. The $P_m^{static} = 0.89\ MPa$ value triggers the static fracture condition as for this load $K_I = 1.47\ MPa\sqrt{m}$. This P_m^{static} value is used in figure 2.7.

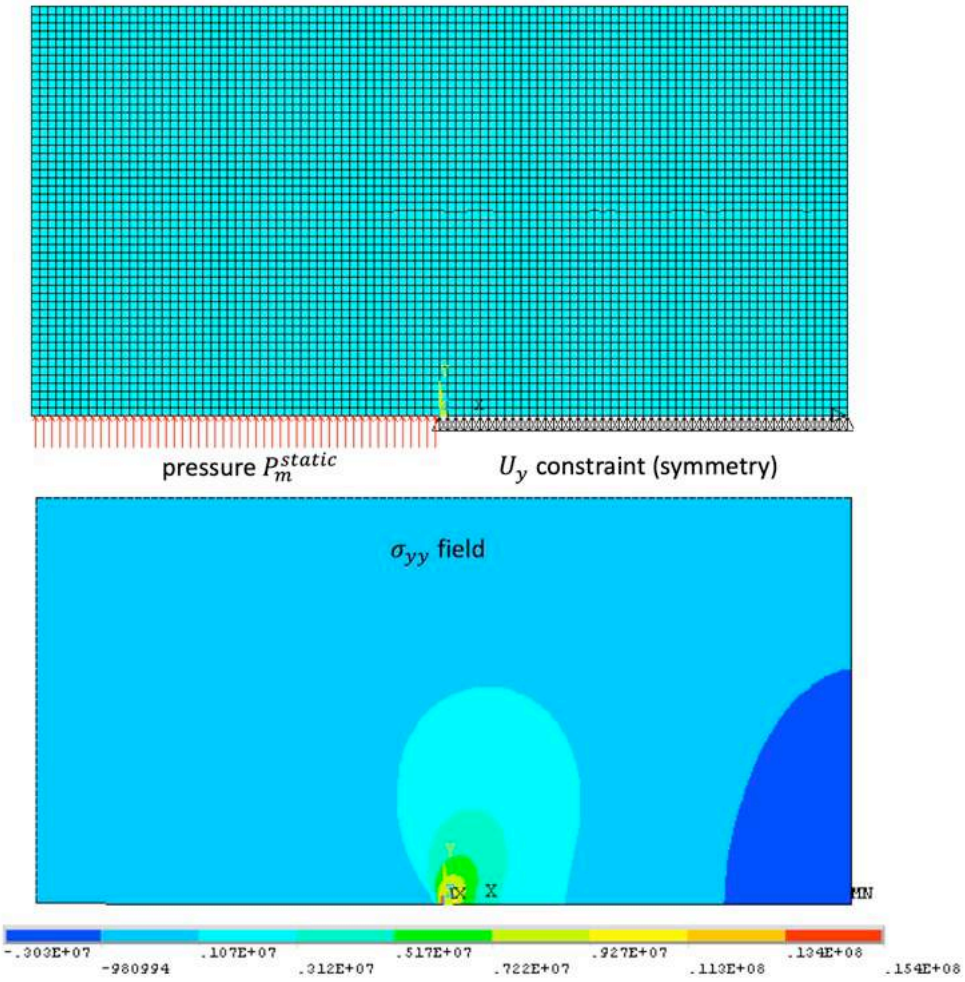

Fig. 2.8. Details and results of FEM simulations used to calculate critical static pressure P_m^{static} for a problem from [4].

Let's briefly summarize the section writing out key points:

- Experiments on crack initiation due to intensive load applied to crack faces are studied using the virtual oscillator approach.

- A rectangular zone is cut in the vicinity of the crack tip forming the oscillator mass. The oscillator spring stiffness is defined in order to make the model applicable in static and quasistatic loading conditions. The zone size is a fitting parameter.

- The loading force is evaluated from analytic solutions for the corresponding elasticity problems.

- If the zone size is selected to be equal to the sample thickness, the experimental points are fit surprisingly well.

- The oscillator model is able to describe (at least qualitatively) key dynamic fracture effects observed in the studied experiments on cracks: strength dependence on loading rate [1] and fracture delay [4].

2.3 Experiments on spallation in rods by Mikhailova et al. [3]

In this section the oscillator model will be calibrated to theoretically describe experimental data on the material strength and dynamic fracture from spallation tests. We will work with the results from work [3], where steel samples were used. The essence of the spallation test is the following: the sample is hit by a projectile which generates a compressive wave travelling through the sample; the compressive wave reflects from the sample free boundary and converts to a tensile stress wave which causes fracture. The stress profile can be measured using the free surface velocity detection with consequent processing. The loading rate can be altered through the projectile length and velocity variation. As a result, material strength – stress rate dependence can be experimentally constructed (figure 10 in [3]). Moreover, results of the work [3] are particularly interesting since fracture delay was observed: in some experiments spallation was registered at the decrease stage of the tensile stress (figure 4b in [3]).

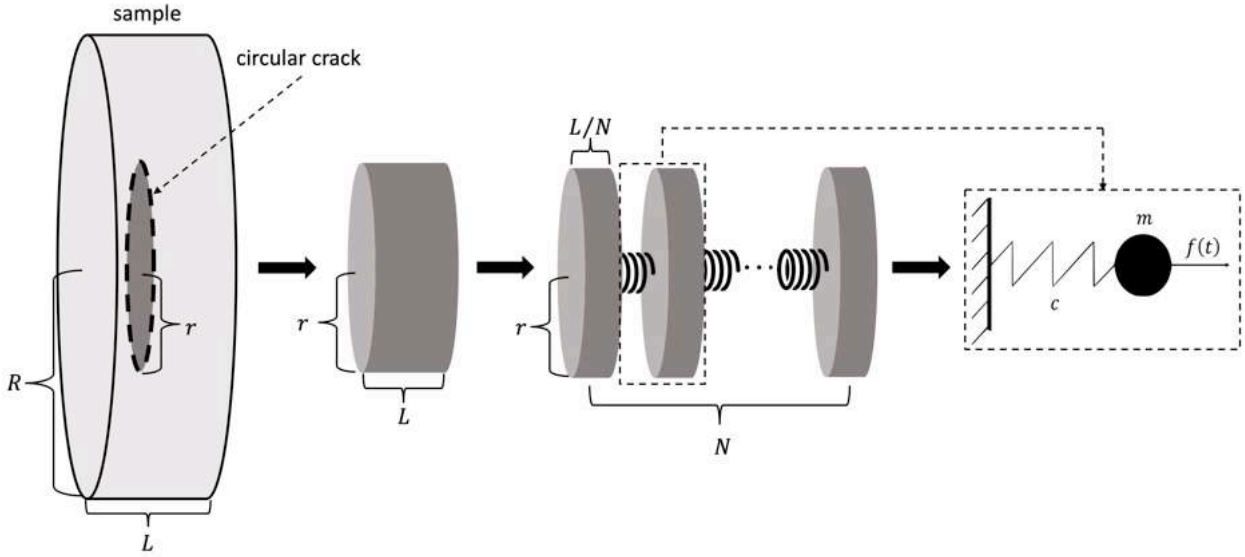

Fig. 2.9. Reduction of spallation problem to an oscillator failure problem.

Here we again try to reduce the rod spallation problem to a failure of an oscillator described by (2.10). The procedure consists of the following steps (the steps are schematically shown in figure 2.9):

1) The sample is substituted by a rod with radius of an experimentally observed crack r and length L which equals the tested sample thickness.

2) The rod is then sliced into N pieces connected by $N-1$ springs. Summation of all masses yields the initial rod mass:

$m_{rod} = \rho SL = Nm,\ S = \pi r^2 -$ the rod cross section area (2.23)

3) The following considerations are made to calculate the single spring stiffness c. Suppose we fix one end of the rod and apply force f to its free end. Since we suppose that the rod deformation ε follows Hooke's law $\varepsilon = \sigma/E$ ($\sigma = f/S -$ stress in the rod and $E -$ Young's modulus), the displacement of the free end U can be calculated according to formula

$$U = L\frac{\sigma}{E} = \frac{L}{SE}f = \frac{f}{c_{rod}} \quad (2.24),$$

which can be used to evaluate the rod stiffness c_{rod} which in its turn equals the total stiffness of the oscillator chain. Finally, the stiffness of a singular spring c is calculated according to formula

$$c = c_{rod}(N-1) = \frac{SE}{L}(N-1) \quad (2.25).$$

4) Analogously to 3) we calculate critical mass deflection U_c using critical stress σ_c of the studied steel:

$$U_c = \frac{\sigma_c L}{E(N-1)} \quad (2.26).$$

Next, we will show that a proper choice of the N value lets one obtain experimentally observed dependence of the material strength on stress rate and even an experimentally observed fracture delay effect. The used parameters are listed in table 2.3.

Parameter name and units	**Value**
Young's modulus, E (Pa)	200e9
Density, ρ (kg/m^3)	7850
Sample length, L (m)	0.0091
Oscillator mass, m (kg)	0.033
Oscillator spring stiffness, c (N/m)	6.11e10
Oscillator spring critical deformation, U_c, m	0.1046e-4

Table 2.3. Material data used for the model calibration.

We will operate with the experimental data for the 6th specimen presented in [3]. As seen from figure 4b in [3], fracture occurs after the peak of the stress pulse. If one uses $N = 3$ value and if the oscillator is loaded by force $f(t) = \sigma(t)S$, where $\sigma(t)$ is the stress profile taken for the 6th specimen from figure 4b from [3], the oscillator fails at time $t^*_{oscilator} = 3.2\ \mu s$ which exceeds the stress function maximum point as does the experimentally observed fracture time ($t^*_{experiment} = 3.13\ \mu s$) and thus fracture

delay effect is qualitatively predicted (figure 2.10a). The $N = 3$ value also let us adequately describe the strength – rate curve (figure 2.10b), however $N = 5$ provides a better fit, but in this case fracture delay is not predicted by the oscillator model – the oscillator failure takes place before the stress reaches its maximum value.

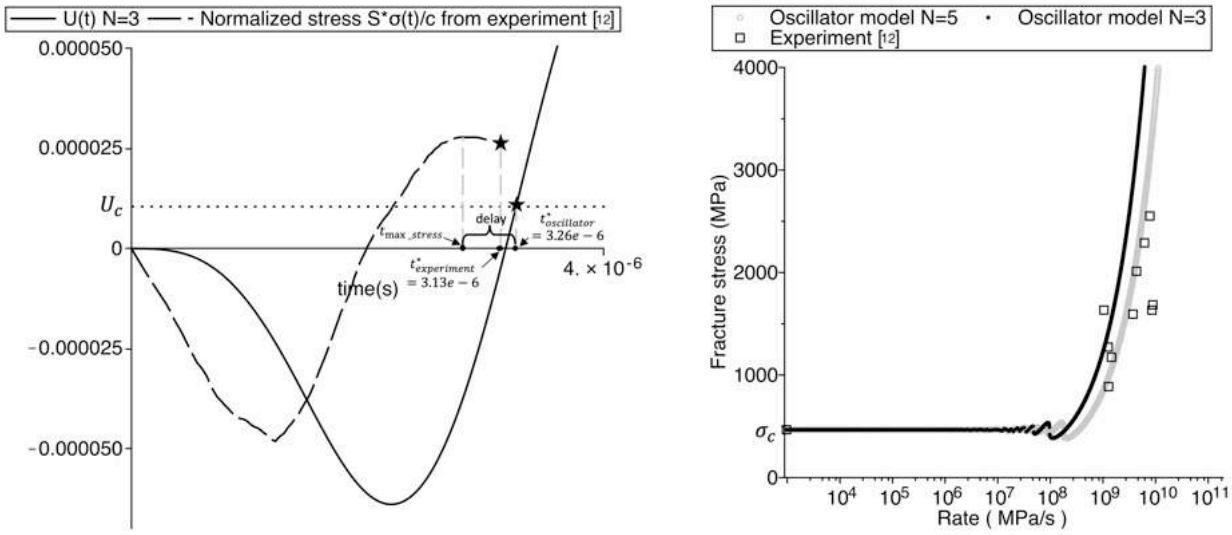

Fig. 2.10. Fracture delay predicted by the oscillator model (left) and strength-stress rate dependence built using the oscillator model for two N values (right).

The strength-stress rate curve in figure 2.10 was constructed using linear loading force applied to the oscillator mass $f(t) = RSt$, where R is rate and S is the rod cross section area. It should be noted that in fact the results do not depend on parameter r – the circular crack radius and thus the cross-section area S is excluded from the calculations. The oscillator mass and stiffness contain S as a multiplier analogously to the load $f(t)$ and thus both sides of differential equation (2.10) can be divided by S. The critical spring deflection U_c (2.26) does not depend on S either. This way, N is the only fitting parameter in the presented case.

Thus, the oscillator model was calibrated using experimental data on spallation providing good fit to strength-rate experimental points and even managing to capture the fracture delay effect reported in work [3].

2.4 Analysis of the obtained results

Chapter 2 shows that the oscillator model can be calibrated to address some complicated dynamic fracture phenomena arising in complex dynamic tests despite being the simplest possible dynamic system with inertia. The oscillator parameters were evaluated from material properties, static strength considerations and some physically motivated values, such as sample thickness. This approach worked surprisingly well requiring small extra adjustments only in one of the considered crack problems. However, we consider the studied examples to serve mostly demonstrational and educational goals as the simulation success based on the described approach might be a pure coincidence. The biggest problem of the demonstrated oscillator model is its crudeness – in fact, extraction of some physical volume with relatively big dimensions is a very rough averaging and simplification. If one would like to build a lattice model of a solid in order to study the dynamic fracture relying on the mases' inertia, the mesh can appear to be unacceptably coarse. For example, in the studied crack problems there would be just one layer of elements throughout the specimen thickness. The other way to apply the proposed model for the engineering purposes is to avoid physical meaning of the oscillator mass and to treat the model as a standard fracture condition. For example, if some problem is solved using dynamic finite element method, the element can be deleted from the mesh if some virtual oscillator breaks due to stresses acting on an area inside this element. Here the oscillator parameters, especially its mass, might serve as purely fitting parameters lacking adequate mechanical and physical meaning.

On the other hand, it is useful to show that some inertia can be attributed to the dynamic fracture process which helps to understand dynamic fracture effects such as strength increase for high loading rates or the fracture delay. The oscillator model shows that these effects are to be expected when short and/or high-rate loads are applied to the system. Moreover, the discussed model does not contain any first order time derivatives and thus, no explicit rate sensitivity terms are involved – all the effects are observed in a purely elastic system and are due to the model inertia.

It is also worth noticing that in Chapter 1 and in work [148] a purely virtual oscillator was attributed to the dynamic fracture process and the oscillator was defined with accuracy to the eigen frequency. Here a more straightforward approach was used as material volume was cut from the sample forming the oscillator mass. In both cases some frequency ω was introduced bringing characteristic time into the system – the natural oscillation period $T = 2\pi/\omega$. As shown in section 2.1 (figure 2.1), the oscillator static strength $f_c = cx_c$ and its eigen frequency ω (or period $T = 2\pi/\omega$) define completely the dynamic strength curve. This is very reminiscent of the incubation time fracture criterion (ITFC) used to analyze dynamic fracture, where a characteristic relaxation time called the incubation time τ is introduced to account for microscopic fracture events (e.g. development of micro cracks, coalescence of pores etc.) which precede and cause the macroscopic fracture. According to the simplest implementation of the incubation time approach, fracture at time t^* takes place if

$$\frac{1}{\tau}\int_{t^*-\tau}^{t^*}\sigma(t')dt' \geq \sigma_c \qquad (2.27),$$

where σ_c is the static material strength. It can be shown that the parameter couple (τ, σ_c) completely defines the strength stress rate curve. If rising stress profile is considered ($\sigma(t) = rt$ with r being stress rate), fracture stress $\sigma^* = rt^*$ can be evaluated in terms of the loading rate r after $\sigma(t) = rt$ is substituted into criterion (2.27):

$$\sigma^* = \sigma_c + \frac{\tau r}{2} \qquad (2.28).$$

If we consider two model materials characterized by couples of parameters (τ_1, σ_{c1}) and (τ_2, σ_{c2}), where $\tau_1 > \tau_2$ and $\sigma_{c1} < \sigma_{c2}$, the corresponding material – stress rate curves will intersect, meaning that material 2 is stronger in in static loading conditions, but for high loading rates material 1 exhibits higher strength – see figure 2.11.

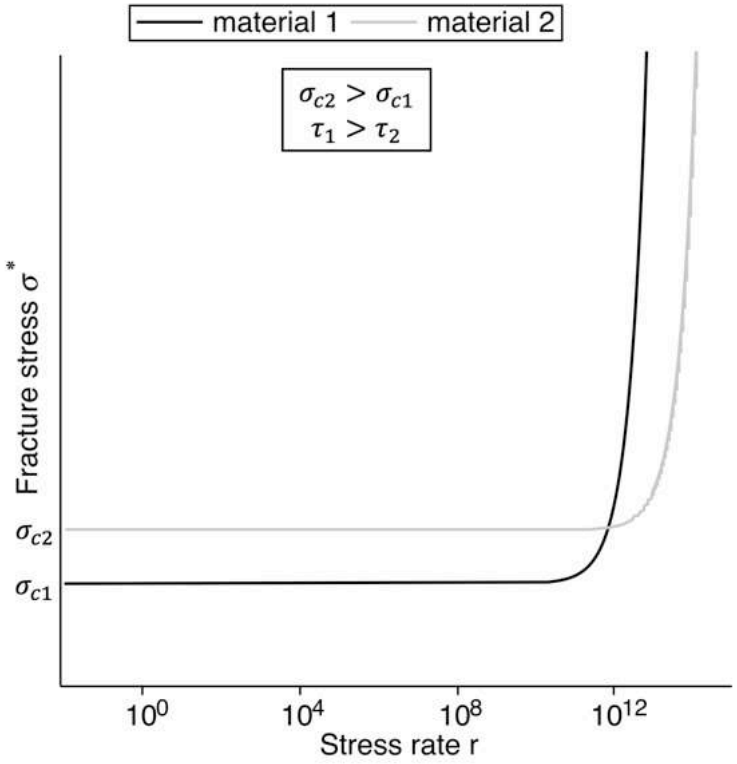

Fig. 2.11. Strength – rate curves built using incubation time fracture model.

According to the ITFC for relatively low stress rates ("static branch" of the strength-rate curve) the material strength is controlled by static ultimate stress σ_c. The material performance for higher rates is defined by the incubation time value – the "dynamic branch" is shifted left for higher τ values and vice versa. This is a complete analogy to the oscillator failure for different loading rated discussed in section 2.1 of this Chapter. For low rates the system's strength is obviously defined by the spring static strength – critical force f_c and the system's dynamic strength is controlled by the eigen frequency of the oscillator $\omega = \sqrt{c/m}$: lower ω (and thus higher natural period $T = 2\pi/\omega$) shifts the "dynamic branch" of the strength curve to the left and vice versa. The discussed spring model cannot be considered as an alternative to the ITFC which has been proven to be a robust tool for the dynamic phenomena investigation. See also work [157] for similar approach to the ITFC. The spring model can be rather regarded as a simplified illustration of the ITFC operation. However, the demonstrated results may be interesting for researchers working with elastic lattice method providing some

insight into possible element size, though, as discussed above, it might appear to be unacceptably big.

2.5 Chapter 2 conclusions

The second Chapter of the thesis discusses failure of the linear oscillator subjected to short and high rate loads and corresponding dynamic fracture effects were investigated. A simple fracture condition was applied – when the oscillator mass deflection reaches some critical value, the system fails. Firstly, it was shown that two modes of the oscillator failure can be observed when the system is loaded with relatively short force pulses: the oscillator can break with a delay (the failure takes place after the load finished) and without a delay – the failure takes place before the loading pulse termination. The latter situation means that the system was overloaded and lower amplitudes pulse amplitudes can be used to cause the oscillator failure. For both failure regimes lower load pulse durations expectedly require higher amplitudes in order to cause the system failure. If rectangular load pulses are considered, a minimal pulse amplitude sufficient for the system failure exists: the pulse amplitude must equal at least half of the static critical force. Secondly, loads with different rates were studied. It was shown that higher load rates result in higher force values acting at the fracture time and two branches of the fracture force – loading rate curve (or strength – rate curve) are clearly demonstrated – a static branch where the fracture force value equals static strength of the oscillator spring and a dynamic branch with higher fracture force values for higher loading rates. In addition to this it was shown that higher static strength of the system does not necessarily mean its superior performance for high loading rates – the strength – rate curves may intersect. This result is analogous to behavior of real brittle materials when high loading rates are explored. Moreover, it can be shown that the oscillator failure is indeed very similar to dynamic fracture of real materials subjected to high rate loads and the oscillator model exhibits features which are similar to the incubation time fracture criterion (ITFC): according to both models the strength – rate curve shape is controlled by static strength and some

characteristic time – the incubation time for the ITFC and a natural oscillation period in case of the oscillator.

This way, it has been shown that inertia of the mass of an oscillator provides possibility to investigate two key effects of dynamic fracture: the system strength dependence on the loading rate and fracture delay.

Next, three sets of experimental results have been processed using the calibrated oscillator model. It was shown that even such simple model yields surprisingly good fit of experimental data requiring little or no extra fitting. The obtained results serve demonstrational and educational purposes: key dynamic fracture effects observed in multiple experiments are shown to be very natural and easy to understand since they can be observed in the simplest possible dynamic system – a “mass on a linear spring” model.

More information can be found in [33,34].

Chapter 3. Features of dynamic fracture processes observed in periodic structures

The third Chapter examines fracture of a chain of identical linear oscillators. The considered system consists of an arbitrary finite number of links. The first mass of the chain is supposed to be motionless. The following problem is studied: at the initial moment of time the chain is uniformly stretched, further it performs free oscillations due to a sudden release – a relaxation wave propagates through the chain. The problem is solved analytically – the motion equation for the masses of are obtained. The study of the obtained solution made it possible to identify the dynamic fracture effect, which is associated with the discrete structure of the system: the relaxation wave propagating through the chain is distorted, and the deformation of some links can exceed the critical value even under non-destructive initial static loading (the initial deformation of the links is supposed to be subcritical). The obtained solutions for the chain of oscillators are compared with the solution of a similar continuum problem – the problem of an elastic rod unloading. The work demonstrates that the effect observed in a chain of oscillators cannot be detected in a one-dimensional rod. In addition to this, calculations using the finite element method have been carried out, confirming the hypothesis about the possibility of secondary fracture following the rupture of one of the components of the preloaded periodic structure.

3.1 Statement of the problem for a single oscillator

This subsection repeats the formulation of the problem of a single oscillator fracture, discussed in previous Chapters, however it contains a procedure for transition to dimensionless coordinates, which plays an important role in the analysis of oscillations and fracture of a chain with an arbitrary number of links. Let’s consider an oscillator with free vibrations described by the equation

$$m\ddot{x} + cx = 0 \quad (3.1).$$

In (3.1) m – is the oscillating mass and c – is the spring stiffness. Let's consider the following condition for the system integrity

$$x \leq x_{crit} \quad (3.2)$$

Linear variable change $T = t\sqrt{c/m}$ provides an equation with dimensionless parameters with differentiation with respect to T:

$$\ddot{x} + x = 0 \quad (3.3)$$

Let's perform another variable change $q = x/x_{crit}$. Transition to a new variable will allow one to rewrite the equation and integrity condition in the following form:

$$\ddot{q} + q = 0, \quad q \leq 1 \quad (3.4).$$

From the same point of view, consider a chain of n connected oscillators with one free end and one fixed end (the chain is uniformly stretched). The chain integrity is the main focus of the study. Let's assume that the oscillating masses and springs are identical and equal m, c respectively. At the initial moment of time, the chain integrity condition is supposed to be satisfied.

3.2 System of two oscillators

Let's consider a system consisting of two links. Let's introduce generalized coordinates q_1, q_2that describe the displacement of masses from the equilibrium position in the absence of load. The movement of masses is described by a system of linear differential equations of the second order

$$A\ddot{Q} + CQ = 0 \quad (3.5),$$

where

$$A = \begin{pmatrix} m & 0 \\ 0 & m \end{pmatrix}, C = \begin{pmatrix} 2c & -c \\ -c & c \end{pmatrix}, Q = \begin{pmatrix} q_1 \\ q_2 \end{pmatrix} \quad (3.6).$$

Differentiation is with respect to time t. The link fails if its deformation exceeds a certain critical value, and, accordingly, the condition for the integrity of the system for the chain has the following form:

$$\begin{cases} q_2 - q_1 \le l_{crit} \\ q_1 - q_0 \le l_{crit} \end{cases} \quad (3.7).$$

Here $q_0 = 0$, meaning that the edge of the chain is fixed, the mass with the zero number is motionless, l_{crit} – the critical distance between the masses. We will assume that at the initial moment of time the chain is uniformly deformed, and the relative deformation of each link is equals to l_{crit}. This way, the initial conditions take the following form:

$$\begin{cases} q_2(t=0) - q_2(t=0) = l_{crit} \\ q_1(t=0) = l_{crit} \\ \dot{q_1}(t=0) = 0 \\ \dot{q_2}(t=0) = 0 \end{cases} \quad (3.8).$$

By a variable change $T = t\sqrt{c/m}$ the system of equations with dimensionless parameters is obtained. As a result, the matrices are transformed:

$$A = \begin{pmatrix} 1 & 0 \\ 0 & 1 \end{pmatrix}, C = \begin{pmatrix} 2 & -1 \\ -1 & 1 \end{pmatrix} \quad (3.9).$$

Let's move on to new generalized coordinates $l_1 = q_1 - q_0$, $l_2 = q_2 - q_1$. In matrix form, the dependence of the new coordinates on the old ones can be written in the following way:

$$L = \begin{pmatrix} 1 & 0 \\ -1 & 1 \end{pmatrix} Q = SQ, L = \begin{pmatrix} l_1 \\ l_2 \end{pmatrix} \quad (3.10).$$

Hence, $Q = S^{-1}L$. System (3.5) takes the form $\ddot{L} + FL = 0$, where

$$F = SCS^{-1} = \begin{pmatrix} 1 & -1 \\ -1 & 2 \end{pmatrix} \quad (3.11).$$

The integrity condition for the links takes the form:

$$\begin{cases} l_1 \le l_{crit} \\ l_2 \le l_{crit} \end{cases} \quad (3.12).$$

Let's put

$$U = \begin{pmatrix} u_1 \\ u_2 \end{pmatrix} = \begin{pmatrix} l_1/l_{crit} \\ l_2/l_{crit} \end{pmatrix} \quad (3.13).$$

Then the system of equations can be rewritten as follows:

$$\ddot{U} + FU = 0 \quad (3.14),$$

As a result of the coordinates change, the integrity condition form: $U_1 \le 1, U_2 \le 1$. The initial conditions, accordingly, have the following form: $U_1(t=0) = 1, U_2(t=0) = 1$. Let us solve the system (3.14) considering the initial conditions and the first mass fixation.

Solving the equation $Det(F - \lambda E) = 0$ allows one to determine the eigenvalues of the matrix F(Det denotes the matrix determinant), which are the squares of the natural frequencies of oscillations of the system:

$$\omega_{1,2} = \sqrt{\frac{3 \pm \sqrt{5}}{2}} \quad (3.15).$$

Let's define the eigenvectors of the matrix F:

$$V_1 = \begin{pmatrix} 1 \\ \frac{\sqrt{5}-1}{2} \end{pmatrix}, V_1 = \begin{pmatrix} 1 \\ -\frac{\sqrt{5}+1}{2} \end{pmatrix} \quad (3.16).$$

Thus, accounting for the initial and boundary conditions, the solution to the system of equations (3.14) reads as:

$$U_1 = \frac{\sqrt{5}+3}{2\sqrt{5}}\cos(\omega_1 t) + \frac{\sqrt{5}-3}{2\sqrt{5}}\cos(\omega_2 t) \cong$$

$$\cong 1.17\cos(\omega_1 t) - 0.17\cos(\omega_2 t) \quad (3.17).$$

$$U_2 = \frac{\sqrt{5}+1}{2\sqrt{5}}\cos(\omega_1 t) + \frac{\sqrt{5}-1}{2\sqrt{5}}\cos(\omega_2 t)$$

In fact, in (3.17) T should be used to denote time, considering the performed variable change. However, starting from this moment, for convenience we will suppose $c = m = 1$ and, accordingly, $T = t$.

Note that in the formula for U_1 the cosines are multiplied by factors of different signs, and when added they give a number greater than one. Let's find a moment in time t^* when $\cos(\omega_1 t) = 1$, a $\cos(\omega_2 t) = -1$:

$$\omega_1 t^* = 2\pi i, \qquad i = 0,1,2,3, \ldots \quad (3.18a)$$

$$\omega_2 t^* = \pi + 2\pi k, \qquad k = 0,1,2,3, \ldots \quad (3.18b).$$

From (3.18) we obtain:

$$\frac{\omega_2}{\omega_1} = \frac{3-\sqrt{5}}{2} = \frac{1+2k}{2i} \quad (3.19).$$

Meaning $(3-\sqrt{5})/2$ (the golden ratio) will be approximated by continued rational representation:

$$\frac{1}{2}; \frac{1}{3}; \frac{2}{5}; \frac{3}{8}; \frac{5}{13}; \frac{8}{21} \ldots \quad (3.20).$$

Let's choose the fraction $3/8$, then $k = 1, i = 4, t^* = 15.534$ and $t^* = 15.250$ according to (3.18a) and (3.18b), respectively. When substituting these values, one gets $U_1 > 1$ – meaning failure of the first link. The choice of a proper rational representation of (3.19) allows one to evaluate t^* from (3.18) with any needed accuracy.

3.4. A chain with an arbitrary finite number of links

Let's consider a chain with an arbitrary number of links n. The chain is supposed to be uniformly stretched and at the initial moment of time relaxation wave (generated for example by a link break, figure 3.1) starts to propagate through the system.

Fig. 3.1. A statically loaded chain of an arbitrary finite number of oscillators. The dotted line indicates a broken link.

The movement of masses is described by a system of differential equations

$$M\ddot{Q} + CQ = 0 \qquad (3.21).$$

The change $T = t\sqrt{c/m}$ provides the transition to dimensionless matrices:

$M = E$ is $n \times n$ unity matrix

$$C = \begin{pmatrix} 2 & -1 & \cdots & 0 & 0 \\ -1 & 2 & -1 & \cdots & 0 \\ & \ddots & \ddots & \ddots & \\ 0 & & -1 & 2 & -1 \\ 0 & 0 & \cdots & -1 & 1 \end{pmatrix} \qquad (3.22).$$

The integrity conditions for the chain are written for each link: $|q_i - q_{i-1}| \leq l_{crit}$, $\forall i = 1..N$, the initial conditions are the following:

$$\begin{cases} q_i(t=0) - q_{i-1}(t=0) = l_{crit} \\ \dot{q}_i(t=0) = 0 \end{cases} \qquad (3.23)\ .$$

The fixation condition is $q_0(t) = 0\ \forall t$. Let's introduce new generalized coordinates in the following way:

$$\begin{aligned} &l_i = q_i - q_{i-1}, \forall i = 1..n, \\ &L = (l_1, l_2, \dots, l_n)^T \end{aligned} \tag{3.24}$$

The variable change is carried out using a transition matrix S:

$$S = \begin{pmatrix} 1 & 0 & \cdots & 0 & 0 \\ -1 & 1 & 0 & \cdots & 0 \\ & \ddots & \ddots & \ddots & \\ 0 & & -1 & 1 & 0 \\ 0 & 0 & \cdots & -1 & 1 \end{pmatrix} \tag{3.25},$$

and, therefore $Q = S^{-1}L$, $L = SQ$. Thus, we get a system of differential equations

$$\ddot{L} + FL = 0 \tag{3.26},$$

where

$$F = SCS^{-1} = \begin{pmatrix} 1 & -1 & \cdots & 0 & 0 \\ -1 & 2 & -1 & \cdots & 0 \\ & \ddots & \ddots & \ddots & \\ 0 & & -1 & 2 & -1 \\ 0 & 0 & \cdots & -1 & 2 \end{pmatrix} \tag{3.27}.$$

The initial conditions read as:

$$\begin{cases} l_i(t=0) = l_{crit} \\ \dot{l}_i(t=0) = 0 \end{cases} \forall i = 1..n \tag{3.28}.$$

The fixation condition is $l_0 = 0\ \forall t$. The chain integrity conditions have the following form:

$$|l_i(t)| \le l_{crit}, \qquad \forall t, \forall i = 1..n \tag{3.29}.$$

Let's make a change of variables $u_k = l_k / l_{crit}$ to get a system of differential equations with the initial conditions:

$$\begin{cases} \ddot{U} + FU = 0 \\ u_k(t=0) = 1 \\ \dot{u_k}(t=0) = 0 \end{cases} \forall k = 1..n \qquad (3.30),$$

and conditions of the integrity of the links

$$|u_i(t)| \leq 1, \qquad \forall t, \forall i = 1..n \qquad (3.31)$$

and the fixation condition $U_0 = 0\ \forall t$.

Natural frequencies of the system

Natural frequencies are determined by calculating the eigenvalues of the matrix F using the equation $Det(F - \lambda A) = 0$. Let's write the equation explicitly:

$$\begin{vmatrix} 1-\lambda & -1 & \cdots & 0 & 0 \\ -1 & 2-\lambda & -1 & \cdots & 0 \\ & \ddots & \ddots & \ddots & \\ 0 & & -1 & 2-\lambda & -1 \\ 0 & 0 & \cdots & -1 & 2-\lambda \end{vmatrix} = 0 \qquad (3.32).$$

Let put $\alpha = 2 - \lambda$, then:

$$\begin{vmatrix} \alpha-1 & -1 & \cdots & 0 & 0 \\ -1 & \alpha & -1 & \cdots & 0 \\ & \ddots & \ddots & \ddots & \\ 0 & & -1 & \alpha & -1 \\ 0 & 0 & \cdots & -1 & \alpha \end{vmatrix} = 0 \qquad (3.33)$$

or $D_n = 0$, where D_k is the determinant of order k. The determinant can be expanded with respect to the last line:

$$D_n = \alpha D_{n-1} - D_{n-2} \qquad (3.34)$$

The recurrent equation (3.34) is supplemented with the conditions

$$D_0 = 1, D_1 = \alpha - 1 \qquad (3.35).$$

We will look for a solution to equation (3.34) in the form $D_n = p^n$. Substituting this expression into (3.34) and dividing by p^{n-2}, we obtain a quadratic equation $p^2 - \alpha p + 1 = 0$. It has the following roots:

$$p_{1,2} = \frac{\alpha \pm \sqrt{\alpha^2 - 4}}{2} \tag{3.36}$$

This way we get the expression for D_n

$$D_n = c_1 p_1^n + c_2 p_2^n \tag{3.37}$$

Let's make another variable change $\alpha = 2\cos(\theta)$. Thus $p_1 = e^{i\theta}, p_2 = e^{-i\theta}$. From the system

$$\begin{cases} c_1 + c_2 = 1 \\ c_1 e^{i\theta} + c_2 e^{-i\theta} = e^{i\theta} + e^{-i\theta} - 1 \end{cases} \tag{3.38}$$

one can find the constants c_1 and c_2, then substitute them into (3.37) and obtain the transformed equation:

$$2sin\left(\frac{\theta}{2}\right) cos\left(\frac{(2n+1)\theta}{2}\right) = 0 \tag{3.39}$$

The roots of (3.39) are $\theta_1 = 2\pi k, \theta_2 = \frac{\pi(2k+1)}{2n+1}, k = 1..n$. The first set should be discarded (the stiffness matrix is non-degenerate). The second set of roots provides a series of n squared eigen frequencies

$$\lambda_k = 2 - 2cos\left(\frac{\pi(2k-1)}{2n+1}\right), k = 1..n \tag{3.40}$$

Thus, the formula for natural frequencies reads as:

$$\omega_k = 2sin\left(\frac{\pi(2k-1)}{4n+2}\right), k = 1..n \tag{3.41}$$

Determination of the stiffness matrix eigenvectors

Considering the initial conditions, the general solution of the system of differential equations describing the movement of the chain reads as:

$$U(t) = \sum_{j=1}^{n} c_j \boldsymbol{R_j} \cos(\omega_j t) \quad (3.42).$$

Here $\boldsymbol{R_j}$ – are the eigenvectors of the stiffness matrix F, and c_j are the constants satisfying the initial conditions.

Let's find the eigenvectors of the matrix F. For the i^{th} component of an eigenvector number j the recurrent formula can be easily derived:

$$r_i^{(j)} = (2 - \lambda_j) r_{i-1}^{(j)} - r_{i-2}^{(j)} \quad (3.43).$$

Let's put $r_1^{(j)} = 1, \forall j = 1..n$. Also note that $r_2^{(j)} = 1 - \lambda_j, \forall j = 1..n$. Let's put $r_0^{(j)} = 1$ so that for $r_2^{(j)}$ the recurrent formula would be also be valid.

In order to satisfy the condition $u_j(t = 0) = 1, \forall j = 1..n$, it is necessary to satisfy the following equalities:

$$\begin{cases} \sum_{k=1}^{n} c_k = 1 \\ \sum_{k=1}^{n} c_k (1 - \lambda_k) = 1 \\ \vdots \\ \sum_{k=1}^{n} c_k r_n^{(k)} = 1 \end{cases} \quad (3.44).$$

Let's determine the components of the eigenvectors. Let's denote $2 - \lambda_j = \nu_j$. Then the recurrent relation for the components of the eigenvectors (3.43) would read as:

$$r_i^{(j)} = \nu_j r_{i-1}^{(j)} - r_{i-2}^{(j)} \quad (3.45).$$

This recurrent formula coincides exactly with the recurrent formula for the Chebyshev polynomials. Let's recall the formulas for Chebyshev polynomials:

$$T_i(y) = 2yT_{i-1}(y) - T_{i-2}(y) \quad (3.46).$$

In this case, particular values are specified for the first two polynomials:

$$T_0(y) = 1, T_1(y) = y \quad (3.47).$$

Let's temporarily omit the index (j) to simplify the calculations. In our case, the recurrence relation has the following form:

$$r_i(x_j) = 2x_j r_{i-1}(x_j) - r_{i-2}(x_j) \quad (3.48),$$

where $x_j = v_j/2$ and thus $r_1(x_j) = 1, r_2(x_j) = 2x_j - 1$. Note that if we choose $r_0(x_j)$ to equal 1, the recurrent relation will give correct expressions for the components starting from the second one.

We cannot use the formula for the Chebyshev polynomials due to the difference in the first two values. Let's turn to the Chebyshev polynomials of the second kind. For them the recurrent relation for them and the zero polynomial coincide with those for the Chebyshev polynomials of the first kind, however, the first polynomial is given by the formula

$$P_1(y) = 2y \quad (3.49).$$

The general formula for the Chebyshev polynomials of the second kind has the following form

$$P_{i-1}(y) = \frac{\sin(i * \arccos(y))}{\sin(\arccos(y))} \quad (3.50).$$

Now let's notice the obvious relation

$$r_i(x_j) = P_{i-1}(x_j) - P_{i-2}(x_j) \quad (3.51).$$

Using formulas (3.48) and (3.49) and considering the relation

$$x_j = \frac{\nu_j}{2} = \frac{2-\omega_j^2}{2} = 1 - 2\sin^2\left(\frac{\pi(2j-1)}{4n+2}\right) = \cos\left(\frac{\pi(2j-1)}{2n+1}\right) \qquad (3.52),$$

let's calculate

$$r_i^{(j)} = \frac{2\sin\left(\frac{1}{2}\arccos\left(\frac{2-\omega_j^2}{2}\right)\right)\cos\left(\frac{2i-1}{2}\arccos\left(\frac{2-\omega_j^2}{2}\right)\right)}{\sin\left(\arccos\left(\frac{2-\omega_j^2}{2}\right)\right)} \qquad (3.53).$$

After trigonometric transformations, the formula for the component with the number i of the eigen vector with number j reads as:

$$r_i^{(j)} = \frac{cos\left(\frac{\pi(2i-1)(2j-1)}{4n+2}\right)}{cos\left(\frac{\pi(2j-1)}{4n+2}\right)} \qquad (3.54),$$

where is n −the number of masses in the chain.

Derivation of formulas for the constants c_j using the initial conditions

Considering formula (3.51), the system of linear equations for g the constants c_j has the following form:

$$\begin{pmatrix} P_0(x_1) & P_0(x_2) & \cdots & P_0(x_n) \\ P_1(x_1) - P_0(x_1) & P_1(x_2) - P_0(x_2) & \cdots & P_1(x_n) - P_0(x_n) \\ \vdots & \vdots & \vdots & \vdots \\ P_{n-1}(x_1) - P_{n-2}(x_1) & P_{n-1}(x_2) - P_{n-2}(x_2) & \cdots & P_{n-1}(x_n) - P_{n-2}(x_n) \end{pmatrix} \begin{pmatrix} c_1 \\ c_2 \\ \vdots \\ c_n \end{pmatrix} = \begin{pmatrix} P_0(1) \\ P_1(1) - P_0(1) \\ \vdots \\ P_{n-1}(1) - P_{n-2}(1) \end{pmatrix} \qquad (3.55).$$

On the right side of the system there is a single column, written in a convenient for the transformations way. Row additions allows one to transform the system as follows:

$$\begin{pmatrix} P_0(x_1) & P_0(x_2) & \cdots & P_0(x_n) \\ P_1(x_1) & P_1(x_2) & \cdots & P_1(x_n) \\ \vdots & \vdots & \vdots & \vdots \\ P_{n-1}(x_1) & P_{n-1}(x_2) & \cdots & P_{n-1}(x_n) \end{pmatrix} \begin{pmatrix} c_1 \\ c_2 \\ \vdots \\ c_n \end{pmatrix} = \begin{pmatrix} P_0(1) \\ P_1(1) \\ \vdots \\ P_{n-1}(1) \end{pmatrix} \quad (3.56).$$

If explicit formula for the polynomials is used the system can be rewritten in the following way:

$$\begin{pmatrix} 1 & 1 & \cdots & 1 \\ x_1 & x_2 & \cdots & x_n \\ \vdots & \vdots & \vdots & \vdots \\ {x_1}^{n-1} & {x_2}^{n-1} & \cdots & {x_n}^{n-1} \end{pmatrix} \begin{pmatrix} c_1 \\ c_2 \\ \vdots \\ c_n \end{pmatrix} = \begin{pmatrix} 1 \\ 1 \\ \vdots \\ 1 \end{pmatrix} \quad (3.57).$$

The matrix of the system (3.57) is the Vandermonde matrix and an expression for its determinant is well known. Let's find the constants $c_j$using Cramer's formulas

$$c_j = \frac{\Delta_j}{\Delta} \quad (3.58),$$

where is Δ is the Vandermonde determinant Δ_j is the determinant of a matrix with a j^{th} column replaced by a unity column. The elementary transformations yield:

$$c_j = \frac{(1-x_1)\cdots(1-x_{j-1})(1-x_{j+1})\cdots(1-x_n)}{(x_j-x_1)\cdots(x_j-x_{j-1})(x_j-x_{j+1})\cdots(x_j-x_n)} \quad (3.59).$$

The notation $M_n(x) = 2^n \prod_{k=1}^{n}(x - x_k)$ allows one to rewrite (3.59):

$$c_j = \frac{M_n(1)}{M_n{}'(x_j)(1-x_j)} \quad (3.60).$$

Consider the function

$$f(x) = \frac{\cos\left(\frac{2n+1}{2}\arccos(x)\right)}{\cos\left(\frac{\arccos(x)}{2}\right)} \quad (3.61).$$

Let’s show that the introduced x_j are zeros of $f(x)$:

$$f(x)=\frac{\cos\left(\frac{\pi(2j-1)}{2}\right)}{\cos\left(\frac{\pi(2j-1)}{4n+2}\right)}=0 \qquad (3.62).$$

Note that the denominator of the $f(x)$ function is non-zero, since the angle $\frac{\pi(2j-1)}{4n+2}, j=1..n$ belongs to the interval $\left(0,\frac{\pi}{2}\right)$. It is easy to show that $f(x)$ it is a polynomial of degree n if (3.61) is multiplied and divided by $\sin(\arccos(x)/2)$:

$$f(x)=\frac{\cos\left(\frac{2n+1}{2}\arccos(x)\right)\sin\left(\frac{\arccos(x)}{2}\right)}{\cos\left(\frac{\arccos(x)}{2}\right)\sin\left(\frac{\arccos(x)}{2}\right)}=\frac{\sin\big((n+1)\arccos(x)\big)-\sin(n*\arccos(x))}{\sin(\arccos(x))}=P_n(x)-P_{n-1}(x) \qquad (3.63)$$

.

The coefficient of the n^{th} degree term of $P_n(x)$ equals 2^n. Then

$$M_n(x)=2^n\prod_{k=1}^{n}(x-x_k)=\frac{\cos\left(\frac{2n+1}{2}\arccos(x)\right)}{\cos\left(\frac{\arccos(x)}{2}\right)}=P_n(x)-P_{n-1}(x) \qquad (3.64).$$

It is obvious that $M_n(1)=1$ and therefore

$$M_n{}'(x_j)=\frac{(-1)^{j+1}(2n+1)}{2\sin\left(\frac{\pi(2j-1)}{2n+1}\right)\cos\left(\frac{\pi(2j-1)}{4n+2}\right)} \qquad (3.65).$$

Thus, the following formula is valid for the constants:

$$c_j=\frac{(-1)^{j+1}2\sin\left(\frac{\pi(2j-1)}{2n+1}\right)\cos\left(\frac{\pi(2j-1)}{4n+2}\right)}{(2n+1)\left(1-cos\left(\frac{\pi(2j-1)}{2n+1}\right)\right)} \qquad (3.66).$$

This way, the following system solution is obtained:

$$u_i(t)=2\sum_{j=1}^{n}\frac{(-1)^{j+1}\sin\left(\frac{\pi(2j-1)}{2n+1}\right)\cos\left(\frac{\pi(2j-1)(2i-1)}{4n+2}\right)}{(2n+1)\left(1-\cos\left(\frac{\pi(2j-1)}{2n+1}\right)\right)}\cos(\omega_j t) \qquad (3.67).$$

Here is i is the number of the link of the chain, ω_j are the natural frequencies of the system, calculated using formula (3.41).

Calculation results for chains with different numbers of links

Figure 3.2 shows $u_1(t)$ (deformation of the first link of the chain) graphs for chains consisting of 35 and 200 links. The effect of exceeding the initial distance between the masses (and hence the link failure) is obvious in both cases. The proof of the existence of the discussed effect can be carried out on the basis of the Kronecker's theorem [157].

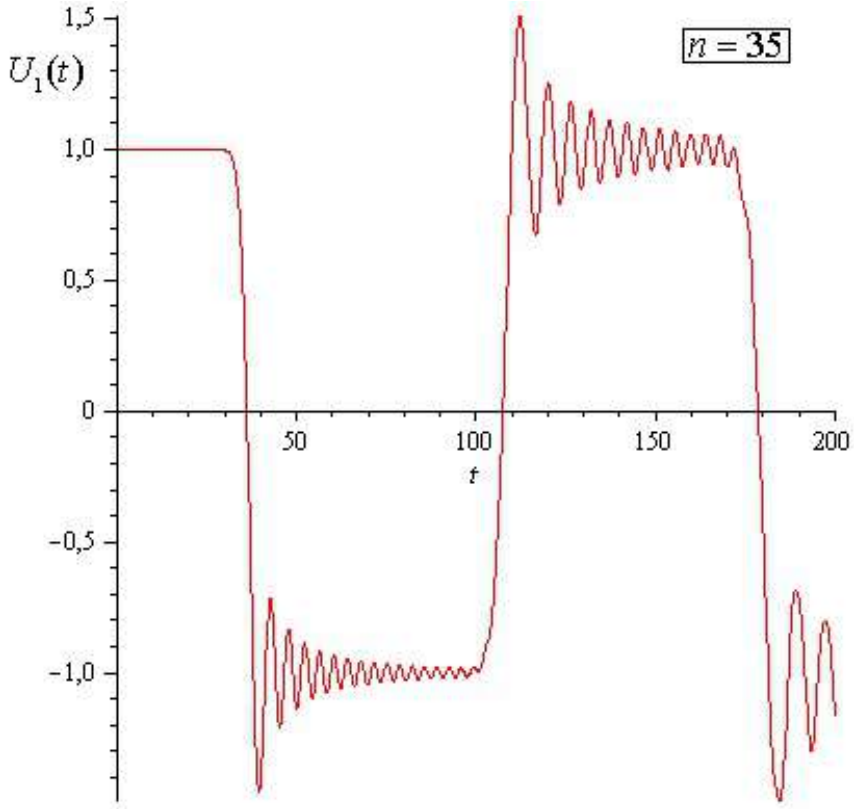

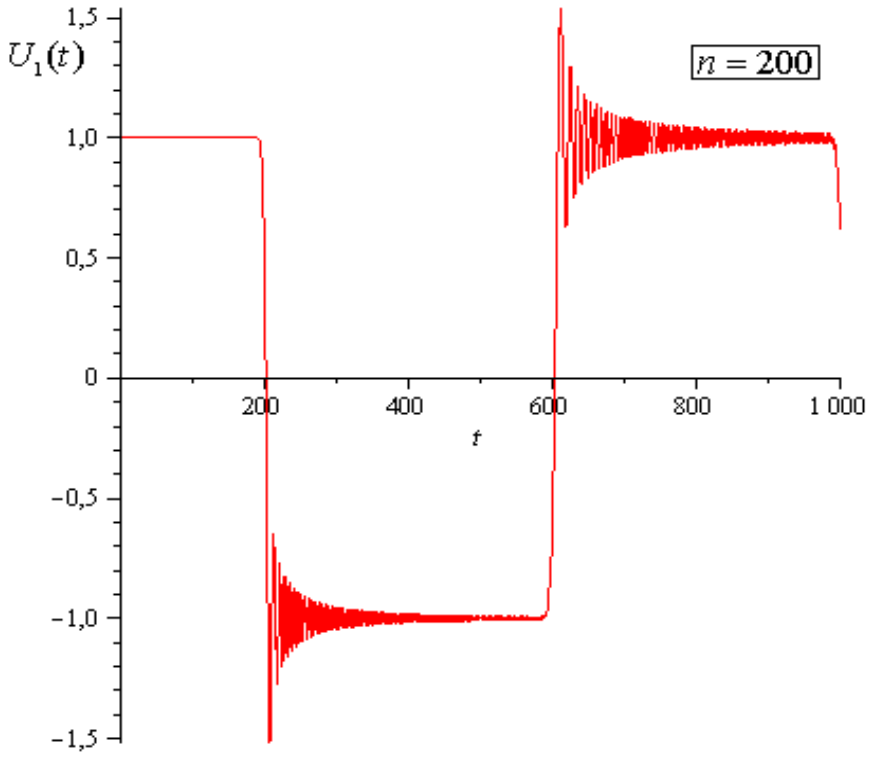

Fig. 3.2. Deformation of the first link for chains with different numbers of links.

3.5 Analysis of the solutions for the chain and for an elastic rod. Gibbs effect

A chain of oscillators can be the basis for deriving a one-dimensional wave equation. If we denote the distance between masses in a state of equilibrium by the parameter $h = \frac{L}{n}$(L – length of the rod), then the formal transition to the limit $h \to 0$ yields the following:

$$\frac{u_k}{h} \to \left.\frac{\partial U(y,t)}{\partial x}\right|_{y=\frac{kL}{n}}$$
$$\frac{q_{k-1} - 2q_k + q_{k+1}}{h^2} \to \frac{\partial^2 U}{\partial x^2} \qquad (3.68).$$

In (3.68) U is the rod deformation. The chain problem can be interpreted as a solution of the wave equation by the finite difference method with a time only discretization. Solution to the corresponding problem for the rod can be found in the form of a piecewise linear function in time if the d'Alembert method is applied.

According to the calculations carried out for different numbers of links, the excess of the initial stretch remains for any number of links, and its value (approximately 54%) does not decrease with increasing number of links n.

Let's consider an effect that is similar to the discussed one – the Gibbs phenomenon for the Fourier series [158]. Let's solve the problem of longitudinal vibrations of an elastic rod fixed at one end using the Fourier method. At the initial moment of time, the rod is supposed to be uniformly stretched. For simplicity, we will consider the length of the rod and the speed of propagation of waves in the rod to be equal to unity, and $\varepsilon = 1$ the be the critical deformation for the studied model material. It the stress in the rod exceeds unity, fracture takes place. We will also assume that at the initial moment of time the stress at all points of the rod was equal to unity.

The wave equation for our system will look like:

$$\frac{\partial^2 U(x,t)}{\partial x^2} = \frac{\partial^2 U(x,t)}{\partial t^2} \qquad (3.69).$$

Here $U(x,t)$is the displacement at point x. In this case, the boundary and initial conditions read as:

$$\begin{cases} U(x,0) = x \\ \left.\dfrac{\partial U(x,t)}{\partial t}\right|_{t=0} = 0 \\ U(0,t) = 0 \\ \left.\dfrac{\partial U(x,t)}{\partial x}\right|_{x=l} = H(-t) \end{cases} \qquad (3.70).$$

The first condition from (3.70) means the uniform rod deformation at the initial moment of time, the third condition denotes the rod end fixation the fastening of one of the ends of the rod, and the fourth – the sudden unloading of the rod at the initial moment of time ($H(t)$is the Heaviside function). Following the Fourier method, solution (3.69) is obtained as an infinite series:

$$U(x,t) = \sum_{k=0}^{\infty} \frac{8(-1)^k}{\pi^2(2k+1)^2} \cos\left(\frac{\pi(2k+1)}{2}t\right) \sin\left(\frac{\pi(2k+1)}{2}x\right) \qquad (3.71).$$

Let's calculate the rod deformation ε deformation in the rod at $x = 0$ (the fixation point).

$$\varepsilon(x=0,t) = \frac{\partial U(x,t)}{\partial x}\Big|_{x=0} = \sum_{k=0}^{n} \frac{4(-1)^k}{\pi(2k+1)} \cos\left(\frac{\pi(2k+1)}{2}t\right) \qquad (3.72).$$

If in (3.72) only partial sums of the series are considered, the solution will exhibit considerable oscillations near points of the solution sign shift. The Fourier solution exceeds the d'Alembert solution by about 18% and this value does not decrease if more terms of the series are considered. This numerical phenomenon is called the Gibbs effect. The figures below show graphs of the relative deformation of the rod at the fixation point versus time. Black stripes show the exact solution for the problem of longitudinal vibrations of a rod, obtained by the d'Alembert method.

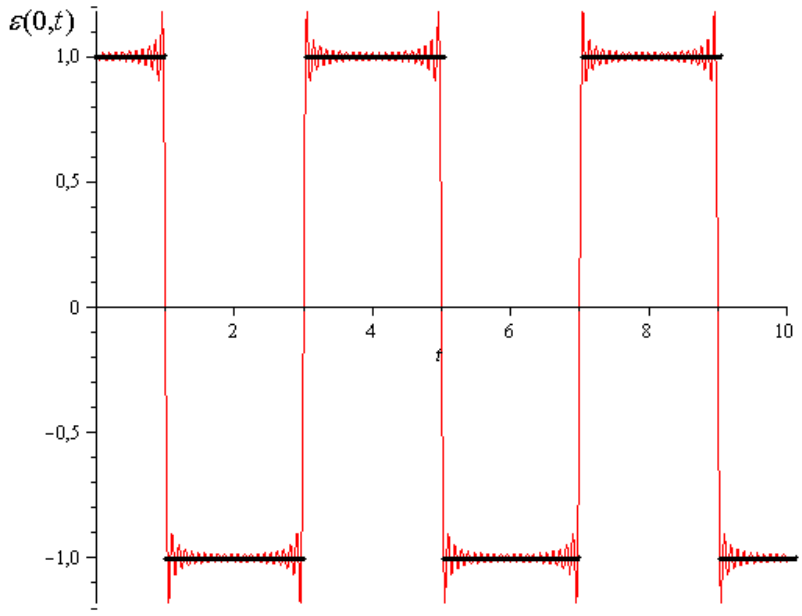

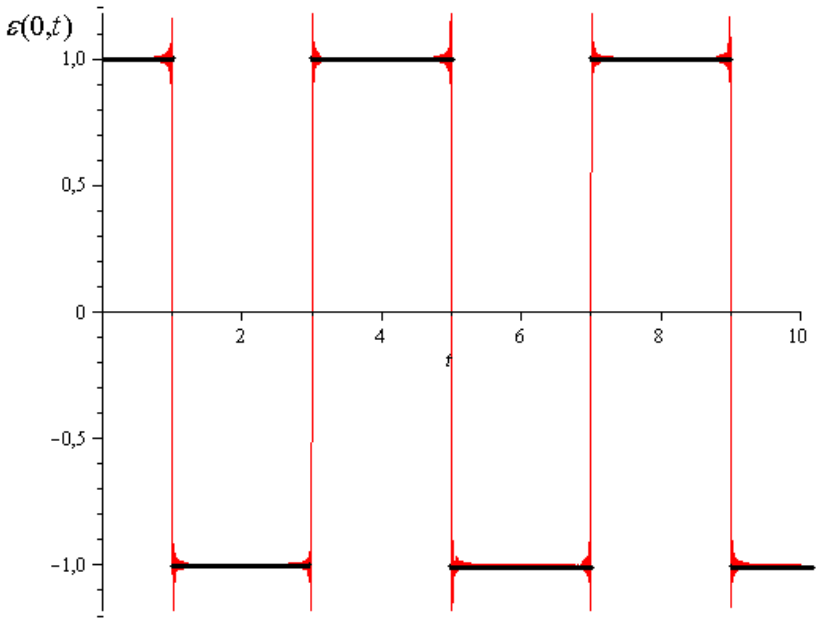

Fig. 3.3. Gibbs effect for a finite sum of the Fourier series of 20 (a) and 200 (b) terms. The black lines are d'Alembert solution.

The Gibbs phenomenon resembles the discovered effect for the chain. The effect observed in the chain is much more pronounced – the excess of the initial deformation is three time bigger for the chain. The effect obtained for the chain of oscillators should be considered as a physical phenomenon, in contrast to the Gibbs effect, which is actually a defect of the numerical scheme.

Thus, the use of numerical methods for solving problems of wave propagation based on spatial discretization of the studied bodies (the finite difference method, the finite element method, and so on) can cause non-physical behavior of the solution and the mesh refinement does not change the situation.

All real materials have a discrete structure. Under highly dynamic loading conditions, the behavior of discrete structures can reveal properties that cannot be accounted for by continuous models. In such situations, the continuum mechanics itself may turn out to be inadequate for the studied phenomenon.

3.7 Numerical study of fracture a periodic structure in course of relaxation

This section provides a numerical study of the effect discovered in the chain of oscillators. The propagation of a relaxation wave in PMMA (polymethyl methacrylate) samples with different shapes, including a periodic structure, was simulated. Samples with a 2mm thickness and 10 mm working area were studied. The primary failure occurs at a certain stress at a certain point of the sample, located near the top of the sample. This primary failure generated a relaxation wave travelling through the sample. After the first rupture, the dynamic problem of the relaxation wave propagation was solved and stresses at a certain point were checked and compared with initial stresses in the sample. Figure 3.4 shows examples of the studied specimens – a standard sample, a sample with discretization. Additionally, a mesh is shown and zones with added weight are demonstrated (in these zones the PMMA was replaced by steel).

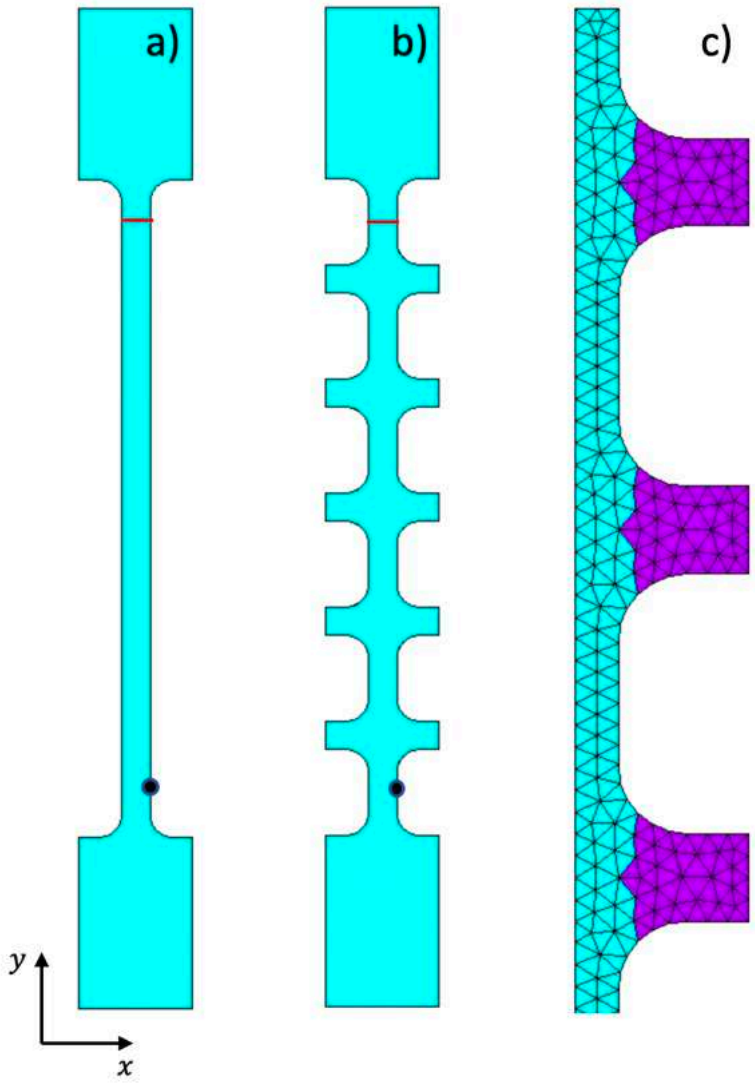

Fig. 3.4. Samples studied used in the numerical study. (a) – standard sample, (b) – sample with a discrete structure and (c) – the finite element mesh, purple color indicates the zones with extra weight where the material properties are changed – the PMMA is replaced by steel. The black circles indicate the points where σ_{yy} stress was calculated, the red line indicates the initial break in the sample.

Figure 3.5 shows the calculation results, namely the dependence of the σ_{yy} stress on time at the points indicated in Figure 3.6. According to the obtained results the initial stress in the sample can be exceeded even in the standard sample, however, the increased stresses act for a relatively short time – 15 μs (only the first excess is considered). This excess may be associated with the numerical features of obtaining a

solution – the use of partitioning the region into finite elements, which is actually a discretization of the region.

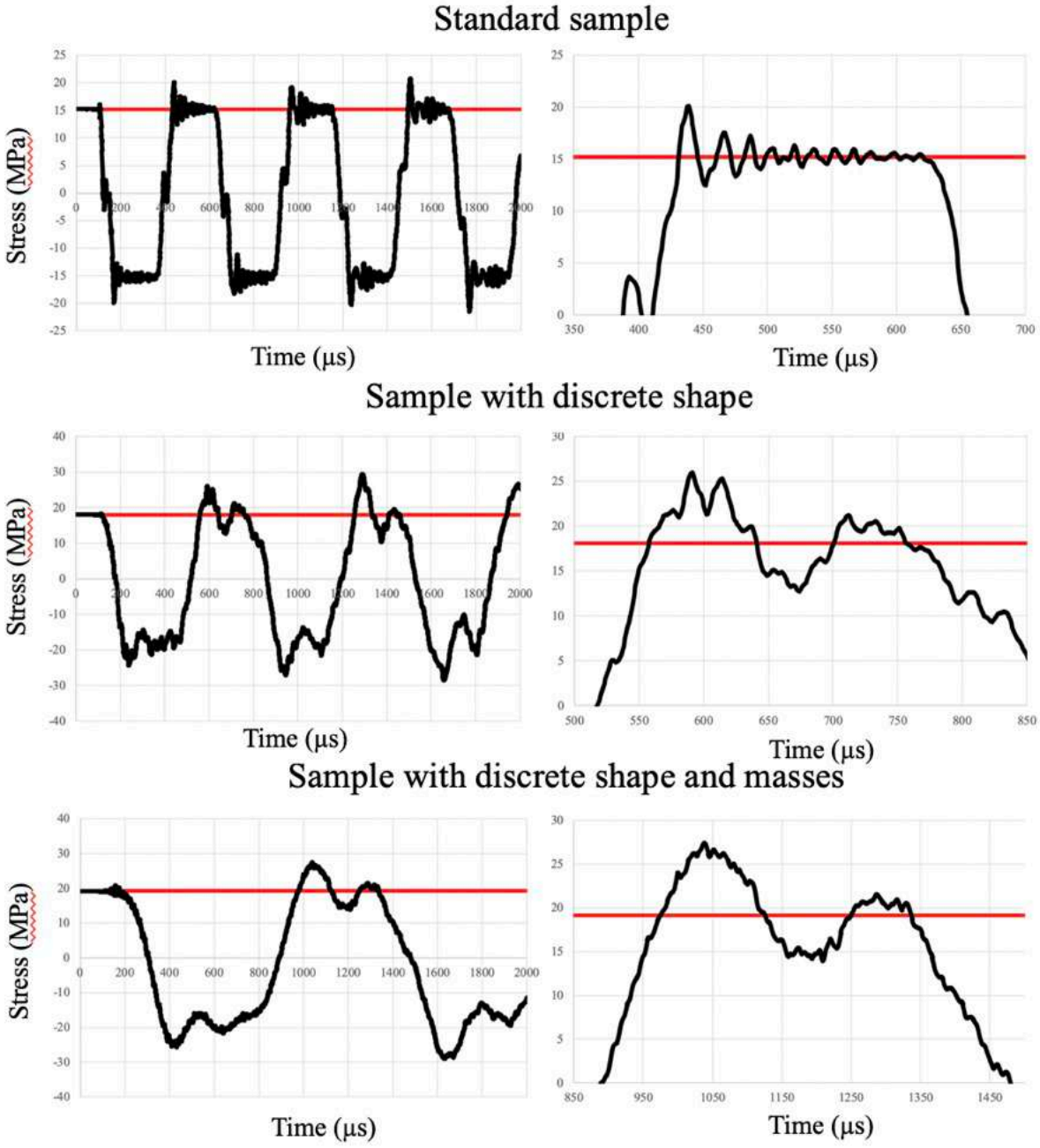

Fig. 3.5. Calculation results. Dependence of the σ_{yy} stress on time at the points indicated in figure 3.4.

In samples with artificial discretization, the maximum excess of the initial stress is by 39.6% and the duration of this excess is 85 μs. The addition of masses leads to the same excess of the initial stress – 38.9%, however, the duration of the excess

increases up to156 μs, and thus the likelihood of a secondary rupture in the system increases.

3.8 Chapter 3 conclusions

An exact analytical solution to the problem of oscillations of a homogeneous finite chain of linear identical oscillators has been found. It has been shown that a preloaded (stretched) chain can fail after the static load has been suddenly removed. This effect is absent in the corresponding continuum model, but occurs for a chain of arbitrary finite length. The studied effect is similar to the Gibbs phenomenon found in trigonometric series, but is much more pronounced and, unlike the Gibbs phenomenon, can be considered as a real physical phenomenon rather than a defect of the numerical scheme. The effect can be important for the analysis of discrete periodic structures in particular the nanostructures.

According to the performed calculations, the effect of fracture following a sudden system unloading (for example, after a primary rupture) can be observed in very real structures and samples. Thus, it has been shown that introducing discreteness into the shape of samples and adding masses to their design (in fact, bringing the properties of the sample closer to the chain of oscillators discussed in the Chapter) leads to a significant excess of the initial stresses in the material (about 40%) for hundreds of microseconds. Such stress field can lead to fracture, and this possibility must be accounted for in the design of real structures.

More information can be found in [17,156].

Chapter 4. Space and time discreetness of the crack propagation process

Chapter 4 discusses the dynamic propagation of cracks in brittle materials under various loading conditions. The propagation of cracks under quasi-static loading, as well as under the shock-pulse loads has been studied. Special attention has been paid to the dependencies characterizing the crack propagation and a non-stationary character of these dependencies. This way, for the case of crack propagation under quasi-static loading, the issue of the crack velocity oscillations has been investigated. The issue related to the variation of stress intensity factor observed in a number of experiments on crack propagation due to intensive loading has been also considered. The research was carried using the finite element method with the incubation time fracture criterion embedded into the numerical scheme. This fracture model fundamentally determines the discrete mechanism of the fracture process at a given scale level. Both quantitative and qualitative comparison of the numerical results with the available experimental data has been carried out. It has been shown that accounting for the spatial and time discreteness of the fracture process makes it possible to predict and explain a number of experimentally observed effects that do not fit into traditional theoretical concepts of the dynamic fracture. A calculation scheme for the modeling of the cracks propagating in arbitrary directions under shock loading conditions has been also developed This numerical model makes it possible to study fragmentation in brittle bodies under dynamic loading, in particular, to study the size distribution of fragments. The results of the application of this numerical model are presented and the results qualitatively correspond to experiments on fragmentation in brittle bodies.

4.1 The incubation time fracture criterion for the crack propagation problems

The incubation time concept has been introduced in the first Chapter (section 1.3). According to the proposed model fracture is not an instantaneous event, and even

though stresses reach certain critical level at some point of the material, a particular time is needed for the fracture to develop (this effect of dynamic fracture is well known among experimentalists, (see ex. [2,5,159]). The observed macroscopic fracture is a result of series of preceding microscopic events, such as growth and coalescence of microcracks and/or micropores, and a notion of preparatory incubation process was introduced in order to account for these events. Terms “macroscopic” and “microscopic” should be regarded just as notations of two scale levels, and dynamic fracture is regarded as an evolution of the “microscopic” fracture into “macroscopic” fracture event, which essentially develops as a relaxation process and can be integrally characterized by a special characteristic time – the incubation time parameter τ, which is used in (1.6). The incubation time is treated as a material property, which can be assessed experimentally. Time-based fracture models were also discussed in [28-30], where fracture criteria involving critical time integrals were presented, but no fundamental temporal material characteristics were introduced. In [2] a short-pulse fracture theory based on assumption that fracture occurs, if stress intensity factor exceeds critical values for some minimal time, was presented. This minimum time interval depends on conditions and history of applied load and clearly reveals itself in a special case of short pulse loading with close to threshold parameters. Historically it was an important step in proclaiming an existence of special preparatory process itself, but the introduced minimum time parameter and corresponding stress intensity factor critical levels cannot be regarded as material properties. It is fundamentally important that the incubation time fracture model is able to predict values of all these parameters for various loading conditions.

The incubation time fracture criterion has been successfully used to study and predict some effects of dynamic crack propagation for various materials and loading conditions. Experiments with both quasistatic [16] and dynamic [160] loading were successfully simulated. Numerically obtained crack trajectory together with experimental data from [16] are shown in figure 4.1. The incubation time approach provides a clear interpretation for a lower than theoretical crack velocity: the crack is

"slowed down" by the preliminary microscopic fracture process which require time to develop due to acting stress field.

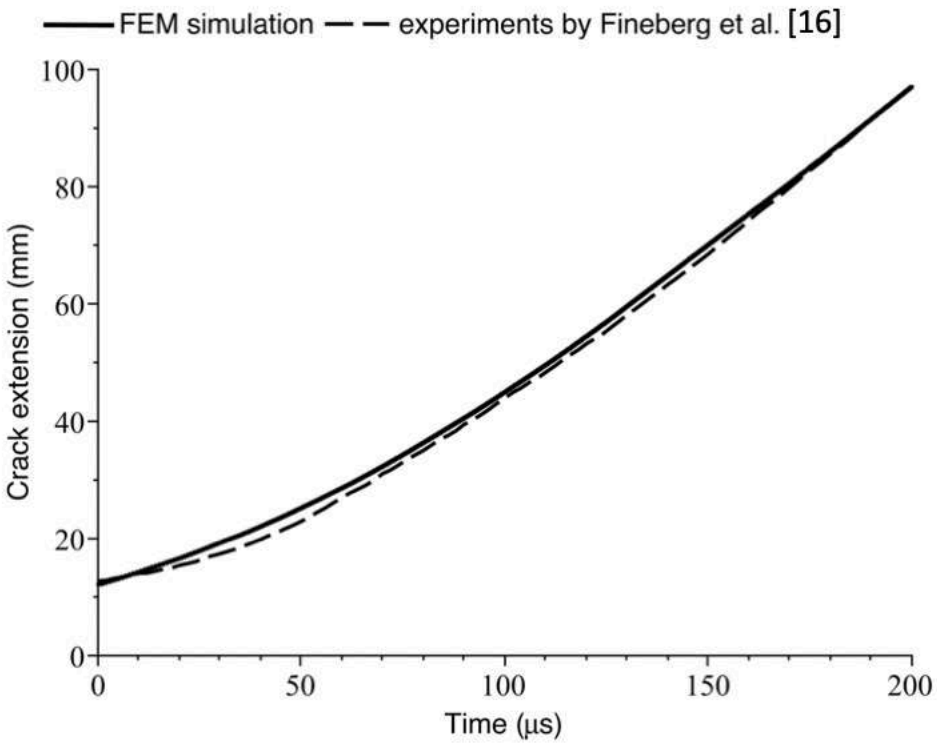

Fig. 4.1. Crack trajectory obtained using FEM and incubation time criterion compared to experimental data on quasistaic loading [16].

4.2 Numerical implementation of the incubation time approach for the dynamic crack propagation problems

For the numerical investigation of the dynamic crack propagation, the fracture criterion (1.6) is used in combination with the finite element method. Criterion (1.6) has been implemented into the ANSYS calculation software as an external procedure designed to control the crack propagation process. Integration by spatial coordinate and time in (1.6) is performed numerically. The procedure saves the history of stresses in the nodes lying on the crack trajectory, which makes it possible to calculate the time integral at each step of the problem solution. Spatial integration is performed at several nodes lying in the interval $[0, d]$, counting from the crack tip. This calculation scheme

allows one to solve problems of a straight crack propagation in symmetrical samples and with a symmetrical method the load application and the crack trajectory coinciding with the line of symmetry. Despite the fact that dividing the area into elements with size d provides satisfactory results, elements with size $d/3$ along the crack trajectory have been used. A regular mesh with equal square elements has been used along the crack trajectory. The size of the elements was gradually increased towards the top of the sample in order to reduce the total number of elements and therefore to improve the performance of the numerical scheme. The full mesh and the enlarged area near the top of the crack with a regular mesh are shown in figure 4.2.

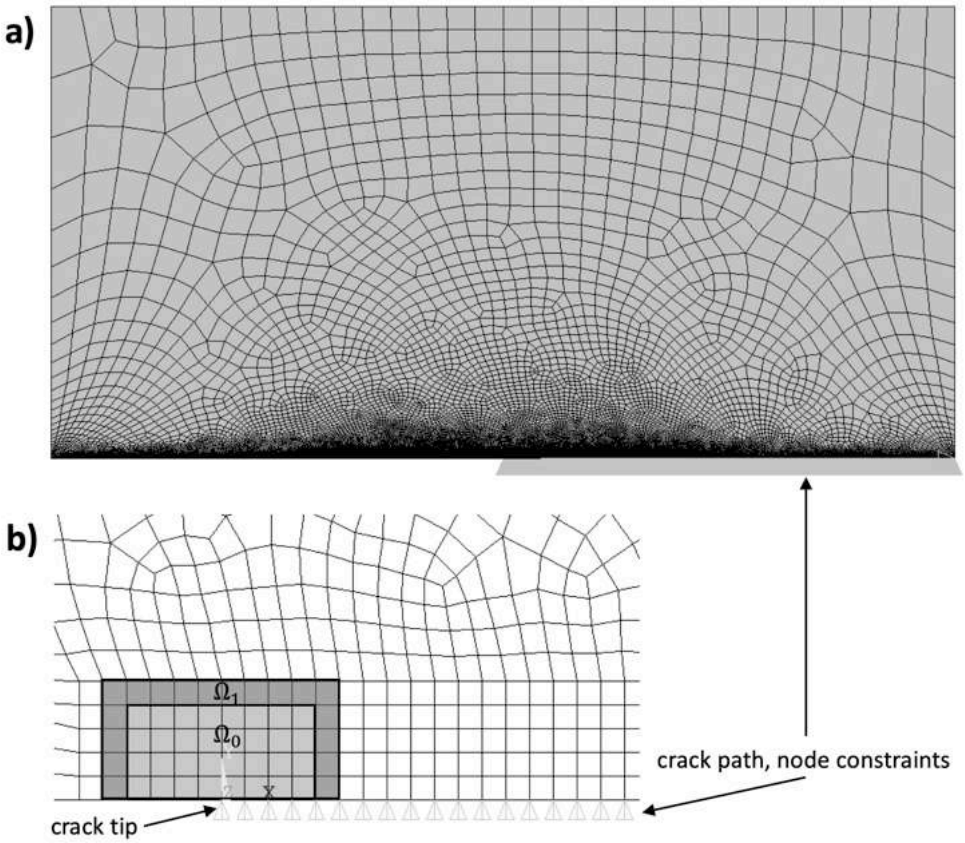

Fig. 4.2. Meshed used in the computations; a) – full model; b) – crack tip region with a regular mesh. Areas involved in J-integral calculations are indicated.

If condition (1.6) holds in a particular set of nodes forming the fracture process zone, displacement restrictions are removed from these nodes and crack tip travels to a subsequent node forming a new crack tip. This way, minimal distance of crack propagation equals d, which lies within the framework of the incubation time

approach: crack increments smaller than d are not regarded as fracture on the considered scale level. Solution time step dt is calculated according to formula $dt = d/c_d$, where c_d is the fastest elastic wave velocity. Integrals in (1.6) are computed numerically according to a trapezoid formula for both time and space integrals. The computations use the stored history of tensile stresses (σ_{yy}) in nodes, which are located on the crack path.

Material of the simulated specimens is supposed to exhibit linear elastic behavior, which can be described by Lame equations and Hooke's law:

$$\rho \frac{\partial^2 U_i}{\partial t^2} = (\lambda + \mu)\nabla_i\left(\nabla \cdot \vec{U}\right) + \mu \Delta U_i$$
$$\sigma_{ij} = \delta_{ij}\lambda \, \nabla \cdot \vec{U} + \, \mu\left(\frac{\partial U_i}{\partial x_j} + \frac{\partial U_j}{\partial x_i}\right) \qquad (4.1).$$

At time $t = 0$ the specimens are supposed to be stress free and velocities of all points of the body are supposed to be zero. The loading was simulated by displacement of the corner of the crack faces according to linear law. Thus, the initial and boundary conditions take the following form (quasistatic load case is described, figure 4.3):

$$\vec{U}(X, 0) = 0; \frac{\partial \vec{U}}{\partial t}(X, 0) = 0$$
$$\sigma_{22}(X \in \Gamma_3, t) = \sigma_{12}(X \in \Gamma_3, t) = 0$$
$$U_2(X \in \Gamma_2, t) = 0, \sigma_{12}(X \in \Gamma_2, t) = 0 \; - \text{ symmetry condition} \qquad (4.2)$$
$$U_2(X = \Gamma_1, t) = vt, \; v - \text{loading rate}$$

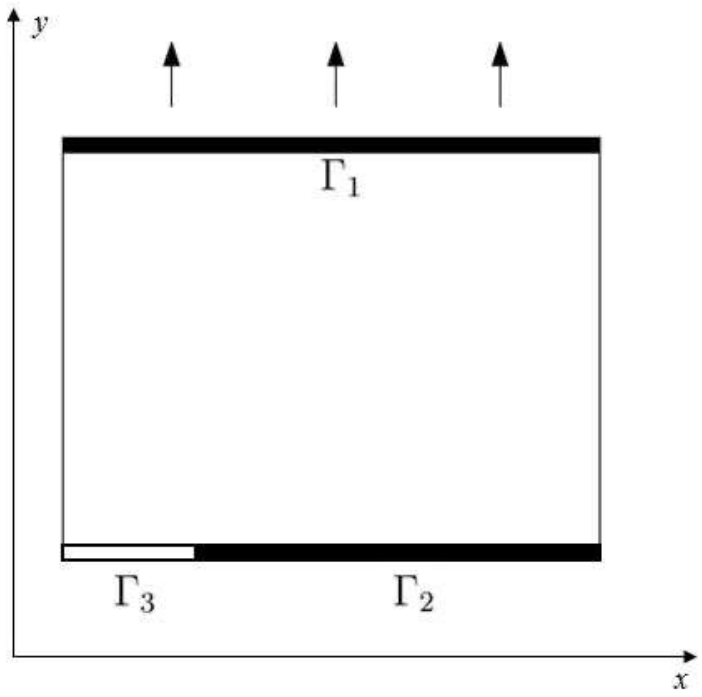

Fig. 4.3. Numerical simulation scheme. Quasistatic load case is shown.

In (4.1) and (4.2) $X = (x_1, x_2)$, $\vec{U}(X,t) = (U_1(X,t), U_2(X,t))$ is the displacement vector, ρ is the material density, λ and μ are the Lame constants.

Computation of the stress intensity factor

The stress intensity factor is computed using the J-integral which is computed with a specially developed software. The computation procedure is based on a formula for the J-integral:

$$J = \lim_{\Gamma \to 0} \int_{\Gamma} \left[(U+T)m_1 - \sigma_{ij} m_j \frac{\partial u_i}{\partial x_1} \right] \qquad (4.3).$$

A more detailed expression for the J-integral can be obtained if integration over area Ω is considered (area bounded by contours Γ and Γ_0, figure 4.4a) using divergence theorem and expression for kinetic energy $T = \frac{1}{2}\rho \frac{\partial u_i}{\partial t}\frac{\partial u_i}{\partial t}$. Here linear elastic material is considered, $\vec{n}$ is an external normal to Ω and partial space and time derivatives are

supposed to be connected by formula $\frac{\partial u_i}{\partial t} = -v\frac{\partial u_i}{\partial x_1}$, where v is the crack velocity [163,164].

$$J = \int_{\Gamma_0} \left[(U+T)n_1 - \sigma_{ij}n_j \frac{\partial u_i}{\partial x_1}\right] d\Gamma + \int_{\Omega} \rho \frac{\partial^2 u_i}{\partial t^2}\frac{\partial u_i}{\partial x_1} d\Omega - \int_{\Omega} \rho \frac{\partial u_i}{\partial t}\frac{\partial^2 u_i}{\partial x_1 \partial t} d\Omega - \int_{f^+ \cup f^-} t_i \frac{\partial u_i}{\partial x_1} d\Gamma \quad (4.4).$$

In (4) and (5) U and T are strain energy and kinetic energy densities, Γ is a shrinking contour close to the crack tip, while Γ_0 is a distant curve around the crack tip, f^+ and f^- denote the crack faces with applied traction $\vec{t}$, u_i is the displacement vector component and $\vec{n}$ and $\vec{m}$ are the normal vectors (figure 4a). In order to evade inaccurate contour integration in (5), the virtual crack extension method [163,164] is applied and thus, contour integration is substituted by integration over area. Additional contour Γ_1 bounding area Ω_1 is constructed (figure 4.4b) and a smooth transition function $q(x,y)$ equaling 1 at Ω_0 and Γ_0 points and 0 at Γ_1 points is introduced.

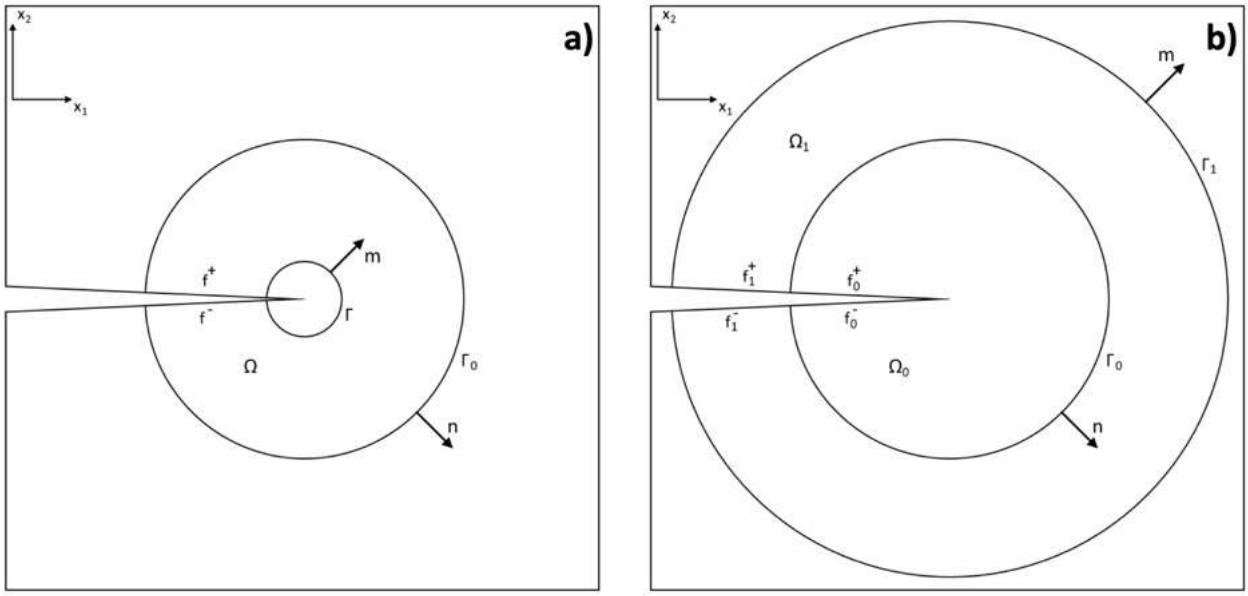

Fig. 4.4. Contour schemes used for J-integral evaluation.

The Ω_1 boundary is composed of contours Γ_1, Γ_0 and the crack faces f^+ and f^- with external normal $\vec{m}$. Hence the following expression holds, if $q(x,y)$ properties and formula for traction on the crack faces $t_i = \sigma_{ij}m_j$ are accounted for:

$$\int_{\partial\Omega_1}\left[(U+T)m_1 - \sigma_{ij}m_j\frac{\partial u_i}{\partial x_1}\right]qd\Gamma = \int_{\Gamma_0}\left[(U+T)m_1 - \sigma_{ij}m_j\frac{\partial u_i}{\partial x_1}\right]d\Gamma - \int_{f_1^+\cup f_1^-} t_i\frac{\partial u_i}{\partial x_1}qd\Gamma \quad (4.5).$$

On the other hand, the integral on the left side of (4.5) can be rewritten using the divergence theorem and thus expression for the contour integral over Γ_0 can be deduced:

$$\int_{\Gamma_0}\left[(U+T)n_1 - \sigma_{ij}n_j\frac{\partial u_i}{\partial x_1}\right]d\Gamma = \int_{\Omega_1}\left[\sigma_{ij}\frac{\partial u_i}{\partial x_1} - (U+T)\delta_{1j}\right]\frac{\partial q}{\partial x_j}d\Omega + \int_{\Omega_1}\rho\frac{\partial^2 u_i}{\partial t^2}\frac{\partial u_i}{\partial x_1}qd\Omega - \int_{\Omega_1}\rho\frac{\partial u_i}{\partial t}\frac{\partial^2 u_i}{\partial x_1\partial t}qd\Omega - \int_{f_1^+\cup f_1^-} t_i\frac{\partial u_i}{\partial x_1}qd\Gamma \quad (4.6).$$

In (4.6) δ_{1j} is Kronecker symbol. Finally, substitution of (4.6) into (4.4) yields formula for J-integral used in the calculations:

$$J = \int_{\Omega_1}\left[\sigma_{ij}\frac{\partial u_i}{\partial x_1} - (U+T)\delta_{1j}\right]\frac{\partial q}{\partial x_j}d\Omega + \int_{\Omega_{01}}\rho\frac{\partial^2 u_i}{\partial t^2}\frac{\partial u_i}{\partial x_1}qd\Omega - \int_{\Omega_{01}}\rho\frac{\partial u_i}{\partial t}\frac{\partial^2 u_i}{\partial x_1\partial t}qd\Omega - \int_{f_{01}^+\cup f_{01}^-} t_i\frac{\partial u_i}{\partial x_1}qd\Gamma \quad (4.7),$$

where $f_{01}^{\pm} = f_0^{\pm}\cup f_1^{\pm}$ и $\Omega_{01} = \Omega_0\cup\Omega_1$.

The J-integral calculations are significantly simplified since regular mesh is built along the crack path. Area Ω_0 is a square centered at the crack tip with 8 elements on the side, while the Ω_1 area is a 1-element thick layer covering Ω_0. However, due to symmetry of the problem the J value calculation involves only half of the area (figure 4.2b) and then the obtained result is multiplied by two.

At each time step the displacement values for node n of element e and their time derivatives $\left((u_i)_n^e, \left(\frac{\partial u_i}{\partial t}\right)_n^e, \left(\frac{\partial^2 u_i}{\partial t^2}\right)_n^e\right)$ are imported from ANSYS. Additionally, the following approximation is used for the $q(x, y)$ transition function:

$$(q)_n^e = \begin{cases} 1, \text{if node n of elment e belongs to } \overline{\Omega_0} \\ 0, \text{otherwise} \end{cases} \tag{4.8}.$$

The $(u_i)^e, \left(\frac{\partial u_i}{\partial t}\right)^e, \left(\frac{\partial^2 u_i}{\partial t^2}\right)^e$ and $(q)^e$ (all denoted as f^e for short) values at arbitrary point (ξ_1, ξ_2) inside the element e can be calculated using the element shape functions $N_i(\xi_1, \xi_2)$ and values at nodes f_n^e:

$$\begin{aligned} f^e(\xi_1, \xi_2) &= \sum_{i=1}^{4} f_i^e N_i(\xi_1, \xi_2) \\ N_1(\xi_1, \xi_2) &= (1 - \xi_1)(1 - \xi_2) \\ N_2(\xi_1, \xi_2) &= \xi_1(1 - \xi_2) \\ N_3(\xi_1, \xi_2) &= \xi_1 \xi_2 \\ N_4(\xi_1, \xi_2) &= (1 - \xi_1)\xi_2 \end{aligned} \tag{4.9}.$$

Approximation (4.9) is also used to evaluate spatial derivatives in (4.7). Integrands in (4.7) are calculated from displacements using formula for small deformations and Hooke's law. The area integrals in (4.7) are calculated by summing integrals over elements comprised by the area, which are evaluated using Gauss integration rule.

The applied J-integral calculation method does not rely on assumption that stresses are characterized by inversed root singularity which is an advantage over standard methods which are embedded into the majority of FEM software.

The stress intensity factor for a moving crack is then formally calculated using formula

$$K_I = \sqrt{\frac{EJ}{(1-\nu^2)A(\dot{a})}} \qquad (4.10a),$$

where

$$A(\dot{a}) = \dot{a}^2\alpha_d/\big((1-\nu)c_s^2 D\big), D = 4\alpha_d\alpha_s - (1+\alpha_s^2)^2,$$
$$\alpha_d = \sqrt{1-\dot{a}^2/c_d^2}, \alpha_s = \sqrt{1-\dot{a}^2/c_s^2} \qquad (4.10b).$$

In (4.10a,b) J is calculated using (4.7), E and ν are the material's elastic parameters, c_d and c_s are dilatational and shear wave velocities in the material and $\dot{a}$ is the crack velocity. The developed scheme was tested for the case of a dynamically loaded stationary crack. In the test problem history of the numerically computed SIF (using both standard ANSYS procedure CINT and the developed software implementing (4.7)) and analytical solution from [153] (formula 3.15) are compared. The sample is loaded using the pressure applied to the crack faces: linear rise region switches to the constant value at time T. The results and the load are shown in figure 4.5. The ANSYS generated values coincide with the analytical formula, while the values obtained using (4.7) lie slightly lower. This can be attributed to the fact that the developed software does not utilize any kind of asymptotic solutions, while ANSYS procedures and the analytical solution suppose inverse square root behavior of stresses in the vicinity of the crack tip.

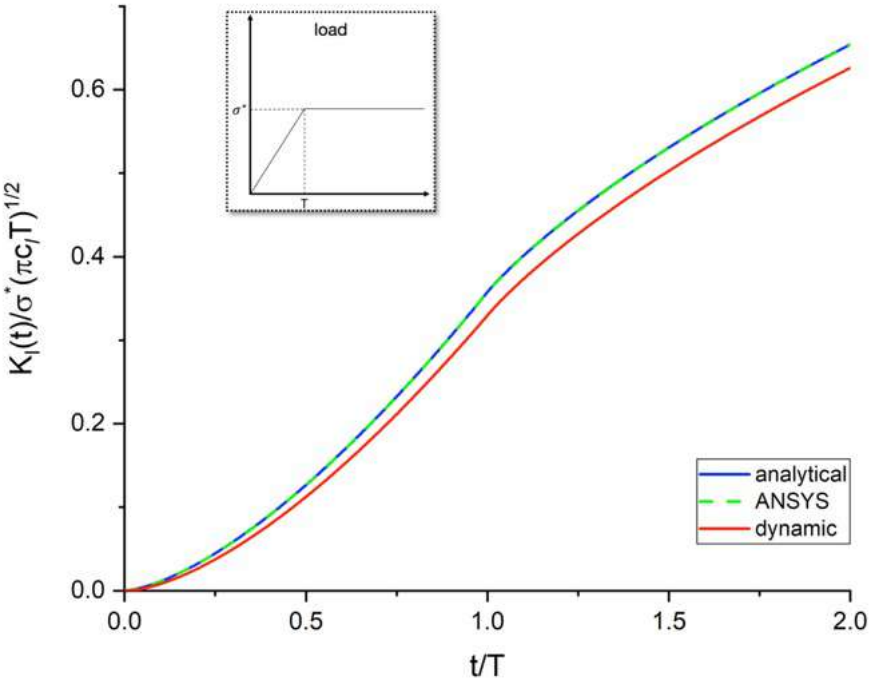

Fig. 4.5. Comparison of analytical solution for $K_I(t)$ dependence with numerical results. Red curve represents values obtained using the developed numerical scheme.

4.3 Instability of SIF for moving cracks

Paper [82] presents experimental data on dynamic crack propagation in Araldite B specimens of three types: double cantilever beam (DCB), single edge notches specimen (SEN) and a mixed type specimen. In order to measure stress intensity factor for a moving crack, method of caustics was used. In addition to this, crack tip position was registered and thus crack velocity could be assessed. All specimens had an artificial initial crack, which started to grow due to wedge loading. Shape and dimensions of the investigated specimens are shown in figure 4.6.

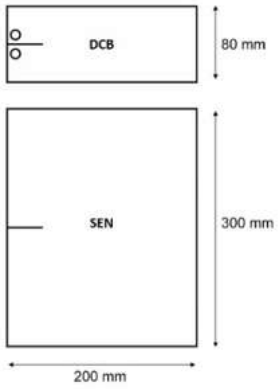

Fig. 4.6. Geometry of specimens studied in [82].

Material properties for the simulations were taken from [163]. Incubation time is still not available for Araldite B and value 1.1 μs was used.

Results of the performed calculations together with experimental points from [82] are shown in figure 4.7. Since time and spatial integration in (1.6) provide possibility to account for history of stresses and therefore consider the processes, which precede minimal crack expansion, numerically obtained crack velocities match experimental values. Good coincidence of experimental and numerical $K_I - \dot{a}$ data was achieved, especially for high crack velocity regimes, which are the most representative for the studied problem. It is important to stress, that material properties for both DCB and SEN samples were identical.

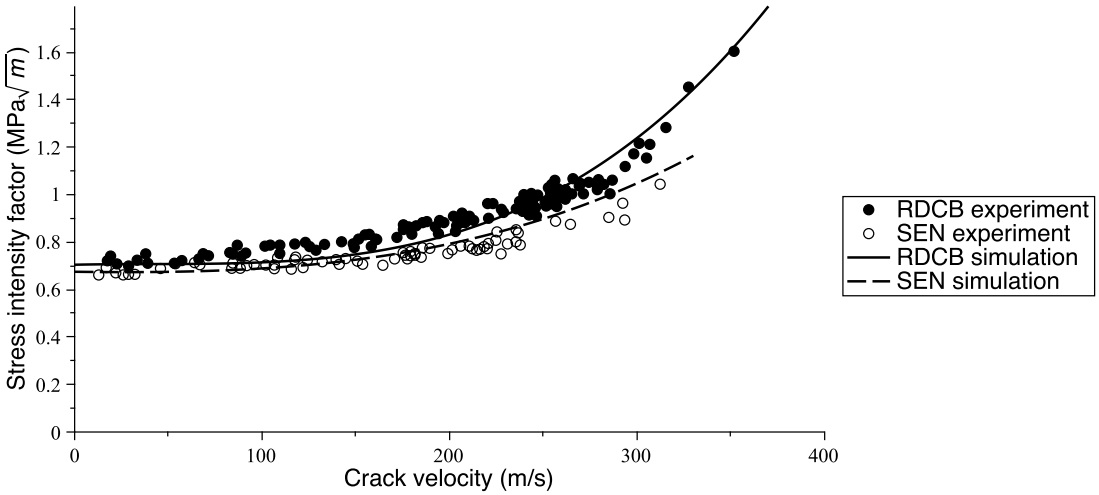

Fig. 4.7. Stress intensity factor – crack velocity dependence for DCB and SEN samples. Experimental data from [82] and the simulation results.

According to works by Ravi-Chandar and Knauss [70] a wide range of stress intensity factor values can correspond to a crack, moving with a constant velocity for the case of dynamic loading by uniform pulse pressure applied to the crack faces. On the contrary, slow or quasistatic loading resulted in a well-established $K_I - \dot{a}$ dependence. In order to study these two cases, crack propagation process was simulated for a model material with properties similar to PMMA properties. For both studies samples had a square shape with a 200 mm side. Quasistatic case was implemented using application of slow displacement to the corners of the crack faces and pulse loading was applied to whole area of the crack faces representing Ravi-Chandar and Knauss loading scheme. Figure 4.8 shows numerically obtained values of the $K_I - \dot{a}$ dependence together with the loading schemes.

Both scatter results (separate vertical bars of the K_I values for a discrete set of the crack velocities) and fitting are shown on the SIF – velocity graph in figure 4.8a. According to the incubation time approach, crack propagates with finite increments, which equal d and transient solution implies a particular value of the solution time step. This way, crack velocity obtains discrete values, as the crack tip remains for a number of time steps in a certain node and then travels the d distance, when (1.6) holds. Such numerical discretization qualitatively reflects experimentally observed data on incremental crack propagation, since discontinuous crack tip trajectories were observed experimentally (see e.g. [164]). Fitting of the scatter data was performed in order to obtain classic shape of the $K_I - \dot{a}$ curve for the quasistatically loaded samples presented in figure 4.8a. The same fitting procedure was also utilized in simulation of Kalthoff's tests for the DCB and SEN samples in figure 4.7.

Figure 4.8b shows only scatter data, as fitting for this loading scheme is inapplicable and thus no classic $K_I - \dot{a}$ can be obtained for the case. Faces of the initial crack were loaded with a trapezoidal pressure pulse. Amplitude and shape of the pulse were adjusted in order to initiate the crack movement during pressure growth time interval. Only several crack velocity values were observed in course of this simulation and a wide range of the SIF values correspond to each of them. This corresponds to

experimental results, obtained by Ravi-Chandar and Knauss [1,69-71] and thus, both quasistatic and dynamic loading cases were obtained using numerical simulation and incubation time model with equal shape of the samples and equal material properties. Mesh size variation does not affect this result as it has been seen from the mesh sensitivity testing: the crack velocity value set changed slightly, however the K_I scattering remained.

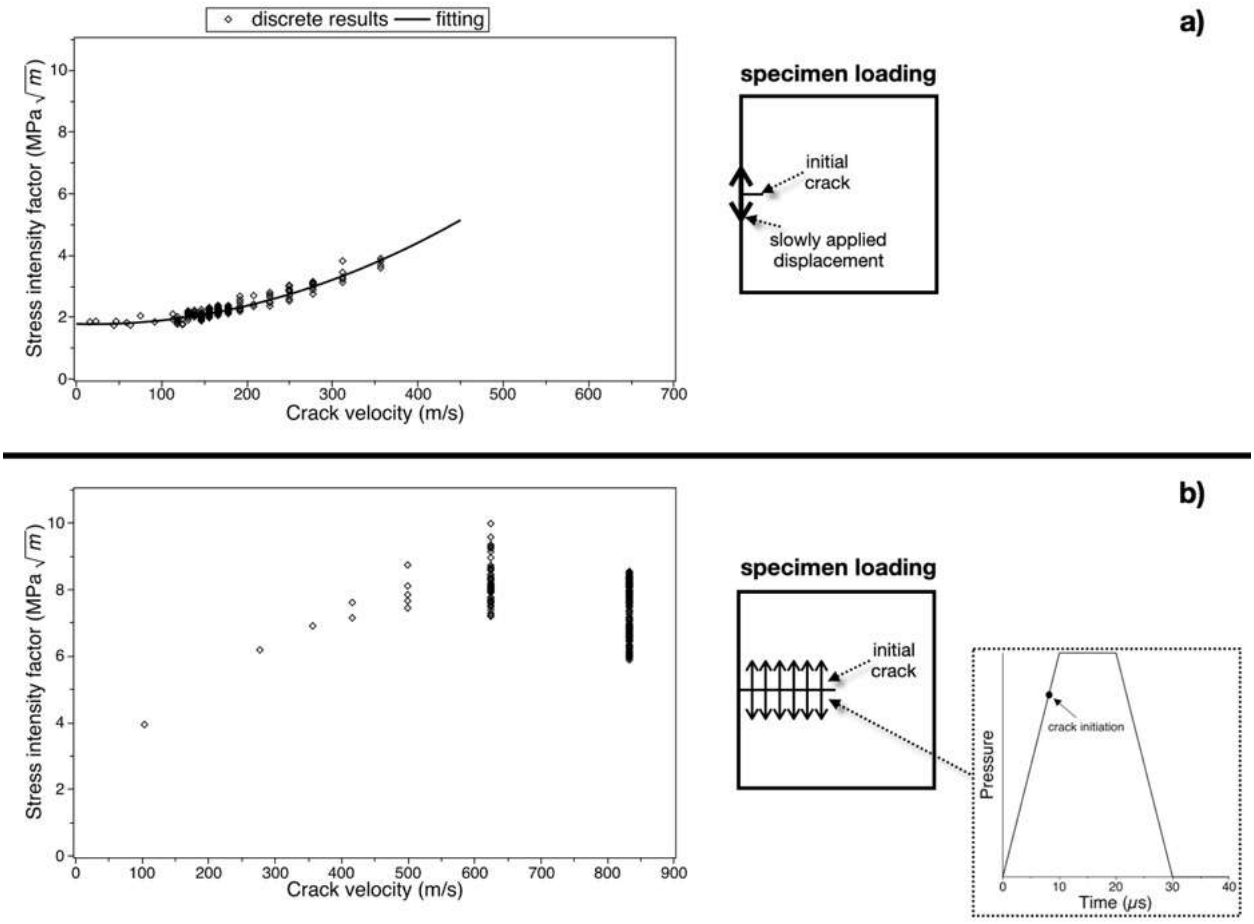

Fig. 4.8. SIF – crack velocity dependencies for a model material for two loading cases; a – quasistatic splitting of the crack faces, b – pulse loading of the crack faces.

4.4 Crack velocity oscillations

As noted above, the dynamic crack propagation can be accompanied by unstable behavior of the characteristics and dependencies describing this process. The SIF

variation effect at relatively high crack velocities considered in the previous section is an example of such instabilities. This section is devoted to the numerical study of the effect of crack velocity oscillations, which has been observed in a number of experimental works (see, for example, [15,16,164,165].

In [16], the propagation of cracks in PMMA plates due to displacements applied to the upper and lower boundaries of the samples was investigated. The authors of [16] recorded the position of the crack tip and the current crack velocity. At the same time, the authors discovered considerable fluctuations in the crack velocity.

Figure 4.9 shows experimental data from [16], as well as the results of calculations using criterion (1.6). The choice of the characteristic size $d = 0.2$ mm according to the formula $d = 2K_{Ic}^2/\pi\sigma_c^2$ allows one to numerically obtain crack velocity oscillations with the amplitudes corresponding well to the experimentally observed phenomenon.

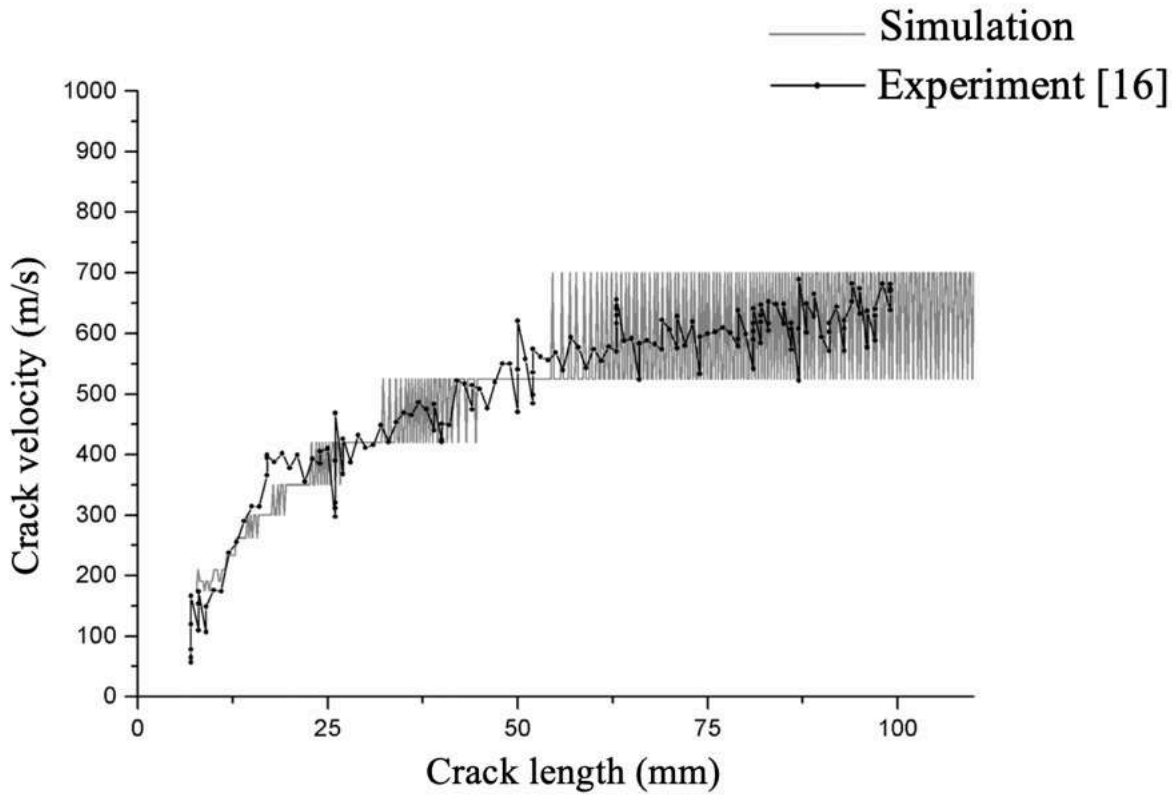

Fig. 4.9. Crack velocity oscillations. Experimental data from [16] and the simulation results.

In [15], the results on experimental and numerical studies of the dynamic crack propagation in PMMA samples are presented (experimental studies were conducted by I.V. Smirnov). The application of the developed numerical approach, made it possible to obtain a fairly accurate correspondence between the numerical results and experimental data. For example, the dependence of the crack length on time almost completely coincides with the experimental curve (figure 4.10). Some discrepancy is observed in the crack acceleration – in the experiment, the crack velocity reaches a constant value faster.

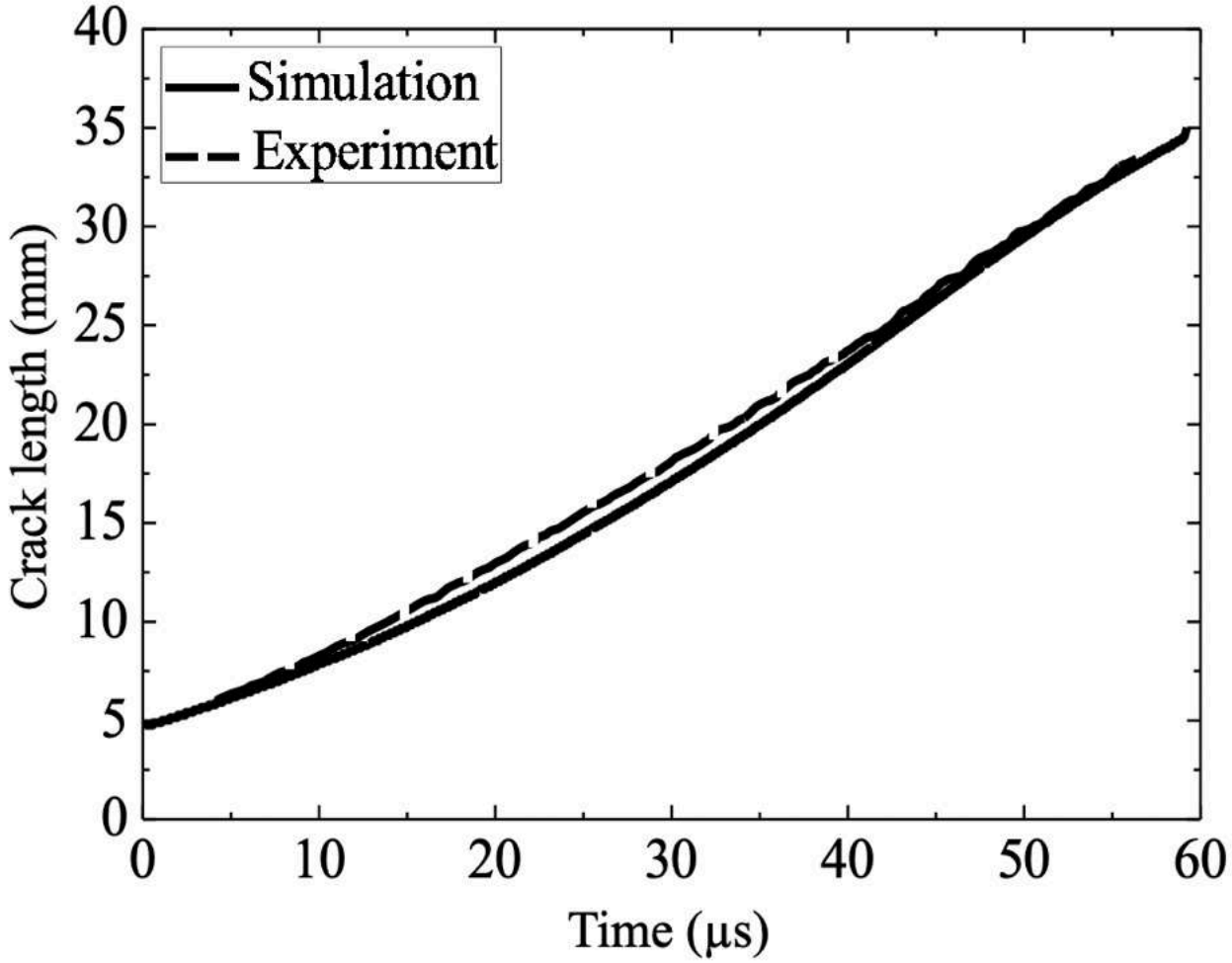

Fig 4.10. The dependence of the crack length on time. The experiment and processing of the experimental results were carried out by I.V. Smirnov.

The stages of the numerical simulation are shown in Figure 4.11: the evolution of the stress field (σ_{22} component) and the crack advancement due to the removal of constraints from the node in which the condition (1.6) was fulfilled.

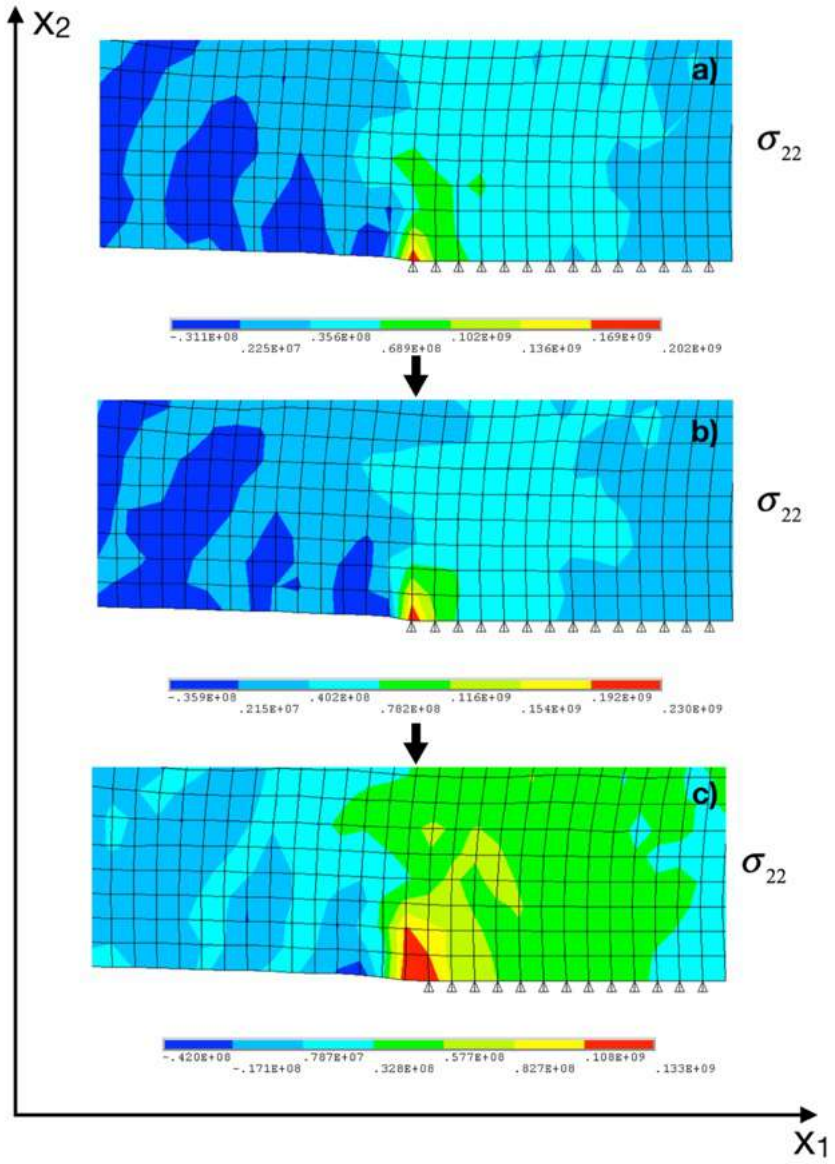

Fig. 4.11. The crack propagation process: the development of a stress state in the vicinity of the crack (a, b) and the subsequent shift of the crack tip to the next node (removal of the constraint in the node) when condition (1.6) is fulfilled (c).

For the experiments carried out in [15], it was also possible to numerically study the crack velocity oscillations. The numerically obtained amplitudes of crack velocity oscillations fit into the experimentally obtained values (Figure 4.12).

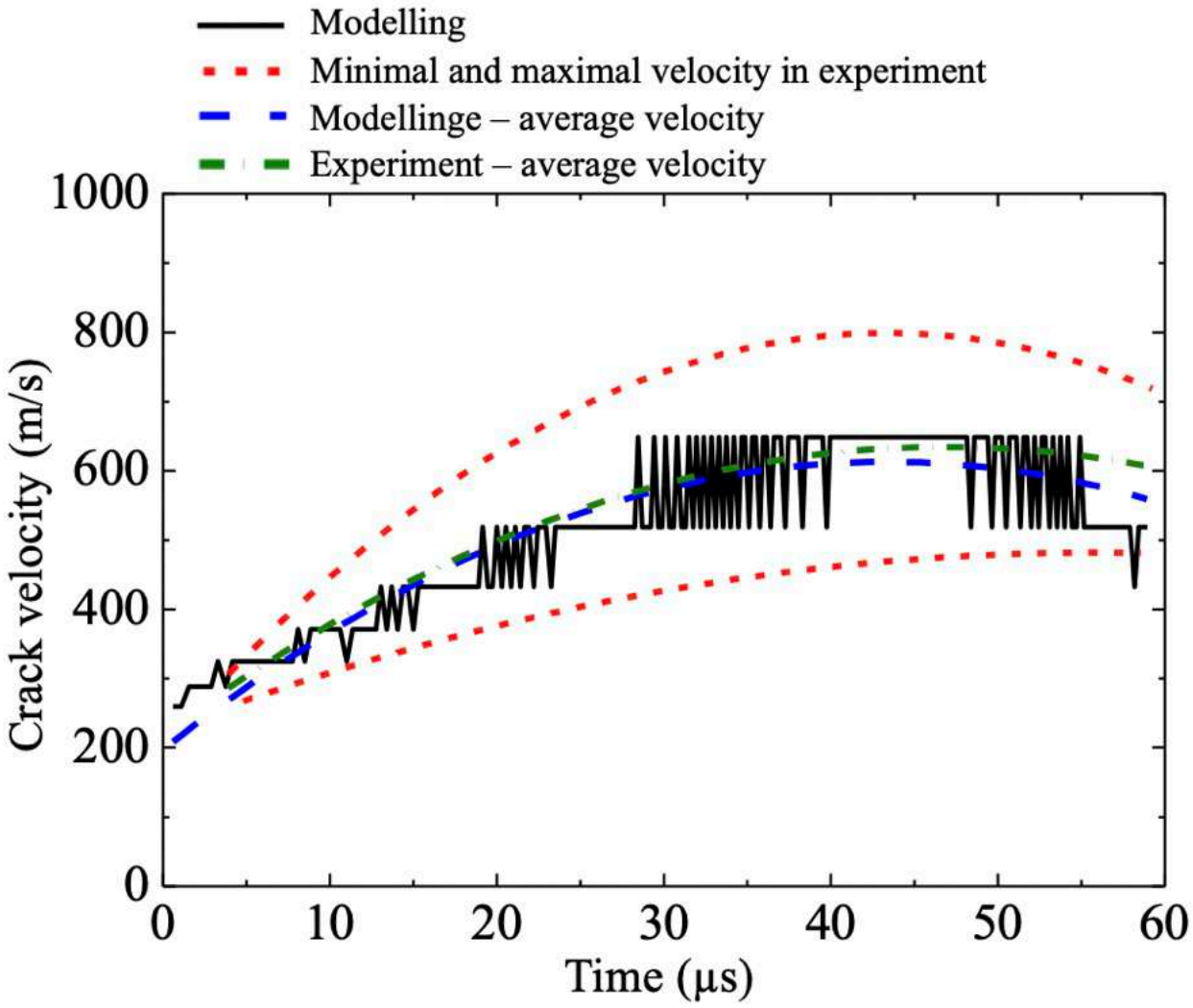

Fig. 4.12. The dependence of the crack velocity on time. 1 – the crack velocity according to modeling; 2 – the smoothed upper and lower bounds of the crack velocities oscillations observed in the experiment; 3 – the average crack velocity according to modeling; 4 – the average crack velocity from the experiment. The experiment and the data processing were carried out by I.V. Smirnov

4.5 The propagation of multiple cracks with arbitrary directions. Dynamic fragmentation

Studies of the dynamic fracture under impact loading conditions lets one investigate transition between the fracture scale levels. In fact, application of the incubation time fracture model for the crack propagation modelling makes it possible to describe this transition. According to criterion (1.6), the fracture scale is defined by

the linear size d, which determines the minimum characteristic size of the zone of recorded destruction. Thus, the propagation of the main crack is a set of discrete increments with a characteristic size d, and in fact, the propagation of the crack is the result of the evolution of the fracture from the scale level characterized by parameter d to the next larger scale level. In the case of the penetration or impact problems, the analogue of such a transition is the fragmentation of the barrier: fracture at a d-sized scale leads to the formation of larger fragments, which can be interpreted as the transition of the fracture process to a larger scale level.

This section presents the results of numerical modeling of the dynamic fragmentation processes observed in brittle materials and the study of the characteristics of this process. In order to study the dynamic fragmentation, a two-dimensional numerical scheme based on FEM and the incubation time criterion has been developed. It is worth noting that in this scheme uses another implementation of fracture compared to the approach developed in the fifth Chapter.

The model problem of penetration of round ceramic barriers by steel cylindrical strikers is considered in the section. The mechanical properties of Al2O3 and ZrO2(Y2O3) ceramics have been used (Table 4.1 [166-168]). Both materials (ceramic target and steel impactor) are considered to be elastic. The target has the following dimensions: a diameter of 100 mm and a thickness of 10 mm, while the length of the steel impactor is 100 mm and the diameter is 10 mm. The developed numerical scheme is based on the finite element method in a two-dimensional axisymmetric formulation with implicit time integration. The ANSYS solver was used to calculate the stress-strain state, and external control procedures were developed to implement criterion (1.6) and to control the solution progress. Figure 4.13 shows a part of the finite element mesh and the complete model with the symmetry extension applied.

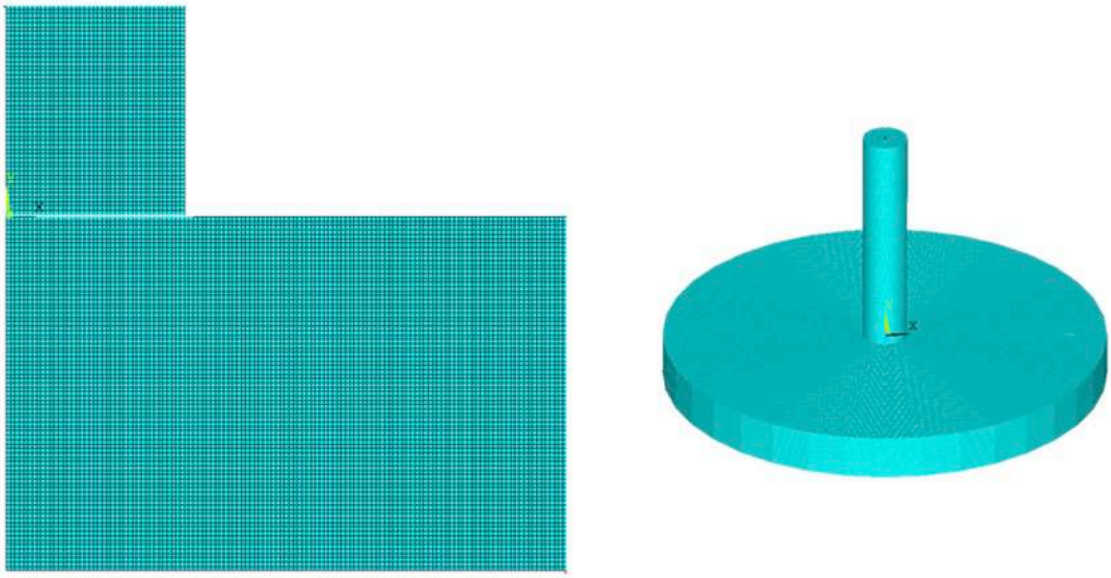

Fig. 4.13. Part of the finite element mesh (contact zone) and full model with symmetry expansion applied.

	Al2O3	ZrO2(Y2O3)	Steel projectile
Young's modulus, E, GPa	366	200	200
Poisson's ratio, ν	0.21	0.25	0.25
Density, ρ, kg/m^3	3880	6000	7860
Ultimate stress, σ_c, MPa	260	750	–
Incubation time, τ, μs	1	1	–

Table 4.1. Mechanical properties of the materials used in the calculations.

The mesh for the finite element solution was constructed manually for the studied problem. Elements do not share nodes, however nodes with equal coordinates have coupled degrees of freedom acting as a single node. This restriction is maintained until the condition (1.6) holds. When fracture occurs according to (1.6), nodes are decoupled and elements are separated leading to the fracture surface generation (see figure 4.14). Since the axial symmetry is applied, each crack contributes to the total fracture surface area (S) according to equation $S = S + 4d * 2\pi R$, where R is distance between the crack and the symmetry axis.

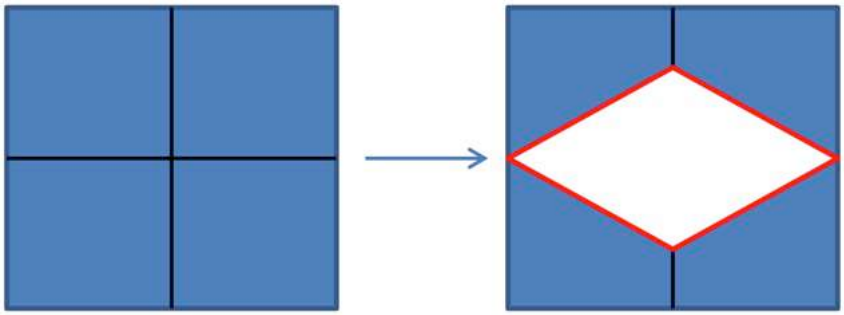

Fig. 4.14. Decoupling of the matching nodes and fracture surface generation.

Element size equals d and thus minimal fracture increment is also d which lies within the incubation time approach framework. The solution time step is chosen to be smaller than the time needed for the fastest wave to travel the d distance.

In order to investigate fragmentation of the ceramic targets a separate program was developed. The finite element mesh is regarded as a graph with the mesh elements being nodes of the graph. This way, separate fragments of the target are connected components of the element graph.

Dynamic fragmentation modelling results

Fracture surface area. This section presents results of the fracture surface area calculations. Figure 4.15 shows typical evolution of the fracture surface are on time: abrupt growth of the surface area indicates active cracking of the sample and the fracture surface area value reaches its maximum and stops growing when the fracture process is completed.

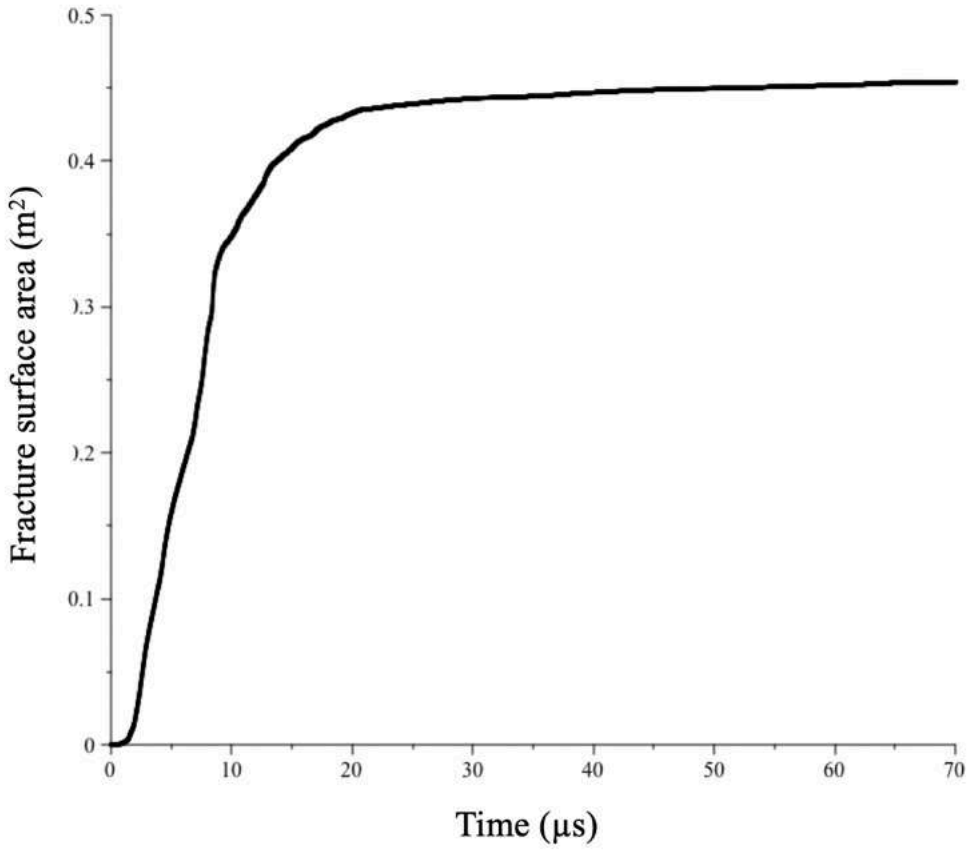

Fig. 4.15. Fracture surface area evolution. The data for the Al2O3 target and 350 m/s impactor velocity is presented.

The computations were made with 1 μs incubation time parameter for the both materials. The dependence of the fracture surface area on the impactor velocity is shown in figure. 4.16. For the studied regimes the fracture surface area increases with the growing impactor velocity for the Al2O3 material. However, the results stabilize for the ZrO2(Y2O3) ceramics. This might indicate that maximal level of energy absorption has been reached by the dynamic fracture process.

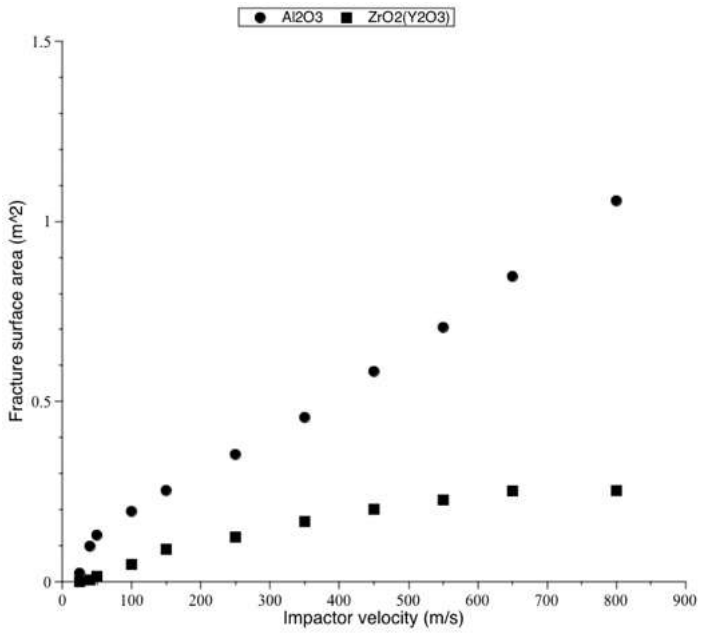

Fig. 4.16. Fracture surface area versus impactor velocity dependence.

Residual impactor velocity. In figure 4.14 dependence of the residual impactor velocity on the initial velocity is presented. Negative residual velocities indicate that the impactor did not penetrate the target and was repulsed from it. For the both materials residual impactor velocity depends linearly on the initial impactor velocity when target is penetrated. In general, the ZrO2(Y2O3) ceramics demonstrated much better ballistic performance with a much higher limit velocity (around 380 m/s) comparing to around 80 m/s for the Al2O3 target. For all the computations in this section 1 μs incubation time was used.

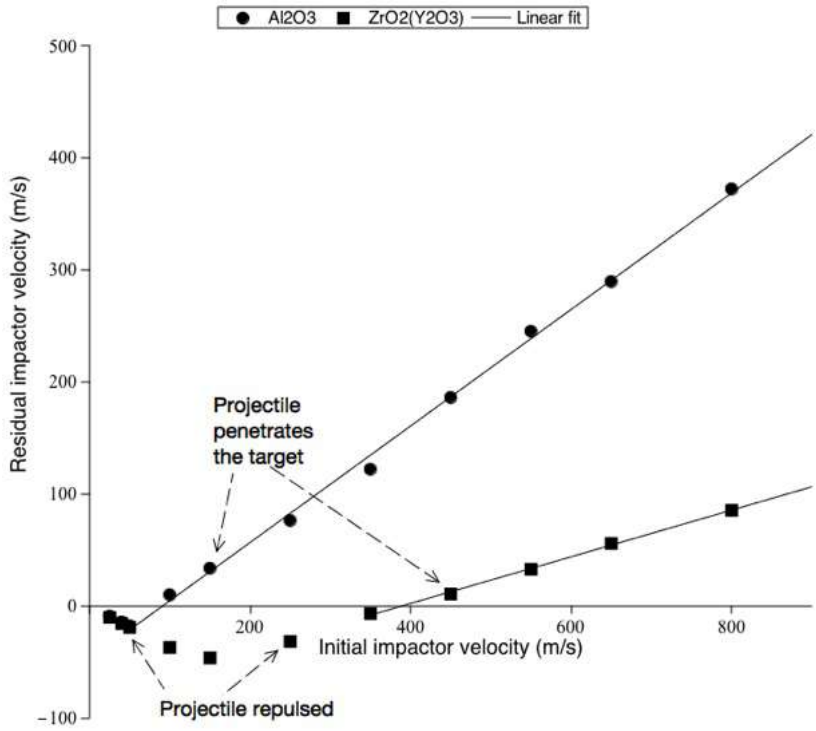

Fig. 4.17. Residual impactor velocity versus initial impactor velocity.

Dynamic fragmentation. Number of fragments. Figure 4.18 presents dependence of the total number of fragments on the impactor velocity. Higher impactor velocities result in a more extensive target fragmentation and higher total number of fragments. This result naturally correlates with the fracture surface are – impactor velocity dependence (figure 4.16): here number of fragments remains almost constant for the 800 m/s impactor velocity comparing to the value obtained for the 700 m/s velocity.

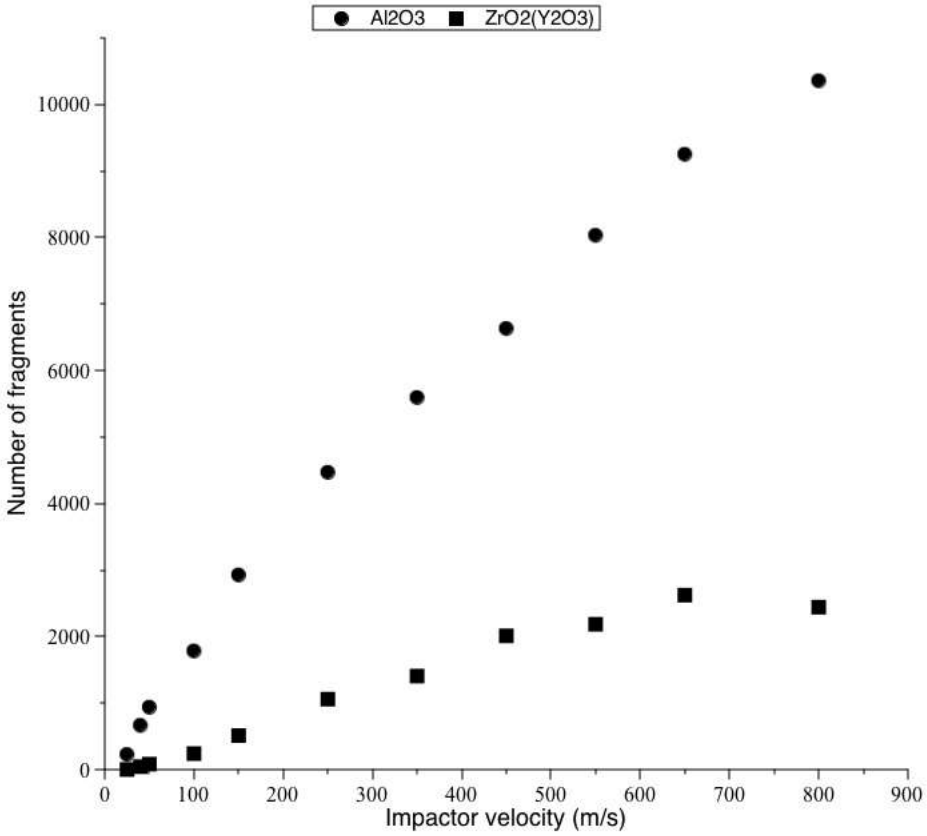

Fig. 4.18. Number of fragments versus impactor velocity.

Dynamic fragmentation. Fragment size distribution. In this section distributions of the fragments are studied. Cumulative size fraction of fragments of all the fragment sizes is presented using logarithmic scale axes. Size of a fragment is measured as the number of elements it consists of. Experimental investigations of the dynamic fragmentation process usually reveal power law distribution of the fragments [89]. The power law approximation (a straight line if logarithmic coordinates are used) works reasonably well for the small fragment region of the distribution, while discrepancies can be encountered for the larger fragments. Figure 4.19 shows fragment size distribution reprinted from work [169], where the above-mentioned trend can be observed.

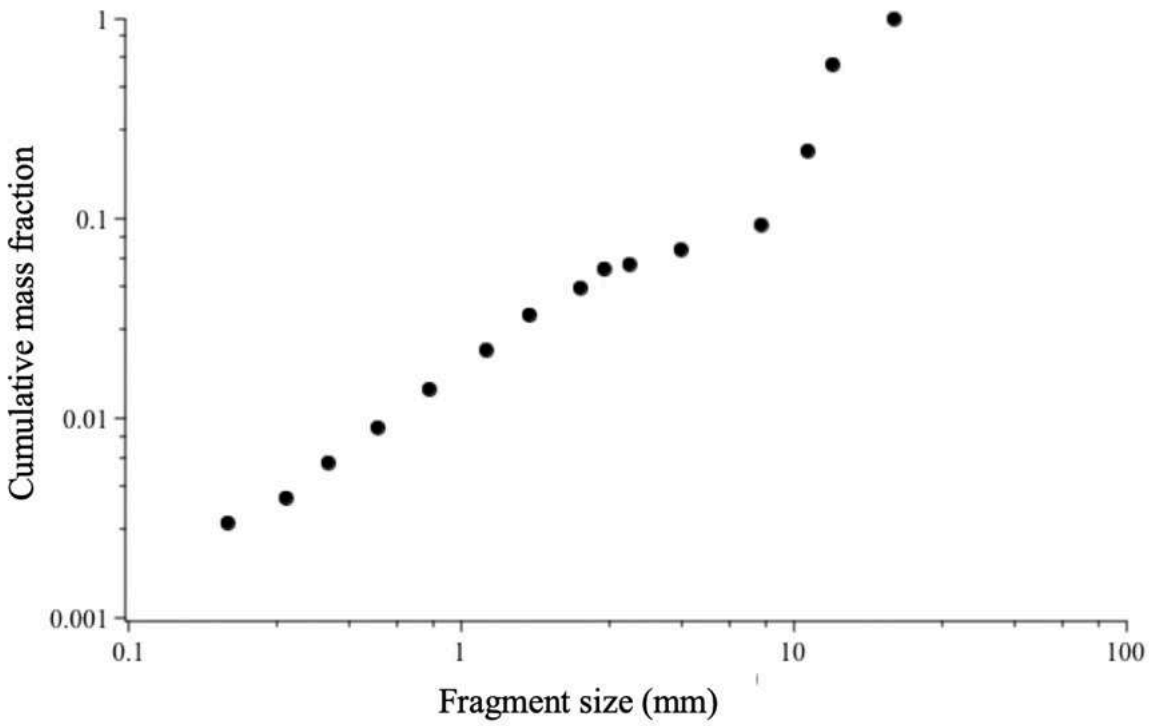

Fig. 4.19. Experimentally observed fragmentation of glass. The figure is reprinted from work [169].

The obtained numerical results qualitatively resemble experimental data – straight lines are observed for smaller fragments with different behavior for medium and larger fragments. It appears that fragments with particular sizes contribute less comparing to the other fragment sizes. Figure 4.20 presents typical distributions of the fragments for both materials and 350 m/s impactor velocity. Corresponding fragmentation patterns, showing fragments distinguished by color (excepting for the smallest one-element fragments which are all colored in black) are shown below each graph.

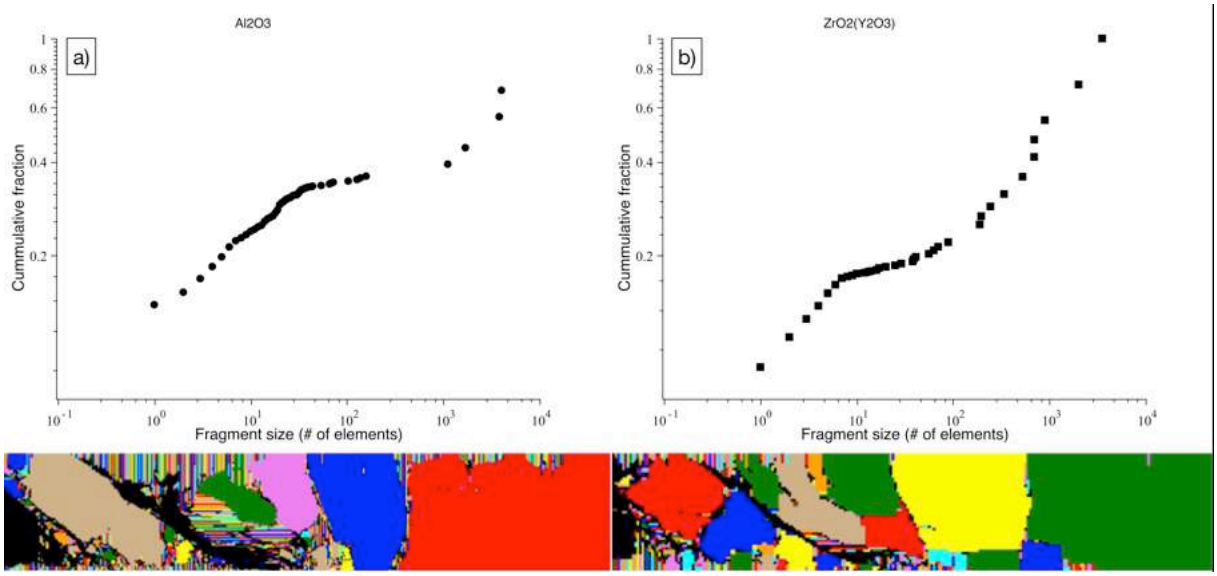

Fig. 4.20. Cumulative distribution of the fragment sizes and corresponding fragmentation patterns; a) – Al2O3, b) – ZrO2. Left edge of the of the presented fragmentation patterns coincides with the target symmetry axis.

4.6 Chapter 4 conclusions

The 4th Chapter discusses nonstationary effects accompanying the dynamic crack propagation in brittle materials. Numerical studies were carried out using the finite element method and the incubation time fracture criterion. The incubation time fracture model implies spatial and time discretization of the fracture process, since, the minimal volume of the fracture material is introduced (in the case of crack movement, the minimum possible crack advancement), as well as the characteristic fracture time – the incubation time.

Discretization of the fracture process within the framework of the incubation time approach allows one to obtain a number of fundamental results consistent with experiments. Firstly, the introduction of a minimum crack advancement provides possibility to numerically investigate the unsteady behavior of the velocity of a moving crack: for example, the experimentally observed oscillations of the crack velocity propagating in PMMA plates under quasi-static loading were obtained. The amplitude

of the crack velocity oscillations obtained by the calculations coincides well with the experimental values.

In addition to this, the use of the incubation time approach made it possible to investigate the problem of uniqueness of the dependence of the stress intensity coefficient on the crack velocity ($K_I - \dot{a}$ dependence). Due to the discrete nature of crack propagation according to the incubation time and FEM, there is a noticeable variation in the values of SIF corresponding to the selected values of the crack velocity. At the same time, the scatter of the SIF values for the case of quasi-static loading is relatively small, and the classical $K_I - \dot{a}$ dependence can be constructed "on average". In the case of high-speed loading, a significant SIF scatter prohibits the construction of such a dependence: the crack can move at an almost constant speed, whereas the intensity coefficient corresponding to its value varies within a wide range. This behavior corresponds to the experiments [70,71].

Thus, on the one hand, application of the incubation time approach allows us to resolve the contradictions that have arisen regarding the uniqueness of the $K_I - \dot{a}$ dependence for a given material, and on the other hand, to simulate fracture without an a priori given $K_I - \dot{a}$ relation. This determines the significant advantage of the developed approach compared to the traditional ones, since the experimental determination of the SIF-crack velocity dependence is a very time–consuming process leading to ambiguous results.

More information can be found in [14,15,86,87,88,183,184,186,187,188,190].

Chapter 5. Incubation time approach for impact problems

The fifth Chapter presents experimental and numerical results on dynamic fracture of PMMA plates subjected to impact loading. The experimental tests were conducted using steel cylinder-shaped projectile accelerated using a gas gun. In order to evaluate performance of the tested specimens, residual impactor velocity was assessed using high-speed photography setup. Square-shaped PMMA specimens with three thicknesses were investigated using various projectile velocities. For all the three specimen types the ballistic limits were experimentally obtained. The conducted experiments were numerically simulated using finite element method with explicit time integration scheme and incubation time fracture model for the material failure prediction. Experiments with all three specimen configurations were successfully simulated using one parameter – incubation time, which was evaluated from existing experimental data on the dynamic fracture of PMMA. In addition to the simulations of the real experiments estimates on performance of a sample with a virtual geometry were made using the developed numerical approach.

Moreover, the fifth Chapter presents an approach to overcome difficulties which are typical for the impact problems – high demands on computing resources and potential numerical instabilities arising from high stresses in the contact zone and high strain rates. The approach is based on the use of artificial neural networks (ANNs) trained on arrays of numerical results. Performance of the approach is demonstrated using the problem of impact of perforated barriers.

5.1 The incubation time approach for numerical simulations of impact fracture

This section is devoted to experimental and numerical studies of dynamic fracture under impact loading conditions, namely, modeling the penetration of obstacles by impactors. Experimental studies were carried out using a gas gun and

high-speed filming equipment. The modeling is carried out using the finite element method (FEM) and the incubation time fracture criterion.

Experiments

Square (100mm x 100mm) PMMA plates with three thicknesses (4 mm, 6 mm and 10 mm) were studied. The sample was clamped in a four-arm holder (see figure 5.1)

Fig. 5.1. The sample mounting device: four grips fixing the specimen.

In order to conduct impact tests a gas gun experimental facility was used. The setup is schematically shown in figure 5.2. The initial projectile velocity was controlled by air pressure in the system and appropriate choice of the membranes placed in the gun shatter. Two membranes were used in the shatter and each could sustain half of the operating pressure. Due to pressure drop in the auxiliary pressure chamber the membranes broke and the projectile started to move through the barrel. The initial velocity was measured using a magnetic coil placed at the exit end of the barrel, while the residual impactor velocity was evaluated using HSFC pro high-speed photography equipment, produced by PCO AG. This setup consists of four Dicam pro modules, which provide possibility to capture eight frames with a variable time interval. For almost all the experiments 150 μs inter-frame time interval.

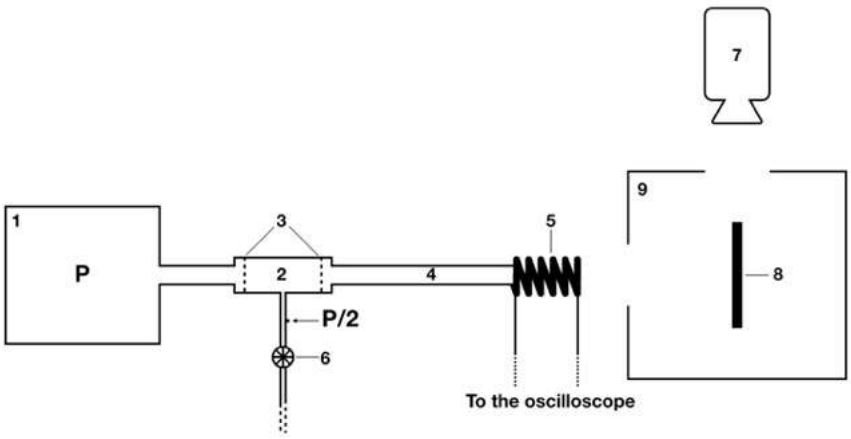

Fig. 5.2. Scheme of the experimental setup; 1 – high pressure chamber, 2 – shatter device, 3 – membranes, 4 – barrel, 5 magnetic coil for the impactor velocity measurements, 6 – pressure drop valve to trigger a shot, 7 – high-speed camera rig, 8 – sample, 9 – protection chamber; P indicates pressure.

Steel cylindrical impactor (diameter 6.9 mm, length 30 mm and mass 8.7 grams) was accelerated to velocities ranging from 40 m/s to 350 m/s. The impactor was placed in a disposable aluminum bed which fitted precisely the gun barrel. The bed was stopped by a barrier at the end of the barrel and the impactor continued to move leaving the bed. The contact between the bed and the barrier caused linkage of the electrical circuit and enabled triggering the high-speed photography setup with a programmable time delay.

Numerical scheme

The developed modelling procedure is based on the finite element method and he incubation time fracture model. The LS-DYNA software was used as a solver. The incubation time approach has been discussed section 1.3.

According to the incubation time model the fracture at point x and time moment $t$takes place if:

$$\frac{1}{\tau}\int_{t-\tau}^{t}\frac{1}{d}\int_{x-d}^{x}\sigma(x',t')dx'dt' \geq \sigma_c \qquad (5.1),$$

where $\sigma(x,t)$ is a time-dependent stress at point x, σ_c is the material static ultimate tensile stress and τ stands for the incubation time.

The left side of inequality (5.1) contains integration over time and thus history of the stresses is accounted for. The microscopic fracture processes are supposed to develop due to these stresses and specific time τ is needed for the macroscopic fracture to evolve. The fracture is non-local and occurs at the areas splitting the considered *d*-sized volume in two parts.

The incubation time parameter τ can be evaluated from experiments on dynamic fracture. In order to calculate the incubation time value, one should register fracture initiation time and the stress – time dependence in the point of interest. The stress – time function is then substituted to formula (5.1) and τ is evaluated as a fitting parameter so that fracture occurs at the registered fracture initiation time. Experiments on spallation or dynamic crack initiation can be used to obtain the incubation time value. It should be noted here that an adequate choice of the fracture scale level is crucial for the sake of the simulation correctness. One should define fracture scale level to be considered in the studied problem and then use an appropriate τ value, which was measured on an appropriate scale level. For a more detailed discussion on the fracture scales please refer to the work presented in [170].

The incubation time fracture criterion was implemented via user defined material (UMAT41 routine) in the LS-DYNA code. Evolution of stresses for each element is stored in additional array parameter and time integral in the inequality (5.1) is computed according to the trapezoidal integration rule. The element size equals linear size d used in the incubation time fracture condition (5.1) and element deletion technique is implemented in order to simulate the fracture development. This scheme fits perfectly the incubation time approach since the minimal characteristic size of a fractured region equals d. Mesh sensitivity testing revealed that further reduction of the element size does not affect the computation results. fully integrated (with 8 integration points) solid element was found to be the most robust in terms of stability

of the numerical simulation. The finite element mesh is shown in figure 5.3. The problem is solved in a three-dimensional statement and the boundary conditions are satisfied due to displacement restrictions imposed on the nodes lying under the holder grips (see figure 5.1).

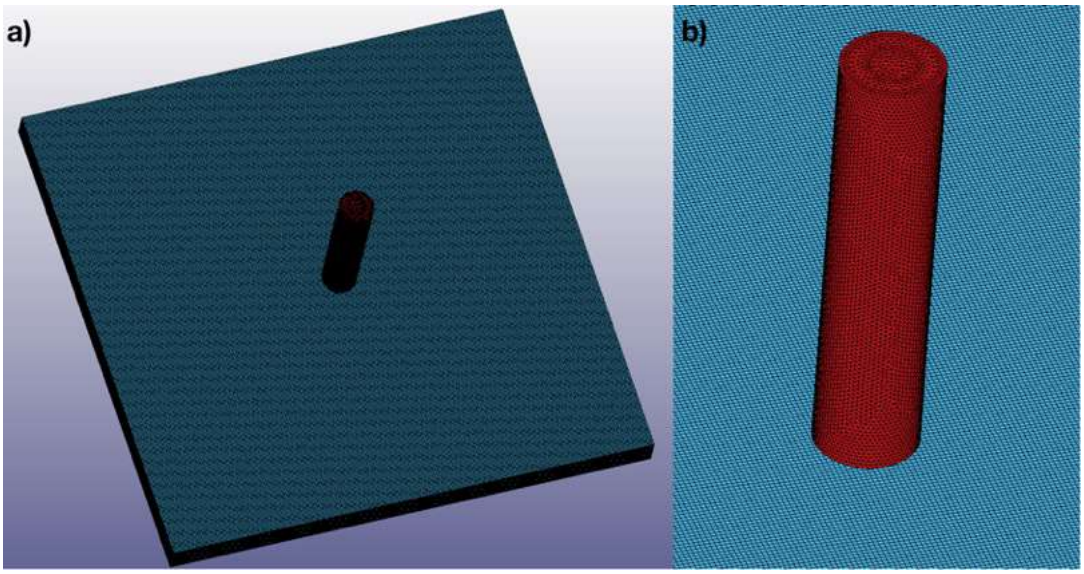

Fig. 5.3. Finite element mesh with an enlarged contact area (b). The model for a 6 mm plate is shown.

The material parameters used in the simulations are listed in Table 1. All the properties were either taken from the material information sheet supplied by the PMMA manufacturer or from elsewhere [171]. The material behavior was supposed to be governed by Hooke's law and thus two material parameters (Young's modulus and Poisson's ratio) were sufficient for the stress-strain dependency description. The incubation of 1 μs provided a good coincidence between the numerical results and the experimental data. This value is close to the PMMA incubation time for a "small" scale level (0.8 μs) calculated in [170]. According to [170] the 0.8 μs value was obtained from experiments on spallation of PMMA rods, where microcracking (small-scale fracture) was registered. Element erosion applied in our scheme can be also considered as a small-scale fracture since the element size is small comparing to the sample dimensions. way, application of a 1 μs incubation time is correct within the studied

case. The incubation time values close to 1 μs have been also used to simulate dynamic crack propagation in PMMA specimens [14,15].

	PMMA target	**Steel projectile**
Young's modulus, E, Pa	3.3e9	2.09e11
Poisson's ratio, ν	0.35	0.28
Density, ρ, kg/m^3	1180	7720
Ultimate tensile stress, σ_c, Pa	72e6	-
Ultimate stress intensity factor, K_{Ic}, MPa	1.7	-
Incubation time, τ, μs	1	-

Table 5.1. Material properties used in the numerical model.

Results

Here we provide both experimentally obtained data and results of numerical simulations using the developed scheme. Figure 5.4 shows typical set of frames from the high-speed camera obtained from the conducted tests. Frames 5-8 were used to calculate the residual projectile velocity.

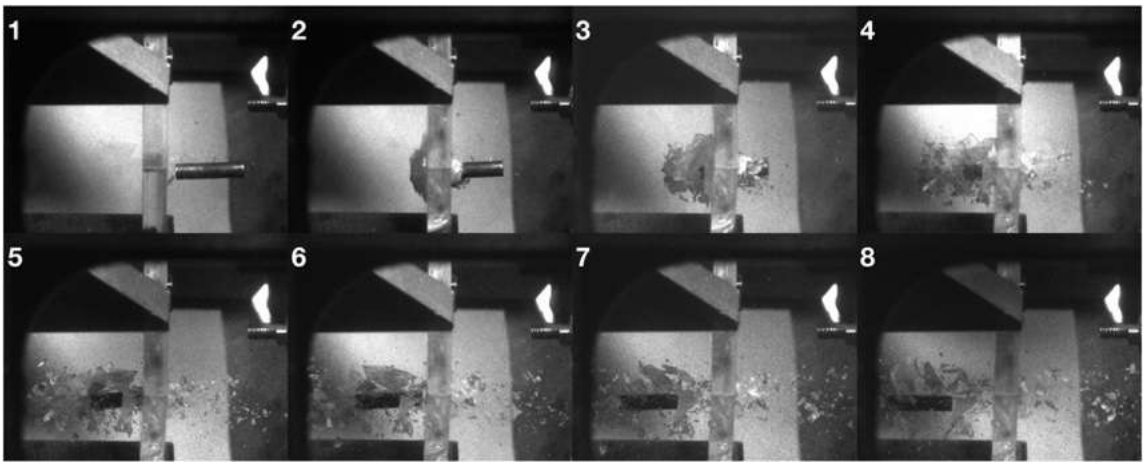

Fig. 5.4. The speed-photography frame sequence used to calculate the impactor residual velocity. 10 mm thick target and 144 m/s initial impactor velocity case depicted. Experiments were conducted with V.V. Balandin and V.V. Balandin Jr.

A typical case of a threshold impactor velocity (ballistic limit) is shown in Figure 5.5 The impactor is almost completely stopped by the target and no penetration is observed, however the target is severely damaged.

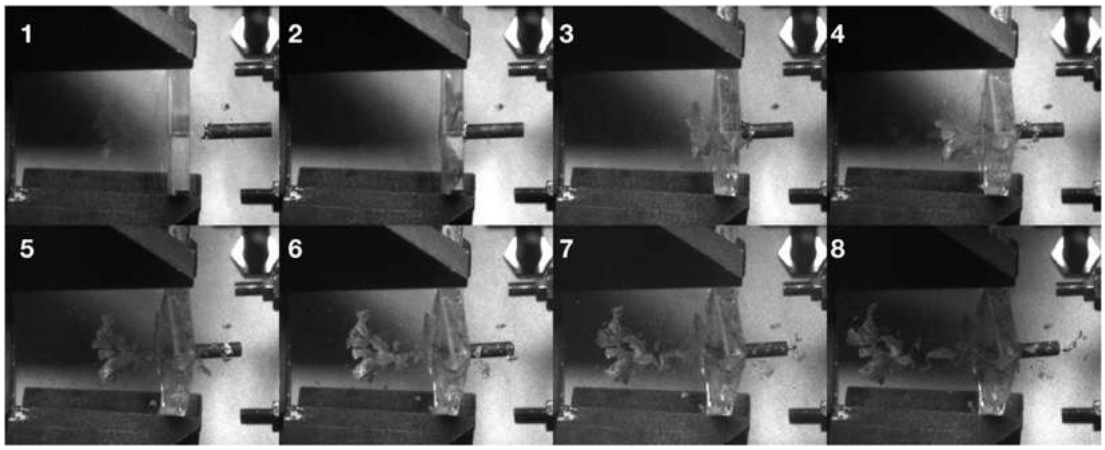

Fig. 5.5. High-speed photography of the threshold velocity impact: 10 mm plate thickness and 70 m/s impactor velocity. Experiments were conducted with V.V. Balandin and V.V. Balandin Jr.

Experimental and numerically obtained dependencies of the residual impactor velocity (V_r) on the initial impactor velocity (V_i) are shown in figure 5.6 together with the ballistic limits. The dependencies can be approximated with a straight line for middle range and high impactor velocities, while the V_r values drop abruptly in the near

ballistic limit velocity range. Some graphs of the numerical results in figure 6 contain negative V_r values, which means that the impactor bounced from the target and no penetration occurred.

The numerical results fit well the experimental data, especially for the thinner plates. In all cases the numerical model could reliably predict the ballistic limit for the studied targets. The $V_r - V_i$ dependence was numerically predicted using the model for a 5mm plate and the ballistic limit for this virtual test configuration was assessed.

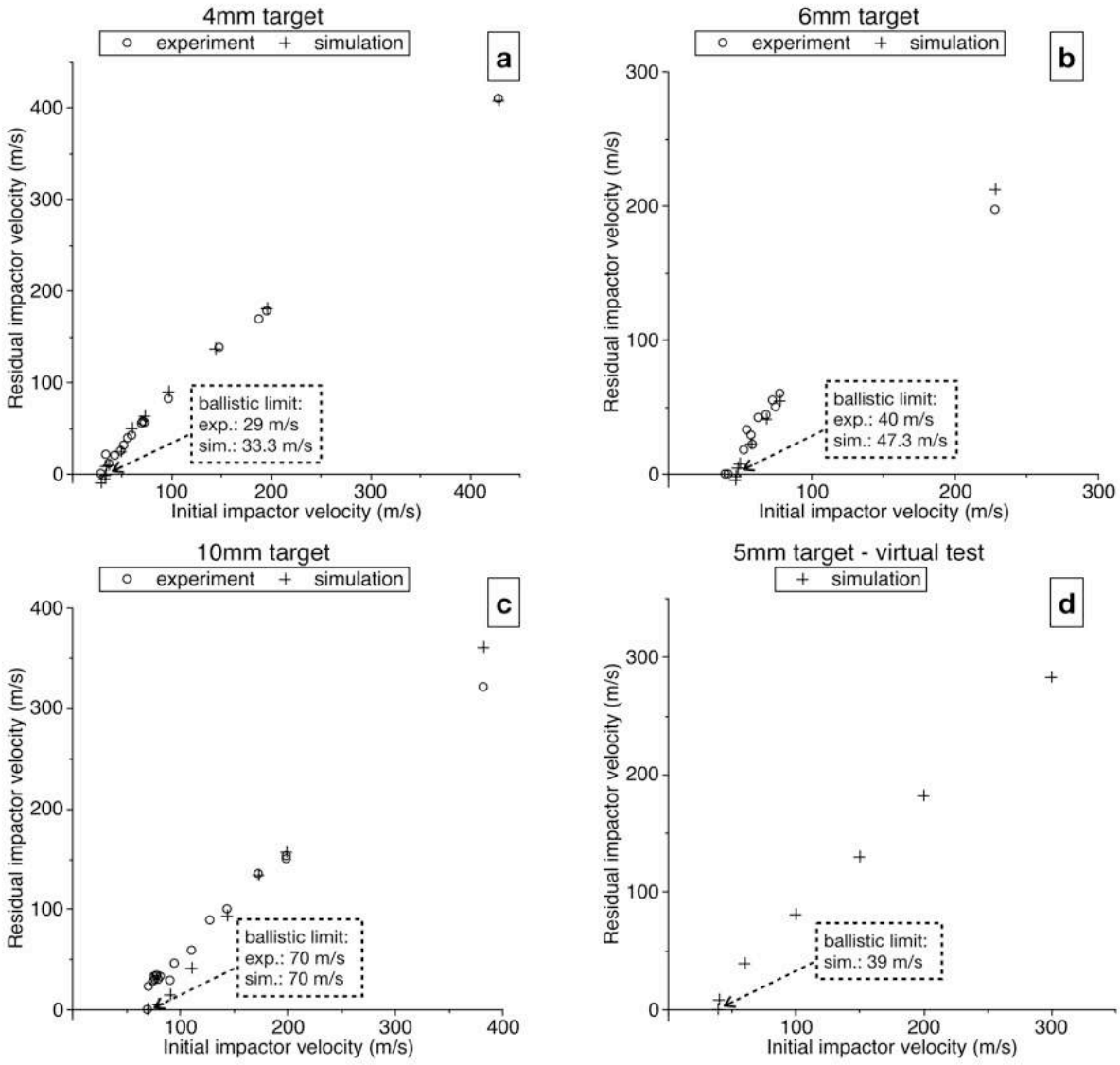

Fig. 5.6. Residual velocity – initial velocity dependencies for different specimen thicknesses; (a)-(c) comparison of the experimental and numerical data (d) a mere numerical prediction and the arrows indicate the ballistic limit.

Fig. 5.7 shows both the experimental and numerically evaluated dependencies of the ballistic limit on the specimen thickness together with the numerical prediction for a 5 mm thick plate.

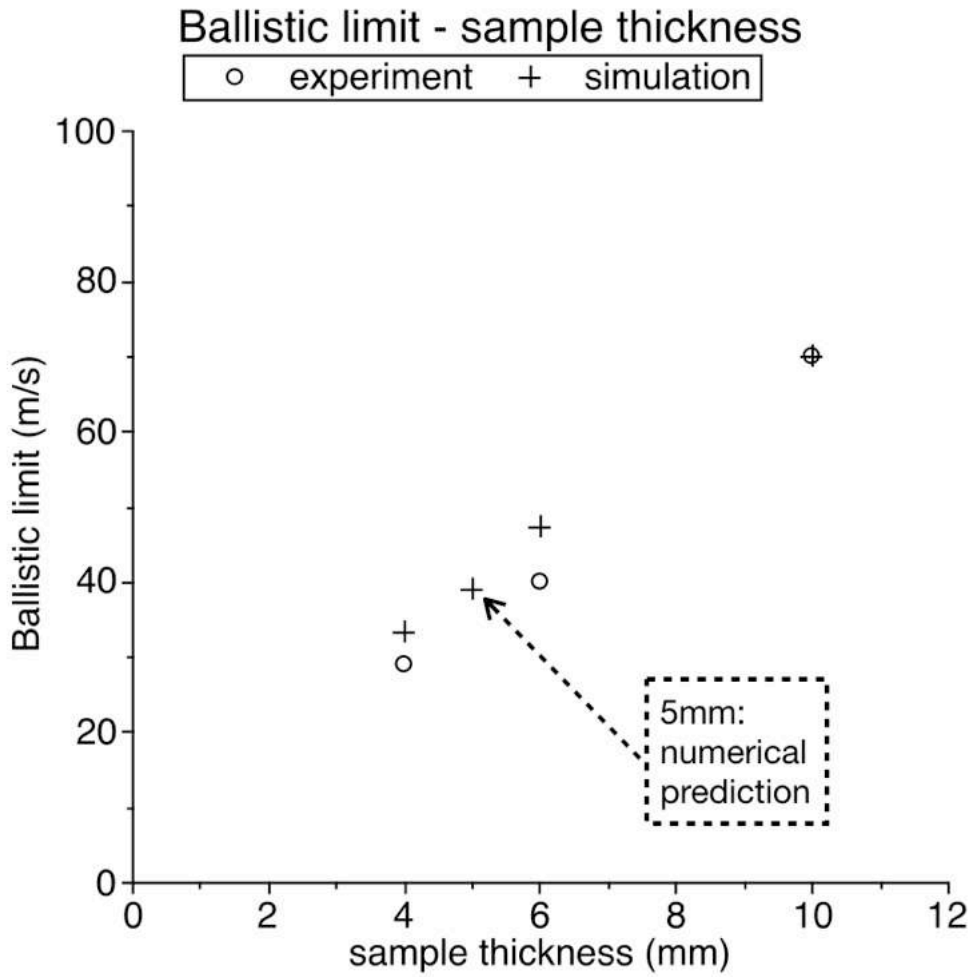

Fig. 5.7. Ballistic limit – sample thickness dependence; 5 mm point is a numerical prediction.

The numerically obtained fracture patterns generally resemble the experimental results. The impact results in crater formation and cracks propagating towards the edges of the sample. For relatively low impactor velocities the fracture pattern is similar. Higher impactor speeds result in shorter cracks comparing to the experimental results. The crack propagation trajectories are defined by the applied boundary conditions – the sample bracing in our case. The fracture patterns for relatively low impact velocities resemble those for the purely quasistatic case – cracks propagating

towards the clamps. The fracture pattern changes for the higher impactor velocities, since the effect of the fixation method is less pronounced in this case due to shorter target – projectile interaction time. Relatively short interaction times lead to concentration of the impact energy in the contact spot leading to a more localized fracture. Figure 5.8 compares numerical results and experimental fracture patterns for the 10 mm thick plate at three impact velocities including a threshold one (70 m/s).

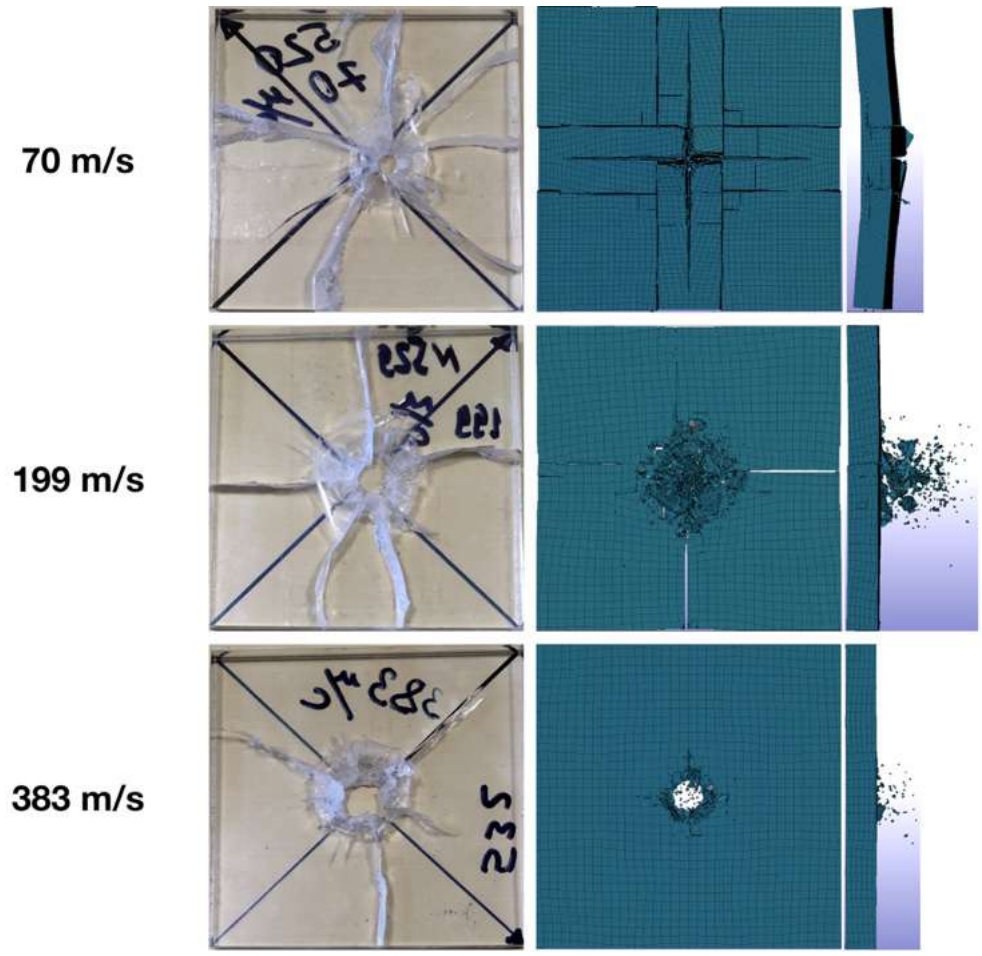

Fig. 5.8. Fracture patterns: experiment and numerical simulation; 10 mm plate results are shown.

Thus, the application of the criterion based on the concept of incubation time allowed a fairly accurate correspondence between the calculated and experimental dependencies describing the dynamic fracture in the impact problems. In particular, the dependence of the residual velocity of the impactor on its initial velocity was obtained, as well as the threshold values of the projectile velocity (ballistic limit) for three sample thicknesses. The applied model actually contains one new material parameter – the

incubation time, as well as a parameter characterizing the spatial discretization of the fracture process and the choice of the fracture scale level.

5.2 Application of artificial neural networks to predict strength of perforated targets

Solving dynamic fracture impact problems usually requires a lot of computing power and takes a lot of time. For example, solution of the problem from the first paragraph of this Chapter required up to 100 gigabytes of RAM and took about 10 hours when using a processor with 16 computing cores. In this particular case, this is largely due to the fracture model – according to the incubation time fracture criterion, the scale level is selected using the parameter$d$, which in turn determines the choice of the element size. In paragraph 5.1, $d = 0.3$ mm and the total number of elements reached 2 million (for a barrier with a thickness of 10 mm). It is impossible to quickly obtain a solution to such a problem, as well as it is impossible to simultaneously solve several such problems. It is also worth noting that computational difficulties are not uncommon when modeling the impact problems. Sometimes the element mesh is heavily distorted due to high stresses in the contact zone and high deformation rates. In particular, when solving the problem from the section 5.1, for the impactor velocities above 150 m/s, the option of forcibly disabling elements from calculations (the so-called erosion of elements) was activated when they are excessively deformed. Such forced removal of the elements leads to a physically non-motivated fracture which naturally reduces the accuracy of modeling.

This section discusses a possible approach to solving the described problems that arise when modeling the penetration of obstacles. As an example, barriers with a discredited structure are used, namely plates with perforations. The method is based on the use of artificial neural networks (ANNs) for rapid numerical estimation of the residual velocity of the impactor for a family of perforated targets made of PMMA (polymethylmethacrylate).

The impact strength of the targets is characterized by residual velocity of the projectile after passing through the target: the higher is the residual projectile velocity the lower is the target impact strength. The trained ANN is able to predict the residual projectile velocity for the configurations which are not present in the training dataset and the strength estimations using the ANNs are instant compared to rather time-consuming FEM calculations. This can be beneficial for certain use cases (e.g. calculations using underpowered mobile devices or for web-based CAD/CAE applications where the result is expected to be obtained instantly and simultaneously by multiple users). Moreover, some plate perforation patterns appear to be problematic and cannot be processed using the developed FEM procedures due to extensive mesh distortion causing a prematurely terminated solution procedure. For such situations the ANN predictions can be useful as the result can be obtained without reducing the solution time step or any other FEM solver tuning. It is worth noticing that inconsistent element behavior is a common problem for the FEM-based impact simulations especially for high projectile velocities and complicated target shapes [172].

Statement of problems

The study objective can be formally stated in the following way: let's consider a family of M problems and each problem is characterized by a vector consisting of N parameters $P^j = \left(P_1^j, P_2^j \dots, P_N^j\right), j \in [1, M]$. Each problem (configuration) P^j is mapped to a result R^j using FEM or any other numerical approach and situations when there is no result ($R^j = \emptyset$) for a particular parameter configuration are not excluded (problematic cases). Thus, the data set (or the configuration family) can be encoded as

$$\left\{P^j \to R^j\right\}, j \in [1, M], P^j = \left(P_1^j, P_2^j \dots, P_N^j\right) \quad (5.2).$$

The goal is to construct an algorithm that would map some new unsolved configuration P^{M+1} to a result R^{M+1} without performing the full problem solution and would possibly process the $R^j = \emptyset$ situations. The problematic $R^j = \emptyset$ cases are supposed to be processed using data obtained from the normally solved problems.

Vector P^j can potentially describe the shape of the sample, material properties, loading or even mixture of them. In this study the P^j vector describes the perforation patterns and artificial neural networks are used as the predicting algorithm while the data set consisting of M solved problems is used to train the ANNs. The data set size M is considered as sufficient for the ANN efficiency to stabilize.

Two problems are considered in the paper: A very simple static plate deformation problem is discussed prior to the main impact problem in order to test the approach and to see how mechanical aspects of the problem can potentially influence the ANN model architecture and efficiency. For the plate deflection problem, the solution is binary: the plate deflects either to left or right. The impact problem solution is a residual projectile velocity.

A two-dimensional formulation is used for the discussed problems, however axial symmetry is applied in the impact problem. The specimen models are composed of two types of square cells – a normal solid cell and a cell with a hole – a perforated cell. Combination of these cells yields the perforation configuration and thus random configurations can be generated forming a configuration set. The cell size can be varied and this way perforation patterns with different numbers of cells (perforation resolutions) can be obtained providing different configuration sets. Thus, in (5.2) N equals number of cells composing the sample and P_i equals zero or unity describing a solid or a perforated cell, while M denotes the size of the data set needed for successful training of the ANN model.

The following issues and questions are to be covered for the problems:

- Sufficient size of the dataset for each configuration set which ensures high efficiency of the ANN model and therefore ability to rapidly obtain the problem solution without performing full FEM analysis.

- Suitable ANN architecture for the particular problem: balance between the architecture complexity, accuracy of the model and required data set size is sought for.

- Possibility to obtain the result for the configurations which cause failure of the FEM solver using the trained ANN models.

- Applicability of the developed ANN models as a fast FEM alternative for the optimization purposes and construction of optimized perforation patterns for higher impact resistance.

For both problems the PMMA material is considered (properties are listed in table 1) and the material behavior is supposed to be elastic.

	PMMA target	**Steel projectile**
Young's modulus, E, Pa	3.3e9	2.09e11
Poisson's ratio, ν	0.35	0.28
Density, ρ, kg/m^3	1180	7720
Ultimate tensile stress, σ_c, Pa	72e6	-
Ultimate stress intensity factor, K_{Ic}, MPa	1.4	-
Incubation time, τ, μs	2.1	-

Table 5.2. Material properties used in the study.

Static deformation of a plate

A rectangular PMMA (properties listed in table 5.2) plate with dimensions 20 mm x 51 mm is considered and plain strain formulation is applied. A 1 mm thick grip area is used and the perforated area is 20 mm x 50 mm. The bottom edge of the plate is fixed and 60 MPa stretching stress is applied to the upper plate edge. Five configuration sets are studied: 2 cells by 5 cells (2x5 notation will be further used for the perforation resolutions), 6x15, 10x25, 14x35 and 20x50. The load causes nonhomogeneous plate deformation and therefore deflection of the specimen to left or right depending on the perforation pattern. In this case the calculation result is the plate deflection side – left or right and the ANN is supposed to predict it for an arbitrary perforation configuration.

ANSYS FEM software is used to both generate the configurations and to obtain the solution. The meshed cells, a configuration example and a resulting deformation

are shown in figure 5.9. The bottom edge nodes are constrained in all directions. The plate deflection is measured using averaged horizontal displacements of the three nodes located on the upper edge of the plate.

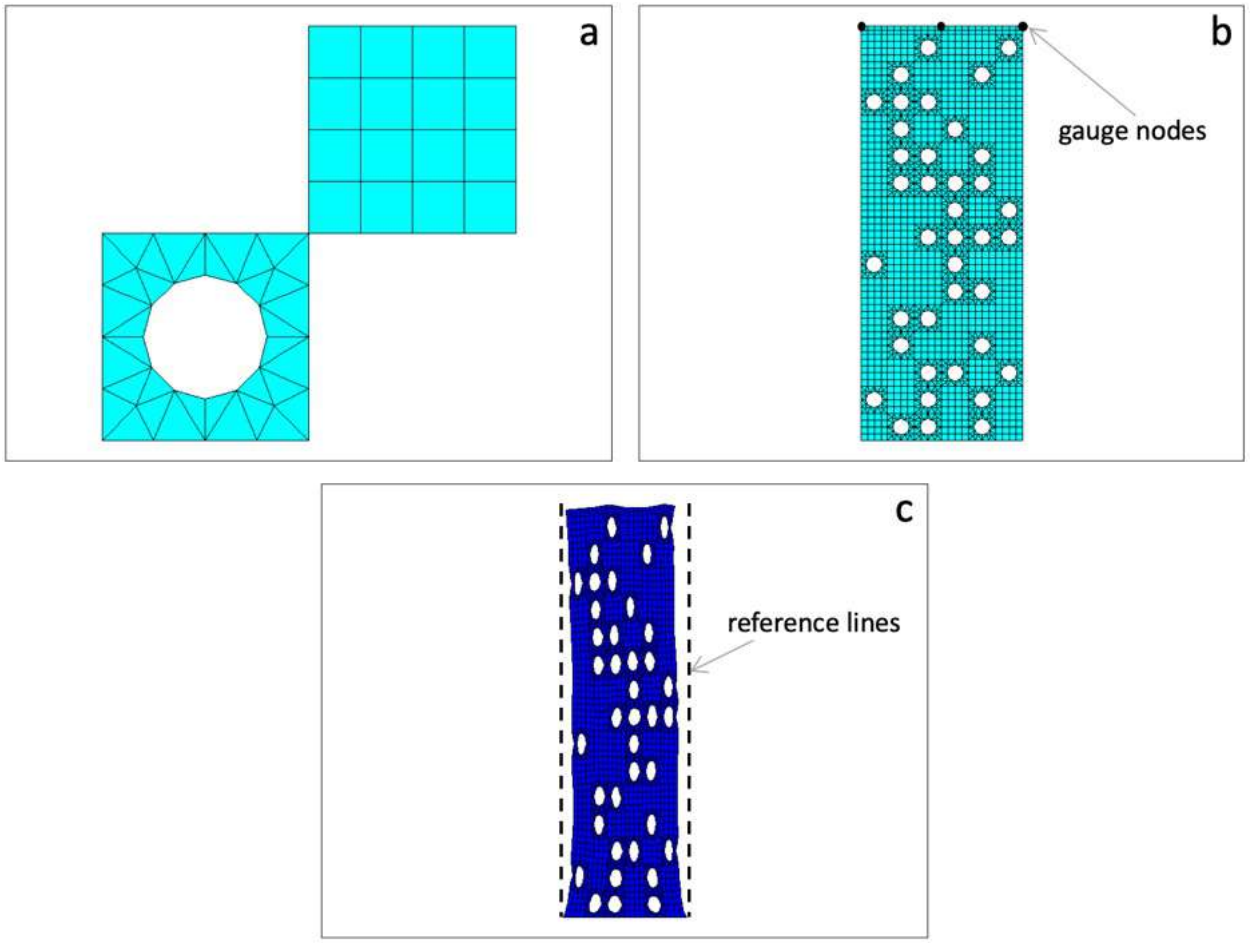

Fig. 5.9. A particular 6x15 configuration for the static problem. Meshed cells (a), whole assembled mesh (b) and a resulting plate deflection to the left as seen from comparison with the dashed vertical reference lines; in (c) 15X magnification is used to show the plate deflection.

Impact problem

A 10 mm thick round PMMA plate with diameter 100 mm is hit by a cylindrical steel projectile (material properties are given in table 5.2). The projectile has the following dimensions: diameter 6.9 mm and 30 mm height. The problem is solved in a two-dimensional statement with axial symmetry applied meaning that the target and

the projectile are both modelled as rectangles and perforation holes are in fact concentric canals inside the target. The target edge is fixed.

The projectile is slowed down due to interaction with the target and the calculation result is the residual projectile velocity. Obviously, the projectile deceleration depends on the perforation configuration, thus the ANN is supposed to predict the projectile's residual velocity for a given perforation pattern.

In this case three perforation resolutions and therefore three sets of configurations are studied: 2 cells x 12 cells (2x12), 4x24 and 8x48, additionally, the plate is supposed to have a non-perforated layer for the contact stabilization – the sample plate models are shown in figure 5.10. The base configuration model (with no perforation) is calibrated using experimental results on the PMMA plates impact discussed in section 5.1.

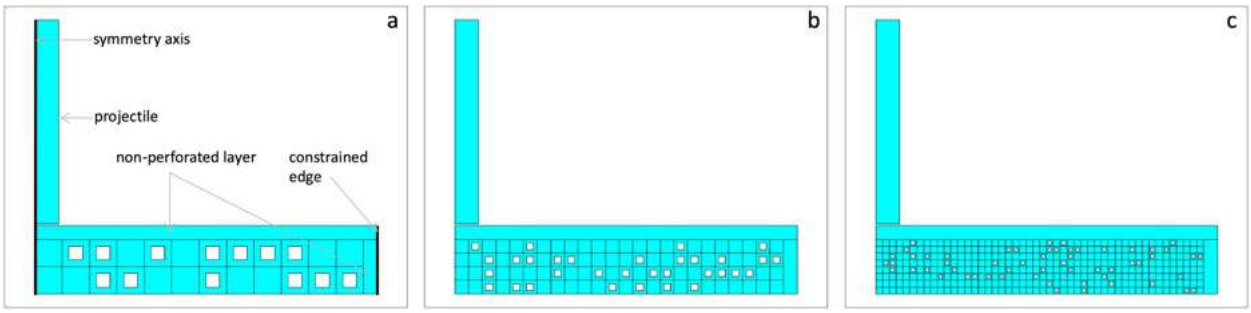

Fig. 5.10. Representatives of the three configuration sets: 2 cells x 12 cells (a), 4x24 (b), 8x48 (c). All the configurations have a nonperforated layer.

Sets of solutions were obtained for each configuration resolution, which made it possible to train neural networks to predict the solution of a problem for a specific configuration without performing a full calculation.

In the impact problem the target meshes are also assembled from solid and perforated cells using ANSYS APDL script. However, the problem is solved using LS-DYNA solver with an explicit time integration scheme. Thus, the LS-DYNA input is generated which is then modified in order to implement the custom dynamic fracture criterion. Square elements with four integration points are used to build the model.

Here all the configurations are meshed with equally sized square elements as the element size is prescribed by the applied fracture model. The model is integrated into the LS-DYNA code using subroutines for the user-defined materials (UMAT41). The stress histories are written to dedicated arrays and the time integration in (5.1) is carried out using trapezoidal integration rule. The mesh element size is chosen to be d (regular mesh with square elements is used for all models) and stress values calculated at four integration points are averaged and thus inner space integral in (5.1) is calculated. If criterion (5.1) predicts fracture for any of eight imaginary areas inside the element, the element is deleted from the mesh. The following area angles are considered (see figure 5.11b): $\alpha = 0, \frac{\pi}{2}, \pm\frac{\pi}{3}, \pm\frac{\pi}{4}, \pm\frac{\pi}{6}$.

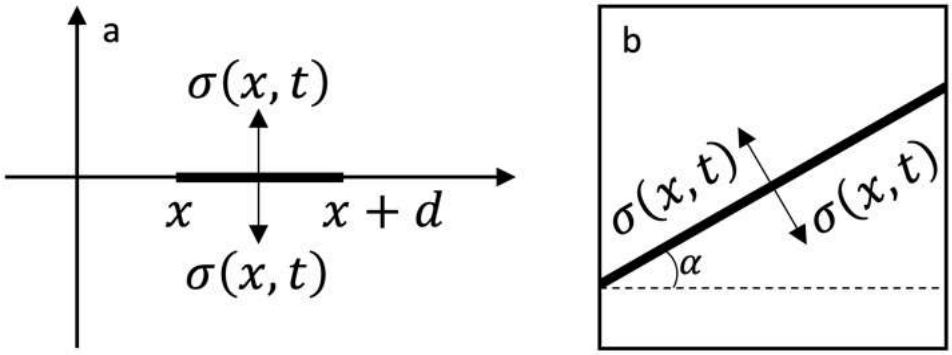

Fig. 5.11. Interval of spatial integration in the incubation time fracture model (a) and element with a fracture area, where $\alpha = 0, \frac{\pi}{2}, \pm\frac{\pi}{3}, \pm\frac{\pi}{4}, \pm\frac{\pi}{6}$.

The developed two-dimensional model is calibrated in order to fit experimental results on the PMMA plates impact: the non-perforated base configuration model with 2.1 μs incubation time yield good matching with the experimental data (see figure 5.12).

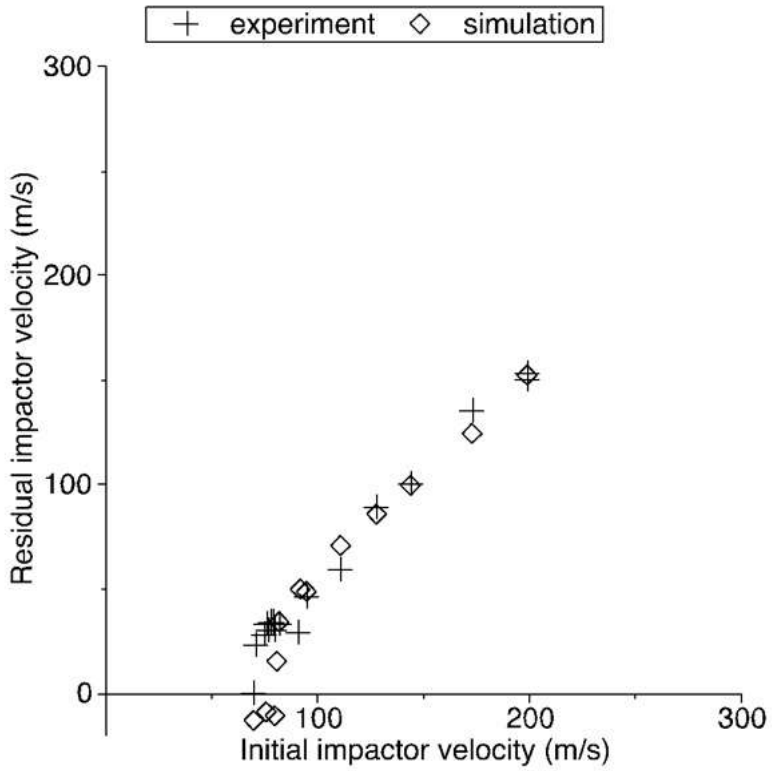

Fig. 5.12. The FEM Model calibration – non-perforated base configuration; experimental results from [109].

The meshed cells, particular hole configuration and a resulting fracture pattern for a 95 m/s impact are shown in figure 5.13.

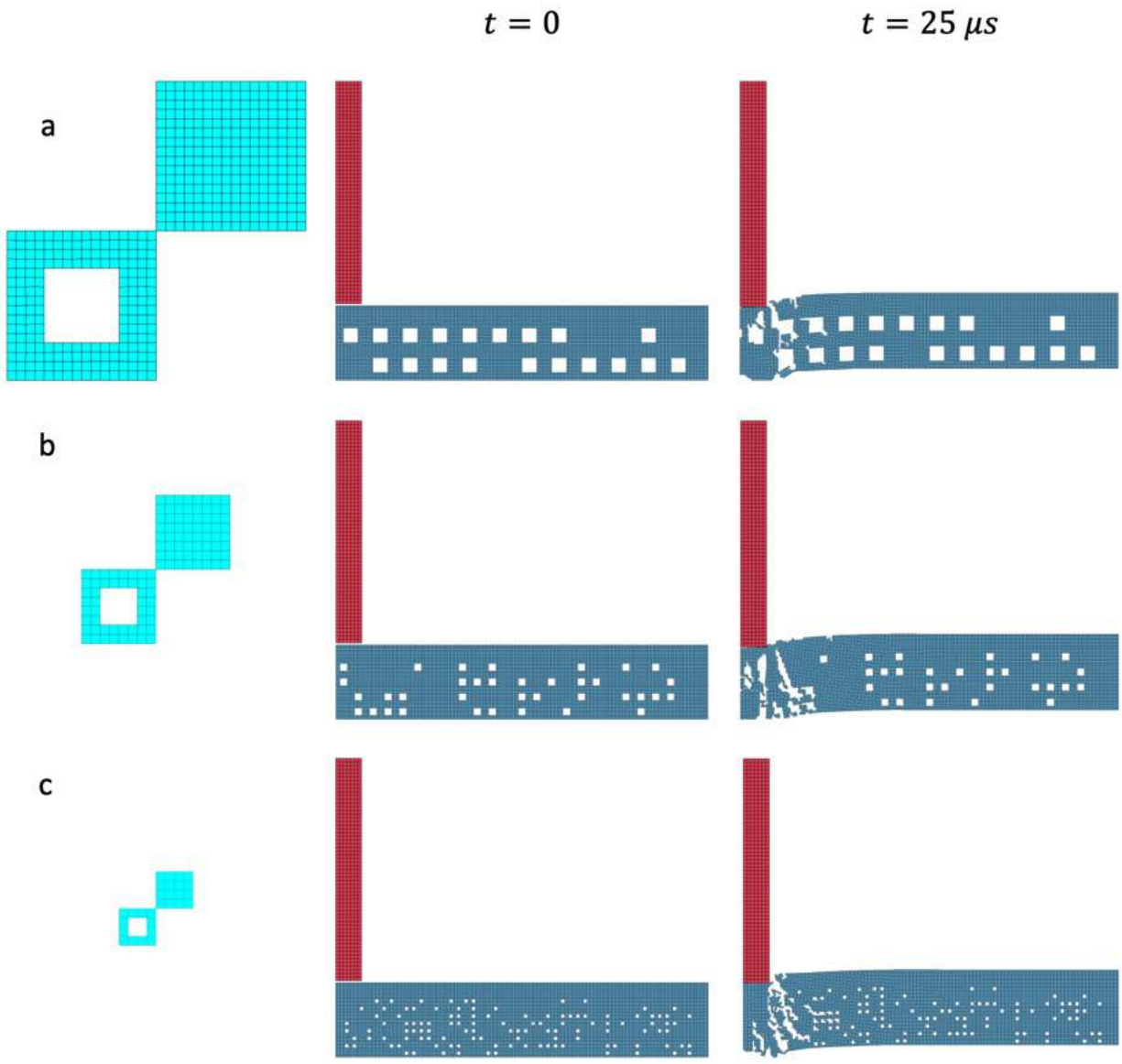

Fig. 5.13. Cells, whole mesh and resulting fracture at time 25 μs for particular 2x12 (a), 4x24 (b) and 8x48 (c) configurations.

Tested architectures of the ANN models

Generally speaking the artificial neural network is a complicated function that is capable of matching some set of data to a certain result. This function contains multiple parameters (weights and biases for the fully connected networks and filter parameters for the convolutional ones) which are adjusted to yield the best possible fit for the given data set and thus some trends and dependencies are established providing the possibility to predict the result with a certain level of accuracy. This parameter adjustment process is known as training. In the studied case the data set member is

encoded with a matrix containing information about the specimen perforation: 1 stands for a perforated cell and 0 – for a solid one. The matrix components are the parameters P^j from (5.2) describing the particular problem. The results R^j are the plate deflection (to the left or to the right) and the projectile residual velocity depending on the problem.

Two types of the ANN models are investigated. Fully-connected models constitute the first class which also contains the very basic linear regression model. The studied problems resemble some known image processing problems (e.g. categorization of the depicted objects) and thus it is fair to suppose that the machine learning techniques used in this area can be applicable for the discussed mechanical problems. Thus, the second used model type is a convolutional neural network (CNN) [173]. Models with different numbers of intermediate layers are tested. The 3x3 filter is used in the convolutional architecture (figure 5.16b).

For the fully connected ANN model the matrix describing the perforation pattern is converted into a single column: the matrix columns are stacked on top of each other and the resulting single column is then used as input for the fully-connected ANN. The convolutional neural networks operate with matrices without conversion. Further in the text the ANN models are denoted using the following notations: FC$[n_1, n_2, \dots, n_m]$ stands for a fully-connected model with n_i-sized m intermediate layers and FC[0] is a simple linear model, while CONV$[n_1, n_2, \dots, n_m]$ denotes convolutional ANN with M convolutional layers containing n_i filters. In all cases ReLu activation was applied. For the CNNs 3x3 filters were used. ADAM algorithm was used for the parameter optimization.

Effectiveness and robustness of the two model architectures are investigated for both static problem and the impact problem. The model architecture selection is made based on the model's efficiency, simplicity (the simplest possible layer and filter design) and universality (high model efficiency for all configuration sets). All the models have been built using Python libraries Scikit-learn and PyTorch.

The model efficiency is evaluated using two metrics depending on the problem. The R2 metric which is a widespread tool for the regression model efficiency assessment is to analyze the ANN models predicting the projectile residual velocity, while *accuracy* metric is utilized for the cases with binary results – the static plate problem and prediction of the FEM calculation failure for the impact problem. The R2 metric is based on the coefficient of determination [174] which shows the model advantage over the baseline prediction – the constant which stands for the data average. If the dataset is an array of n values $\{y_i\}$, the model predictions are $\{p_i\}$ and $\bar{y} = \frac{1}{n}\sum_{i=1}^{n} y_i$ is the data average, then the coefficient of determination is evaluated according to the following expression:

$$\mathrm{R2} = 1 - \frac{\sum_{i=1}^{n}(p_i - y_i)^2}{\sum_{i=1}^{n}(\bar{y} - y_i)^2} \qquad (5.3).$$

Obviously R2 ranges from $-\infty$ to 1 and $\mathrm{R2} = 1$ indicates the highest possible efficiency of the model, while $\mathrm{R2} = 0$ corresponds to the baseline prediction. The *accuracy* metric is a ratio of number of correct predictions to total number of predictions. The 0.5-0.6 *accuracy* scores for the problems with balanced binary results sets (e.g. left or right; yes or no) are considered as poor since the model is essentially guessing.

The data sets are divided into train and test disjoint subsets. For the majority of studied problems, the test section has 1000 problems except for the perforation patterns with lowest resolutions (2x5 and 2x12 problems).

Solution of the static plate deflection problem

Figure 5.14 contains results on training of the ANN models developed for different configuration sets of the static problem. In all the graphs in figure 5.14 the X axis is the number of configurations used to train the model and the Y axis is the model *accuracy* metric. The FC[0] model appeared to be the most effective for this particular static problem: while being the simplest one, it requires the smallest number of

configurations for the model *accuracy* score to stabilize at the highest levels. Much more complicated models with higher numbers of intermediate layers are at most as efficient as the linear model requiring more data for training. Moreover, the convolutional models appear to be far less effective in this case failing to reach even 0.6 *accuracy* score for the higher resolution configuration sets. This probably should be expected as the plate deflection is controlled by how holes in the left and right halves of the plate are balanced. The convolutional neural network looks for certain local patterns which involve neighbor cells ignoring respective hole locations in the left and right plate halves. On the contrary, fully connected neural networks account for position of each cell and thus are able to analyze how holes and whole cells are balanced in the left and right plate halves.

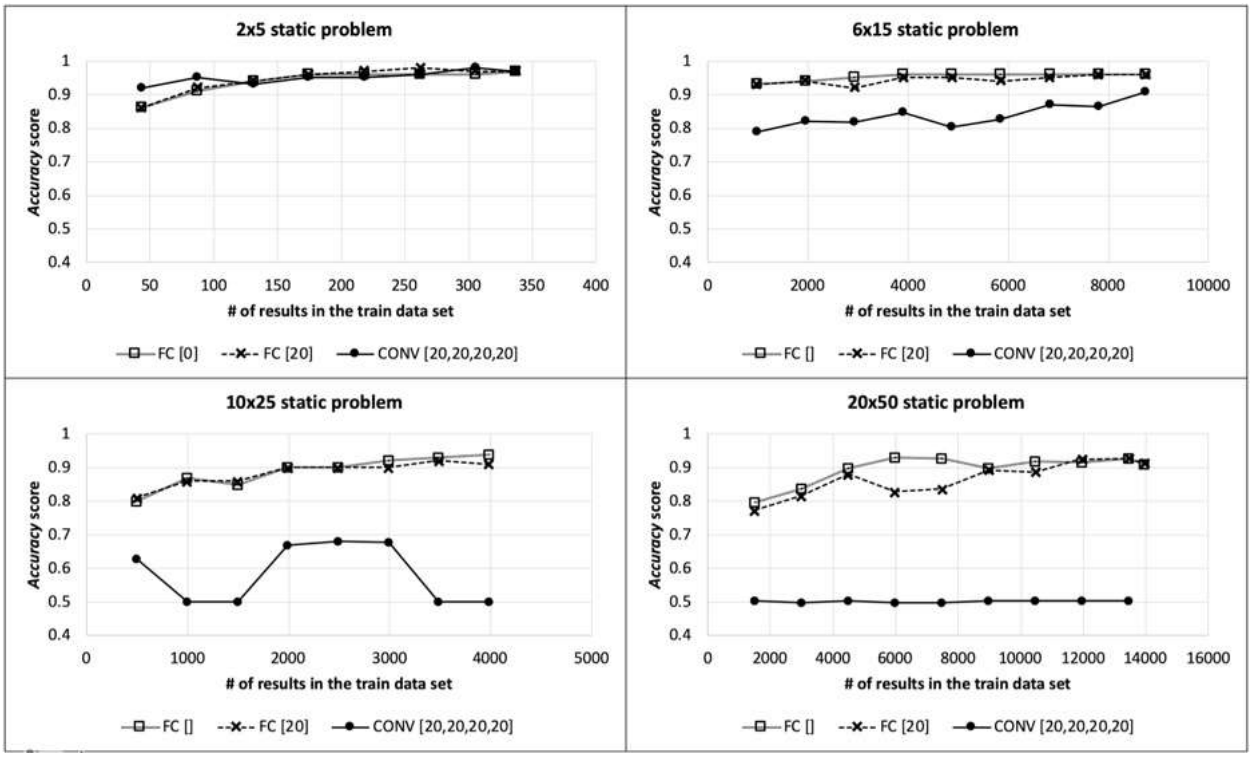

Fig. 5.14. Dependence of the *accuracy* score of the ANN models built for static test problem and different perforation resolutions.

Efficiency of the selected models applied to the different configuration sets with indicated dataset size are provided in table 5.3.

Configuration / ANN architecture	2x5	6x15	10x25	14x35	20x50
FC []	0,97	0,956	0,91	0,937	0,911
FC [5]	0,97	0,954	0,919	0,931	0,936
FC [10]	0,97	0,962	0,902	0,926	0,906
FC [20]	0,97	0,959	0,897	0,91	0,914
FC [50]	0,98	0,952	0,903	0,918	0,92
FC [200]	0,97	0,956	0,906	0,919	0,933
FC [20, 20]	0,98	0,951	0,91	0,906	0,924
FC [20, 20, 20]	0,97	0,958	0,909	0,909	0,916
FC [20, 20, 20, 20]	0,97	0,958	0,908	0,909	0,911
FC [20, 20, 20, 20, 20]	0,97	0,958	0,892	0,918	0,919
CONV [20, 20]	0,96	0,8	0,653	0,683	0,632
CONV [20, 20, 20]	0,97	0,858	0,751	0,687	0,502
CONV [20, 20, 20, 20]	0,97	0,909	0,739	0,754	0,502
CONV [20, 20, 20, 20, 20]	0,97	0,519	0,5	0,644	0,502
CONV [20, 20, 20, 20, 20, 20]	0,96	0,519	0,5	0,644	0,502
CONV [30, 30, 30, 30]	0,97	0,887	0,5	0,764	0,502

Table 5.3. *Accuracy* scores of different ANN architectures for the static plate deflection problem; the optimal one is highlighted. For all configurations the test data subset has 1000 problems except for the 2x5 case with 100 problems in the test subset.

To sum up, the following results were obtained for the static plate deflection problem:

- The ANN models provide high accuracy predictions as it is probably expected, since the observer is able to predict the plate deflection side for lower resolution perforation patterns (2x5, 6x15) just looking at the perforation pattern.

- The simplest fully-connected model appears to be both accurate and easy to build and to train while the convolutional models fail to yield any accurate prediction despite the fact that the problem formulation is similar to the image processing problems – the model is supposed to distinguish the cell configurations.

Solution of the impact problem

For the impact problem a number of architectures of the neural networks are investigated. Table 5.4 contains information about performance of various architectures of the ANN models. In this case two models appear to be preferable in terms of accuracy, universality and required amount of train data: a fully-connected model with two intermediate layers (FC[20,20]) and a convolutional neural network with four layers – CONV[20,20,20,20]. Information on training of these two models for the studied configuration sets is shown in figure 5.15.

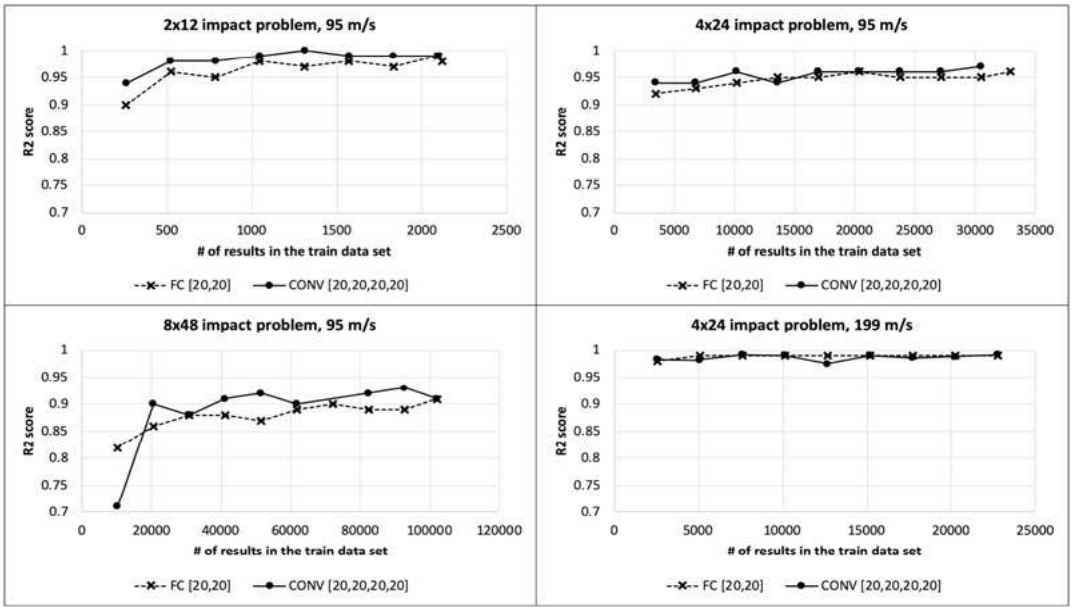

Fig. 5.15. Efficiency (R2 score) of two types of neural networks depending on the dataset size for the impact problem.

Configuration / ANN architecture	2x12 95 m/s	4x24 95 m/s	8x48 95 m/s	4x24 199 m/s
FC []	0,78	0,81	0,78	0,95
FC [5]	0,97	0,92	0,84	0,98
FC [10]	0,97	0,95	0,87	0,99
FC [20]	0,97	0,95	0,88	0,99
FC [50]	0,98	0,96	0,89	0,99
FC [200]	0,98	0,96	0,89	0,99
FC [20, 20]	0,98	0,96	0,91	0,99
FC [20, 20, 20]	0,99	0,95	0,90	0,99
FC [20, 20, 20, 20]	0,98	0,95	0,89	0,99
FC [20, 20, 20, 20, 20]	0,99	0,95	0,89	0,99
CONV [20, 20]	0,97	0,92	0,74	0,98
CONV [20, 20, 20]	0,99	0,95	0,86	0,98
CONV [20, 20, 20, 20]	0,99	0,97	0,91	0,98
CONV [20, 20, 20, 20, 20]	0,99	0,95	0,90	0,98
CONV [20, 20, 20, 20, 20, 20]	0,98	0,95	0,85	0,99
CONV [30, 30, 30, 30]	0,98	0,96	0,91	0,99

Table 5.4. Efficiency (R2 score) of various ANN architectures for different configurations of the impact problem. Projectile velocity is indicated for each problem. Optimal models are highlighted. For all configurations the test data subset has 1000 problems except for the 2x12 case with 500 problems in the test subset.

Figure 5.16 schematically shows two utilized types of the ANN models, while figure 5.17 depicts diagrams with comparison of the ANN predictions with the FEM results. The spread of results for the 199 m/s impactor velocity is smaller compared to

other cases, since for a higher projectile velocity, the result is mainly determined by the number of holes in the contact zone, rather than their exact location – many configurations are indistinguishable from the point of view of the ANN, which reduces the complexity of the task.

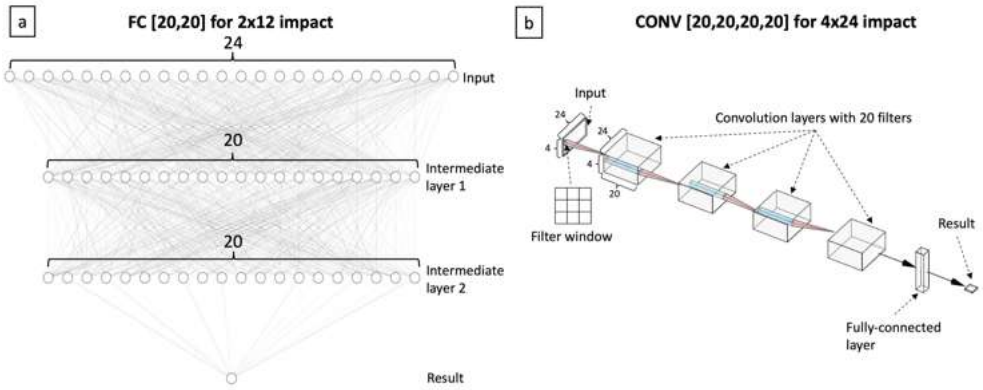

Fig. 5.16. Schematic representation of the two utilized ANN architectures: a) – the fully connected ANN (FC[20,20] for the 2x12 impact problem is shown); b) – convolutional neural network with four convolutional layers with 20 filters each (CONV[20,20,20,20] and a final fully connected layer for categorization.

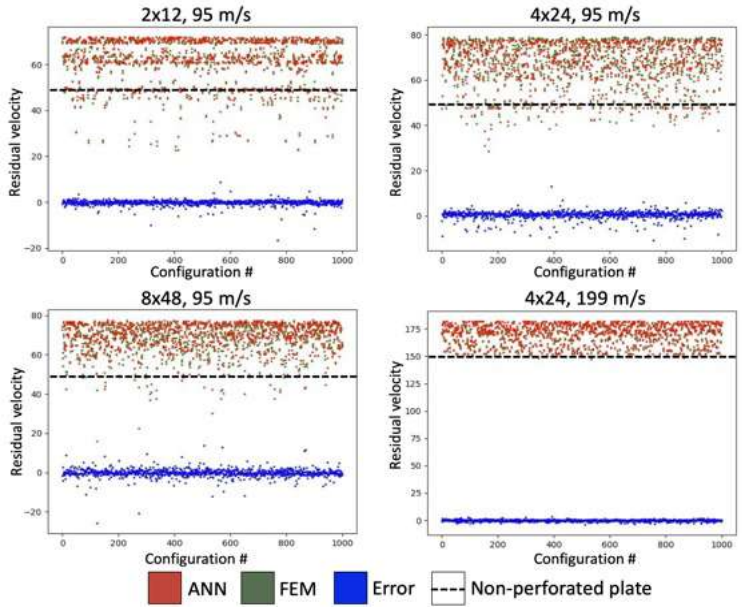

Fig. 5.17. Accuracy of the ANN models developed for the impact problem, each dot indicates one problem from the test configuration set, dashed line indicates performance of the non-perforated target.

As expected the required data set size increases for problems with higher resolution of the perforation patterns and the increase is much more pronounced compared to the plate deflection problem. The 8x48 configuration appeared to be rather complex, requiring a lot of data to safely surpass the R2=0.9 efficiency level.

Predictions using the trained ANN models take considerably less time compared to the full FEM computation: fractions of a second compared to around 50 seconds (8-core processor).

It is known that finite element meshes can be prone to considerable distortion when problems with high deformations are solved leading to errors and premature calculation stoppages [175-177].

General recommendations include reduction of a time step, mesh refinement, alternation of the contact parameters, changes of the material rheology [178], rezoning techniques [175,179] and simple deletion of heavily distorted elements which leads to fracture with no physical motivation. Alternative computational methods can be used to manage with highly deformed media such as Material Point Method, Smoothed Particle Hydrodynamics [180,181], Peridynamics [182-184] or coupling of different methods [185].

All the datasets for the impact problem contain configurations that resulted in an excessive element deformation causing the solver failure. For the 4x24 configuration set and a 95 m/s projectile velocity the solution could not be obtained for 199 configurations (out of 25000). The problem is much more pronounced for the 199 m/s case: 7828 cases of premature computation termination due to error (out of 48000).

Some of the failed configurations were processed using FEM with a reduced time step (from 7.15e-8 s to 5.56e-8 s) leading to a normal termination of the computation. These results were used to evaluate efficiency of the ANN models applied to the problematic configurations and R2=0.961 score was obtained for the 4x24 perforation pattern and 199 m/s projectile velocity. These figures indicate that the

ANN models are applicable to configurations which are hard to process using the developed FEM scheme without tuning and adjustments.

An example of a problematic 4x24 configuration stroke at a 199 m/s velocity is shown in figure 10a and figure 10b depicts a zone with inconsistent mesh behavior leading to an abrupt computation termination. This particular configuration could not be fixed by the time-step reduction and the ANN yields 151.2 m/s prediction for the residual projectile velocity.

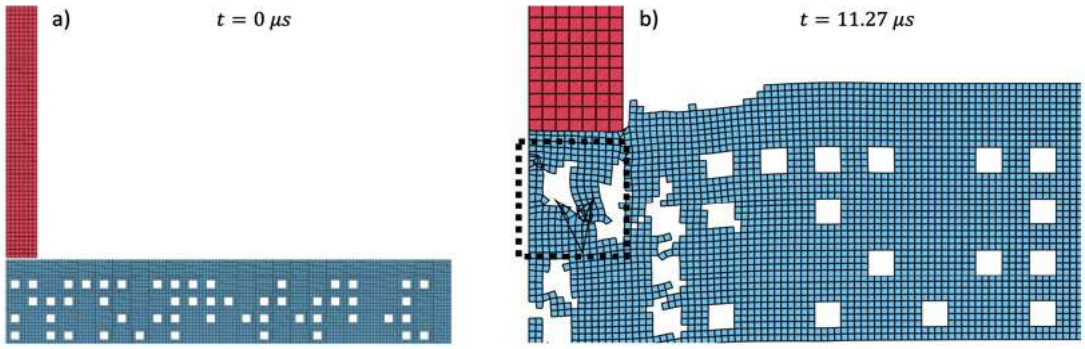

Fig. 5.18. An example of a 4x24 configuration causing the computation failure and a zone with extensive element deformation (b).

The conducted studies have shown that the artificial neural networks were found to be a powerful tool for reduction of computational costs for the particular problem of impact of perforated plates. The networks were trained using a preliminarily obtained set of FEM results and the number of required data is dependent on the perforation pattern resolution. On the one hand considerable computation resources are needed in order to obtain the dataset (for example, more than 100 000 problems should be solved for the 8x48 impact problem), on the other hand after the dataset has been obtained the solution of each next problem can be obtained instantly with high accuracy. Moreover, each next computation run does not require any FEM software which is often costly and requires licenses. Besides this the dataset generation is a completely automated procedure which is also beneficial for reduction of the development costs. This way, if the total number of problems to be solved exceeds the needed dataset size, the ANN based approach is worth considering. Such an approach might be useful for prototyping

when general trends of the designed structure are of interest and many construction variants should be tested to obtain the desirable performance. Another possible use case is simultaneous solution of multiple problems, e.g. web-based CAD/CAE applications. It should be noted that realistic engineering problems would involve a complicated set of parameters to be varied which describe shape of the object, material properties and loading conditions or even a mixture of these parameters and each case should be studied separately. As it has been found even similar problems might require different architectures of the neural networks: while the convolutional neural network appeared to be successful for the impact problem, it was found to be inapplicable for the plate deflection problem due to purely mechanical reasons.

In addition to reduction of computational time and costs the developed approach can be used to overcome some known computational difficulties of FEM (or actually any other numerical method) applied to impact problems such as contact instabilities or inconsistent mesh behavior due to high strains. In the studied case some of the perforation patterns led to FEM failure however the information obtained from the rest of the dataset helped the neural network to predict the solution for the problematic cases too. The problematic configurations were found not to exhibit any specific features which could be distinguished by the neural network and thus they did not form a standalone subclass inside the dataset from the viewpoint of the neural network. This means that the developed ANN could be used to predict results for the problematic cases as they share features with the rest of the dataset. Consider a case when the computation fails for a particular combination of parameters P^j (expression (5.2)) that characterize the problem (e.g. material model parameters or sample fixation and loading method or both, etc.) This problem can be potentially resolved using neural network model trained on a dataset consisting of problems with slightly altered P^j parameters (if alternation of P^j leads to successful FEM computations, of course). Inapplicability of the developed ANN model to prediction of FEM failure or success can be regarded as an indication that the ANN efficiency for the problematic configurations is comparable to the normal cases, since the problematic configurations

do not form a subclass within the main dataset sharing features with the rest of the data and are not distinguished by the ANN model. It is worth noticing that high velocity of the projectile is a common cause of the FEM solution failure and the above described ANN based approach should not be expected to be very successful for the case. If the projectile velocity is included into the parameter array P^j and for all the projectile velocities higher than some critical value FEM fails, the problematic configurations clearly form a separate class. Thus, the train data would lack information about features of the problematic configurations which can possibly reduce the ANN model efficiency or make it completely inapplicable. This approach can be considered as deserving attention since such methodology can be possibly introduced in FEM routines to provide better user experience.

5.3 Chapter 5 conclusions

The work contains experimental and numerical results on impact of PMMA plates with various thicknesses using a steel projectile. Dependence between initial impactor velocity V_i and the residual impactor velocity V_r was experimentally assessed using a gas gun and a high-speed photography setup. In addition to this, the ballistic limit for all three sample types was obtained. The experimental data was used to test and validate a numerical approach, which uses the finite element method and the incubation time fracture model for the material failure predictions. The applied scheme is rather simple and involves a limited number of the material parameters. All of the parameters are either standard material data or can be evaluated from the experiments on the PMMA described in the literature (e.g. the incubation time value).

The simulation results appear to be promising: both ballistic limits for the particular targets and the projectile and the $V_r - V_i$ function can be predicted using relatively simple numerical scheme. This way the developed numerical approach can be applied to predict the impact fracture in other cases: for other brittle materials (e.g. ceramics) and other specimen configurations. For example, numerical estimates for the

ballistic limit and for the $V_r - V_i$ dependence of the 5 mm thick PMMA plate are presented in the work.

The second paragraph of Chapter 5 is devoted to an attempt to partially solve the fundamental difficulties encountered when dynamic fracture due to impact is simulated. The impact problem involving obstacles with a discrete structure – plates with perforation - was chosen as a model problem. The essence of the approach is to solve an array of similar problems (in this case, problems with different perforation schemes) and then to train an artificial neural network on the resulting array. The trained ANN is able to instantly predict the solution for a problem with a new perforation scheme, as well as process problems for which the use of direct calculation using FEM is difficult.

More information can be found in [109,118]

Conclusions

- The work investigates discrete features of the dynamic fracture processes, and offers discrete models for the analysis of this phenomenon. In particular, an analogy between the processes of fracture at the start of a crack under conditions of pulse loading and fracture in the "mass-on-a-spring" system has been discovered. This analogy is based on the incubation time fracture criterion applied to the problem of crack initiation due to pulse loading. The analogy allows one to interpret the dynamic fracture processes as "inertial" processes and, thus, provides a natural and simple explanation of the key fracture effects, for example, the fracture delay effect. A simple engineering approach to fracture under dynamic loads initiation has been also proposed. The model is based on the linear oscillator failure. As shown in the study, the inertia of this system provides possibility to observe the key effects of the dynamic fracture of materials – the dependence of the strength of the system on the loading rate and the fracture delay when short pulse loads are applied. This model was shown to be applicable for prediction of fracture taking place in structural materials subjected to rapidly growing and short loads.

- The results obtained in the work and the developed model emphasize the importance of the incubation characteristics of the dynamic fracture process and allow us to build parallels between the failure of the "mass-on-a-spring" system and the incubation time fracture criterion. Both models imply the existence of characteristic times of dynamic fracture processes and, thus, allow one to set the time scale to be used when these processes are studied.

- The incubation time fracture model is based on the space and time discretization of the dynamic fracture process. According to this approach, a minimum size of the fracture zone is introduced, which allows one to set the scale level of the analysis. In addition to this the incubation time – a characteristic relaxation time of fracture is introduced as a material parameter. The incubation time approach, which assumes, in

particular, the discrete nature of the crack propagation, was introduced into the finite element method, and provided possibility to numerically investigate a number of effects accompanying the crack movement. Thus, it has been shown that the discretization of the crack propagation process makes it possible to obtain experimentally observed crack velocity oscillations. Moreover, the developed numerical approach helped to resolve the question of the uniqueness of the stress intensity factor – crack velocity dependence: for intense loading and high crack velocities, there is a strong variation in the SIF values, which prohibits a single curve construction and thus classic theory applicability is questioned. At slow loads and relatively low crack velocities, the SIF variation is small and the approximation yields the SIF-crack velocity curve. Moreover, the approaches developed for modeling of straight cracks have been redesigned to analyze cracks propagating in an arbitrary direction. This modification of the numerical scheme made it possible to study the fragmentation of brittle bodies under shock loading and to obtain experimentally observed characteristics of the fragmentation process, for example, the size distribution of fragments.

- The transition from continuous models to discrete systems, which in many ways more realistically describe structural materials, provide possibility to explore new effects, which cannot be predicted within the framework of continuum mechanics based on traditional approaches. The chains of linear oscillators were used to demonstrate that a relaxation wave resulting from initial fracture and travelling through the system may cause secondary fracture. Such effect cannot be found in an elastic rod. However, according to the conducted numerical calculations, this effect can be possibly observed in specially designed samples with a discrete periodic structure. Thus, the study of a discrete model – a chain of linear oscillators – made it possible to detect an effect that can be implemented in real structures and which should be considered in the engineering practice.

- The work proposes new numerical methods applicable to the design of structures and the analysis of their strength under shock loading conditions. The developed

numerical schemes are based on the finite element method and the incubation time fracture model. Commercial computer software packages serve as the basis for the developed numerical schemes, which can help to introduce the presented approaches into the engineering practice. The performance of the numerical scheme is demonstrated using the impact problem – experimental dependences of the residual velocity of the projectile from its initial velocity have been numerically constructed, and threshold values of the projectile velocity for the obstacles of different thickness have been determined.

- The application of the developed numerical approach to the impact experiments modelling has fully revealed difficulties which are often encountered in course of the dynamic fracture modelling. Such problems are often very resource demanding and take long time to solve even using powerful computers. In addition to this, in problems with high strain rates and high stress values (the impact problems represent well this category of problems), computational difficulties are often observed due to excessive distortion of elements and unstable operation of contact algorithms. The study proposes an approach that partially solves these difficulties. The approach is based on artificial neural networks (ANNs). The ANNs are trained on an array of solutions to a family of problems and predict the solution of a new representative of this family. In this case, the solution can also be predicted for the problems which are hard to solve using a complete calculation due to computational difficulties.

- The successful application of the developed approach was demonstrated using an example of the impact problem: the barriers with a discrete structure (perforated plates) were hit by projectiles. Each problem was described by a set of discrete parameters characterizing the perforation pattern. Correlation between the perforation pattern and the plate strength was investigated. The developed ANN which was trained on an array of results for various perforation patterns has been shown to be able to predict the result for new perforation schemes. Moreover, one can obtain the result for configurations which are hard to process using the finite method due to computational instabilities. Different values can be used as parameters describing a specific problem

– material properties, sample geometry, loading parameters, and many others. In the considered case, the problem is described by a perforation scheme, which greatly simplifies the application of the proposed approach and makes it possible to solve the considered model problem. The proposed approach looks promising for practical purposes, especially for obtaining approximate solutions in computationally complex cases.

The study used a wide range of methods to solve the formulated problems – from analytical solutions of differential equations to numerical methods and experimental studies. The results obtained in this work can be useful from the theoretical point of view – as a foundation for further research, however, the practical value of the developed approaches is also obvious. For example, the effect of fracture in periodic structures in course of unloading requires experimental confirmation and can be used to load materials with short pulses. Linear oscillator-based fracture models demonstrate the fundamental nature of the key effects of the dynamic fracture and provide simple tool for the fracture analysis. The developed numerical schemes and approaches can be used to analyze strength of the designed structures.

References

1) K. Ravi-Chandar, W.G. Knauss, An experimental investigation into dynamic fracture: I. Crack initiation and arrest, Int J Fract 25, 1984, 247–262

2) J.F. Kalthoff, D.A. Shockey, Instability of cracks under impulse loads, J. Appl. Phys. 48, 1977, 986-993

3) N.V Mikhailova, I.V. Smirnov, V.V. Balandin, V.VI. Balandin, A.M. Bragov, Yu.V. Petrov, The spall failure delay: Experimental observation and theoretical analysis, International Journal of Impact Engineering 164, 2022, 104194

4) A.N. Berezkin, S. I. Krivosheev, Yu. V. Petrov, A.A. Utkin, Effect of Delayed Crack Nucleation under Threshold Pulse Loading, Doklady Physics 45(11), 2000, 617-619

5) D.A. Shockey, D.C. Erlich, J.F. Kalthoff, H. Homma, Short-pulse fracture mechanics, International Journal of Fracture 23(1), 1986, 311-319

6) F. Jiang, K.S. Vecchio, A. Rohatgi, Analysis of modified split Hopkinson pressure bar dynamic fracture test using an inertia model, International Journal of Fracture 126, 2004, 143-164

7) A.G. Dutton, R.A.W. Mines, Analysis of the Hopkinson Pressure Bar loaded Instrumented Charpy Test using an inertial modelling technique, International Journal of Fracture 51, 1991, 187-206

8) Z. Guangping, S. Xinhui, W. Yanwei & C. Zhongliang, Dynamic stress intensity factor of 2A12T4 Al compact tension specimen with loading point displacement and spring mass model, Materials Research Innovations 19(sup9), 2015, S9-42-S9-45

9) J.G. Williams, The analysis of dynamic fracture using lumped mass-spring models, International Journal of Fracture 33, 1987, 47-59

10) L. Slepyan, Dynamics of a crack in a lattice, Sov. Phys. Dokl. 26, 1981, 538-540

11) N. Gorbushin, G. Mishuris, Dynamic fracture of a dissimilar chain, Phil. Trans. R. Soc. A 377, 2019, 20190103

12) H. Gao, A theory of local limiting speed in dynamic fracture, J. Mech. Solids 44(9), 1996, 1453-1474

13) T. Goldman, A. Livne, J. Fineberg, Acquisition of Inertia by a Moving Crack, Physical Review Letters 104, 2010, 114301

14) N.A. Kazarinov, V.A. Bratov, Yu.V. Petrov, Simulation of dynamic crack propagation under quasi-static loading, Doklady Physics 59(2), 2014, 99-102

15) I. Smirnov, N. Kazarinov, Y. Petrov, Experimental observation and numerical modeling of unstable behaviour of a fast crack velocity, Theoretical and Applied Fracture Mechanics 101, 2019, 53-58

16) J. Fineberg, S.P. Gross, M. Marder, H.L. Swinney, Instability in the propagation of fast cracks, Physical Review B 45(10), 1992, 5146-5154

17) Yu.V. Petrov, A.A. Gruzdkov, N.A. Kazarinov, Features of the dynamic fracture of one-dimensional linear chains, Doklady Physics 53(11), 2008, 595-599

18) G. Irwin, Analysis of Stresses and Strains Near the End of a Crack Traversing a Plate, Journal of Applied Mechanics 24, 1957, 361-364

19) E. Cadoni, Dynamic Characterization of Orthogneiss Rock Subjected to Intermediate and High Strain Rates in Tension, Rock Mech Rock Eng 43, 2010, 667–676

20) V.V.Skripnyak, E.G. Skripnyak, V.A. Skripnyak, I.K. Vaganova, A.M. Bragov, A.K. Lomunov, et al., Multiscale Simulation of Porous Quasi-Brittle Ceramics Fracture, AMM 756, 2015, 196–204

21) J. Campbell, The dynamic yielding of mild steel, Acta Metall 1(6), 1953, 706–710

22) W. Mocko, J.A. Rodriguez-Martinez, Z.L. Kowalewski, A. Rusinek, Compressive viscoplastic response of 6082-T6 and 7075-T6 aluminium alloys under wide range of strain rate at room temperature: Experiments and modelling, Strain 48(6), 2012, 498-509

23) N.V. Mikhailova, G.A. Volkov, Y.I. Meshcheryakov, Y.V. Petrov, A.A. Utkin, Failure-delay effect in destruction of steel samples under spalling conditions, Tech Phys 62, 2017, 547-552

24) K. Ravi-Chandar, Dynamic fracture of nominally brittle materials, International Journal of Fracture 90, 1998, 83–102

25) J.W. Dally, W.L. Fourney, G.R. Irwin, On the uniqueness of the stress intensity factor – crack velocity relationship, Int. J. Fract 27, 1985, 159-168

26) A.J. Rosakis, G. Ravichandran, Dynamic failure mechanics, J. Mech. Mater. Struct. 37, 2000, 331-348

27) G.R. Johnson, T.J. Holmquist, An improved computational constitutive model for brittle materials, AIP Conference Proceedings 309, 1994, 981-984

28) V.S. Nikiforovskii, S.I. Sabitova, A.E. Strelyaev, Fracture of solid bodies by dynamic loads, Sov Min Sci 6, 1970, 517-524

29) V.S. Nikiforovskii, Kinetic nature of the brittle fracture of solid bodies, J Appl Mech Tech Phys 17, 1976, 721-726

30) F.R. Tuler, B.M. Butcher, A criterion for the time dependence of dynamic fracture, Int J Fract Mech 4, 1968, 431-437

31) Y.V. Petrov, A.A. Utkin, Dependence of the dynamic strength on loading rate, Sov Mater Sci 25, 1989, 153-156

32) B.A. Crouch, J.G. Williams, Modelling of dynamic crack propagation in the three-point bend impact specimen, J.Mech.Phys.Solids 1, 1988, 1-13

33) N. Kazarinov, Y. Petrov, A. Smirnov, Dynamic fracture effects observed in discrete mechanical systems, Procedia Structural Integrity 28, 2020b, 2168–2173

34) N.A. Kazarinov, S.A. Smirnov, Y.V. Petrov, Revisiting mass-on-spring model to address key dynamic fracture effects, Theoretical and Applied Fracture Mechanics, 132, 2024, 104470

35) M.J. Nieves, A.B. Movchan, I.S. Jones, G.S. Mishuris, Propagation of Slepyan's crack in a non-uniform elastic lattice, Journal of the Mechanics and Physics of Solids 61, 2013, 1464–1488

36) G.S. Mishuris, A.B. Movchan, L.I. Slepyan, Dynamical extraction of a single chain from a discrete lattice, Journal of the Mechanics and Physics of Solids 56, 2008, 487–495

37) J. Wu, C.Q. Ru, A refined cohesive zone model that accounts for inertia of cohesive zone of a moving crack, Mechanics Research Communications, 76, 2016, 78–85

38) S. Chakraborty, A. Shaw, A pseudo-spring based fracture model for SPH simulation of impact dynamics, International Journal of Impact Engineering 58, 2013, 84-95

39) S.K. Hui, T.X. Yu, Modelling of the effectiveness of bicycle helmets under impact, International Journal of Mechanical Sciences 44, 2002, 1081–1100

40) K. Tsubota, S. Wada, Elastic force of red blood cell membrane during tank-treading motion: Consideration of the membrane's natural state, International Journal of Mechanical Sciences, 52, 2010, 356–364

41) A. Szekrényes, Fracture mechanical stability of DCB and 4ENF tests complemented with linear springs, Theoretical and Applied Fracture Mechanics 125 (2023), 103900

42) L.I. Slepyan, Nonstationary elastic waves, Shipbuilding, Leningrad, 1972, 376p. (in Russian)

43) L.I. Slepyan, Crack mechanics, Shipbuilding, Leningrad, 1990, 296p. (in Russian)

44) D.I. Trubetskov, Linear vibrations and wave, Fizmatlit, Moscow, 2001, 465 p. (in Russian)

45) Gladwell G.M.L., Inverse Problems in Vibration, Dordrecht/Boston/London, Kluwer Academic Publishers, 2008, 457p.

46) M.I. Rabinovich, D.I. Trubetskov, Introduction to theory of vibrations and waves, NIC “Regular and chaotic dynamics”, 2000, 560p. (in Russian)

47) L. Brillouin, Wave Propagation in Periodic Structures, Dover Publications Inc., 1953, 255p.

48) V.A. Kuzkin, A.M. Krivtsov, Energy transfer to a harmonic chain under kinematic and force loadings: Exact and asymptotic solutions. Journal of Micromechanics and Molecular Physics 3(1,2), 2018, 1850004

49) Xu, A. Needleman, Numerical simulations of dynamic crack growth along an interface, Int J Fract 74,1995, 289–324

50) S. Zhu, H. Yu, X. Wu, L. Hao, Z. Shen, J. Wang, L. Guo, Dynamic fracture analysis in nonhomogeneous piezoelectric materials with a new domain-independent interaction integral, Theoretical and Applied Fracture Mechanics 122, 2022, 103614

51) D.Yang, X. He, X. Liu, Y. Deng, X. Huang, A peridynamics-based cohesive zone model (PD-CZM) for predicting cohesive crack propagation, International Journal of Mechanical Sciences 184, 2020, 105830

52) A. Karma, D. Kessler, H. Levine, Phase-Field Model of Mode III Dynamic Fracture, Physical Review Letters 87(4), 2001, 045501

53) L. Zhou, Z. Zhu, Y. Dong, Y. Fan, Q. Zhou, S. Deng, The influence of impacting orientations on the failure modes of cracked tunnel, International Journal of Impact Engineering 125, 2019, 134-142

54) Z. Deng, L. Zhou, Z. Zhu, L. Ma, J. Chen, F. Dai, T. Peng, Study of the fracture properties of twin tunnel surrounds subjected to the coupling of dynamic and static loads, Theoretical and Applied Fracture Mechanics 130, 2024, 104308

55) W. Riedel, K. Thoma, S. Hiermaier, Penetration of Reinforced Concrete by BETA-B-500 Numerical Analysis Using a New Macroscopic Concrete Model for Hydrocodes. Proc 9, ISIEMS, Berlin, 1999, 315-322

56) E. Sharon, J. Fineberg, Confirming the continuum theory of dynamic brittle fracture for fast cracks, Nature 397, 1999, 333-335

57) Z. Zhuang, P.E. O'Donoghue, The recent development of analysis methodology for rapid crack propagation and arrest in gas pipelines, Int. J. Fract. 101, 2000, 269-290

58) M.F. Kanninen, P. O'Donoghue, Research challenges arising from current and potential applications of dynamic fracture mechanics to the integrity of engineering structures, Int. J. Solids Structures 32(17/18), 1995, 2423-2445

59) W. Shen, Y.-P. Zhao, Combined effect of pressure and shear stress on penny-shaped fluid-driven cracks, Journal of Applied Mechanics 85(3), 2017, 031003

60) K.B. Broberg On the Speed of a Brittle Crack, J. Appl. Mech. 31, 1964, 546-547

61) K.B. Broberg, The near-tip field at high crack velocities, Int J. Fract. 39, 1989, 1–13

62) B.V. Kostrov, Crack propagation at variable velocity Int J. Fract. 11(1), 1975, 47-56

63) L.B. Freund, Dynamic fracture mechanics, Cambridge University Press, Cambridge, 1990

64) L.B. Freund, Crack propagation in an elastic solid subjected to general loading. I: Constant rate of extension, J Mech Phys Solid 20, 1972, 129–140

65) L.B. Freund, Crack propagation in an elastic solid subjected to general loading. II: Nonuniform rate of extension, J Mech Phys Solid 20, 1972, 141–152

66) L.B. Freund, Energy flux into the tip of an extending crack in an elastic solid. J Elast 2, 1972, 341–349

67) J.D. Achenbach, Z.P. Bazant, Elastodynamic near-tip stress and displacement fields for rapidly propagating crack in orthotropic media. Journal of Applied Mechanics 42, 1975, 183-189

68) J.D. Achenbach, V. Dunayevsky, Fields near a rapidly propagating crack tip in an elastic-perfectly plastic material, Journal of the Mechanics and Physics of Solids 29, 1981, 283-303

69) K. Ravi-Chandar, W.G. Knauss, An experimental investigation into dynamic fracture: II. Microstructural aspects, Int J Fract 26, 1984, 65–80

70) K. Ravi-Chandar, W.G. Knauss, An experimental investigation into dynamic fracture: III. On steady state crack propagation and crack brunching, Int J Fract 26, 1984, 141–154

71) K. Ravi-Chandar, W.G. Knauss, An experimental investigation into dynamic fracture: IV. On the interaction of stress waves with propagating cracks, Int J Fract 26, 1984, 189–200

72) A.S. Kobayashi, B.G. Wade, W.B. Bradley, S.T. Chiu, Crack branching in Homalite-100 plates, Eng Fract Mech 6, 1974, 81–92

73) T. Kobayashi, J.W. Dally, Relation between Crack Velocity and the Stress Intensity Factor in Birefringent Polymers, Fast Fracture and Crack Arrest. ASTM STP 627, 1977, 257–273

74) J.W. Dally, Dynamic photoelastic studies of fracture, Exp Mech 19, 1979, 349–361

75) J.F. Kalthoff, J. Beinert, S. Winkler, Measurements of dynamic stress intensity factors for fast running and arresting cracks in double-cantilever-beam specimens ASTM STP 627, 1977, 161-176

76) A.J. Rosakis, J. Duffy, L.B. Freund, The determination of the dynamic fracture toughness of AISI 4340 steel by the shadow spot method, Journal of the Mechanics and Physics of Solids 34, 1984, 443–460

77) A.T. Zehnder, A.J. Rosakis, Dynamic fracture initiation and propagation in 4340 steel under impact loading, Int. J. Fract 43, 1990, 271–285

78) H. Maigre, D. Rittel, Dynamic fracture detection using the force-displacement reciprocity: application to the compact compression specimen, Int. J. Fract. 73, 1995, 67-79

79) J.F. Kalthoff, Modes of dynamic shear failure in solids, Int. J. Fract. 101, 2000, 1–31

80) Y.V. Petrov, N.F. Morozov, On the modeling of fracture of brittle solids, J Appl Mech 61, 1994, 710–712

81) D.M. Owen, S. Zhuang, A.J. Rosakis, G. Ravichandran, Experimental determination of dynamic crack initiation and propagation fracture toughness in thin aluminum sheets, Int. J. Fract. 90, 1998, 153-174

82) J.F. Kalthoff, On some current problems in Experimental Fracture dynamics, Workshop on dynamic fracture, California Institute of Technology, 1983, 11-25

83) A. Shukla, H. Nigam, A note on the stress intensity factor and crack velocity relationship for Homalite 100, Eng. Fract. Mech 25(1), 1986, 91-102

84) K. Arakawa, T. Mada, K. Takahashi, Correlations among dynamic stress intensity factor, crack velocity and acceleration in brittle fracture, Int. J. Fract. 105, 2000, 311-320

85) Y. Hwangbo, C.-K. Lee, S.-M. Kim, J.-H. Kim, K.-S. Kim, B. Jang, H.-J. Lee, S.-K. Lee, S.-S. Kim, J.-H. Ahn, S.-M. Lee, Fracture Characteristics of Monolayer CVD-Graphene, Scientific Reports 4: 4439 (2014) PMID 24657996.

86) N.A. Kazarinov, Y.V. Petrov, A.V. Cherkasov, Instability effects of the dynamic crack propagation process, Engineering Fracture Mechanics, 242(1), 2021, 107438

87) N.A. Kazarinov, Y.P. Petrov, A.V. Cherkasov, Spatial and Temporal Discreetness as a Crucial Property of the Dynamic Fracture Process, Mechanics of Solids 55(5), 2020, 673-678

88) N.A. Kazarinov V.A. Bratov, Dynamic fracture of ceramic plates due to impact loading. Numerical investigation, Materials physics and mechanics 4(42), 2019, 389-395

89) D.E. Grady, Fragment size distributions from the dynamic fragmentation of brittle solids, International Journal of Impact Engineering, 35, 2018;35: 1557-62

90) O.B. Naimark, S.V. Uvarov, M.M. Davidova, I.A. Bannikova, Multiscale statistical dependencies of the dynamic fragmentation, Physical Mesomechanics 20, 2017, 94-205 (in Russian)

91) A.M Ignatova, O.B. Naimark, M.V. Yudin, V.L. Voronov, M.N. Ignatov, Experimental determination of fragment dynamics of refractory non-metallic silicate material under high-velocity impact. Procedia Structural Integrity 40 2022, 185-193

92) A.V. Gerasimov, S.V. Pashkov, Numerical modelling of natural fragmentation of solids, Physical Mesomechanics 7 (U1), 2004, 313-316 (in Russian)

93) M.B. Liu, G.R. Liu, Smoothed particle hydrodynamics (SPH): an overview and recent developments, Arch Comput Methods Eng 17(1), 2010, 25–76

94) G.R. Johnson, Artificial viscosity effects for SPH impact computations. Int J Impact Eng 18(5), 1996, 477–488,

95) L.E. Kosteski, I. Iturrioz, A. Cisilino, R.B. D'ambra, V. Pettarin, L. Fasce, P. Frontini, A lattice discrete element method to model the falling-weight impact test of PMMA specimens, International Journal of Impact Engineering 87, 2016, 120–131

96) T. Belytschko, P. Krysl, Y. Krongauz, A three-dimensional explicit element-free Galerkin method, International Journal of Numerical Methods in Fluids 24(12), 1997, 1253-1270

97) J. Lee, W. Liu, J-W. Hong, Impact fracture analysis enhanced by contact of peridynamic and finite element formulations, International Journal of Impact Engineering 87, 2016, 108–119

98) P.N. Demmie, S.A. Silling, An approach to modeling extreme loading of structures using peridynamics, J Mech Mater Struct 2, 2007, 1921–1945

99) E. Cadoni, C. Albertini, G. Solomos, Analysis of the concrete behaviour in tension at high strain-rate by a modified Hopkinson bar in support of impact resistant structural design, J. Phys. IV France 134, 2006, 647-652

100) A.M. Bragov, A.K. Lomunov, Methodological aspects of studying dynamic material properties using the Kolsky method, Int.J.Imp.Eng. 16(2), 1995, 321-330

101) J. Fineberg, E. Bouchbinder, Recent developments in dynamic fracture: Some perspectives, Int.J Fract. 196, 2015, 33–57

102) G. Johnson, W. Cook, Fracture characteristics of three metals subjected to various strains, strain rates, temperatures and pressures, Eng. Fract. Mech. 21(1) 1985, 31-48

103) G.R. Johnson, W.H. Cook, A constitutive model and data for metals subjected to large strains, high strain rates and high, Proceedings of the 7th International Symposium on Ballistics, 1983, 541-547

104) M.A. Iqbal, K. Senthil, P. Bhargava, N.K. Gupta, The characterization and ballistic evaluation of mild steel, International Journal of Impact Engineering 78 2015, 98-113

105) D.J. Allen, W.K. Rule, S.E. Jones, Optimizing Material Strength Constants Numerically Extracted from Taylor Impact Data, Experimental Mechanics 37(3) 1997, 333-338

106) S. Chung Kim Yuen, G.N. Nurick, G.S. Langdon, Y. Iyer, Deformation of thin plates subjected to impulsive load: Part III – an update 25 years on, International Journal of Impact Engineering 107, 2017, 108-117

107) Y. P. Zhao, Suggestion of a new dimensionless number for dynamic plastic response of beams and plates, Archive of Applied Mechanics 68, 1998, 524-538

108) Y.V. Petrov, On "quantum" nature of dynamic failure of brittle media, Dokl Akad Nauk SSSR 321(1), 1991, 66-68

109) N.A. Kazarinov, V.A. Bratov, N.F. Morozov, Y.V. Petrov, V.V. Balandin, M.A. Iqbal, N.K. Gupta, Experimental and numerical analysis of PMMA impact fracture, International Journal of Impact Engineering 143, 2020, 103597

110) A. Dorogoy, A. Godinger, D. Rittel, Application of the incubation time criterion for dynamic brittle fracture, International Journal of Impact Engineering 112, 2018, 66–73

111) J.S. Stenzler, N.C. Goulbourne, The effect of polyacrylate microstructure on the impact response of PMMA/PC multi-laminates, International Journal of Impact Engineering 38, 2011, 567-576

112) G.I. Kanel, Spall fracture: methodological aspects, mechanisms and governing factors, Int.J.Fract 163, 2010, 173–191

113) I.P. Parhomenko, A.V. Utkin, Spallation strength of plexiglass, Investigation of properties of matter under extreme conditions, IVTAN, Moscow, 1990 (in Russian)

114) Z. Rosenberg, Z. Surujon, Y. Yeshurun, Y. Ashuach, E. Dekel, Ricochet of 0.3'' AP projectile from inclined polymeric plates, International Journal of Impact Engineering 31, 2005, 221–233

115) D.J. Benson, J. Hallquist, Computation for transient and impact dynamics, Encyclopedia of Vibration, 2001, 278–286

116) V. Kumar, K. Ramamurthy, Meshfree and finite element modelling of impact: A comparative study, International Journal of Impact Engineering 90, 2016, 146-153

117) W.Y. Li, C. Zhang, C.J Li, H. Liao, Modeling Aspects of High Velocity Impact of Particles in Cold Spraying by Explicit Finite Element Analysis, J Therm Spray Tech 18, 2009, 921-933

118) N. Kazarinov, A. Khvorov, Predicting impact strength of perforated targets using artificial neural networks trained on FEM-generated datasets, Defense Technology 32, 2024, 32-44

119) P. Garnier, J. Viquerat, J. Rabault, A. Larcher, A. Kuhnle, E. Hachem, A review on deep reinforcement learning for fluid mechanics, Computers & Fluids 225, 2021,104973

120) X. Zhang, F. Xie, T. Ji, Z. Zhu, Y. Zheng, Multi-fidelity deep neural network surrogate model for aerodynamic shape optimization, Computer Methods in Applied Mechanics and Engineering, 373, 2021, 113485

121) S. Lee, D. You, Data-driven prediction of unsteady flow over a circular cylinder using deep learning. Journal of Fluid Mechanics 879, 2019, 217-254

122) D.W. Abueidda, M. Almasri, R. Ammourah, U. Ravaioli, I. M. Jasiuk, N. A. Sobh, Prediction and optimization of mechanical properties of composites using convolutional neural networks, Composite Structures 227, 2019, 111264

123) M. Lefik, D.P. Boso, B.A. Schrefler, Artificial Neural Networks in numerical modelling of composites, Computer Methods in Applied Mechanics and Engineering, 198(21–26), 2009, 1785-1804

124) C. Yang, Y. Kim, S. Ryu, G.X. Gu, Using convolutional neural networks to predict composite properties beyond the elastic limit, MRS Communications 9, 2019, 609–617

125) I. Sosnovik, I. Oseledets, Neural networks for topology optimization, Russian Journal of Numerical Analysis and Mathematical Modelling 34(4), 2019, 215-223

126) K. Greff, R. M. J. van Damme, J. Koutnik, H.J. Broersma, J.O. Mikhal, C. P. Lawrence, W. G. van der Wiel, J. Schmidhuber, Using neural networks to predict the functionality of reconfigurable nano-material networks, International journal on advances in intelligent systems, 9(3&4), 2017, 339-351

127) H.T. Kollmann, D.W. Abueidda, S. Koric, E. Guleryuz, N.A. Sobh, Deep learning for topology optimization of 2D metamaterials, Materials & Design 196, 2020, 109098

128) M.V. Mousavi, H. Khoramishad, Investigation of energy absorption in hybridized fiber-reinforced polymer composites under high-velocity impact loading, International Journal of Impact Engineering 146, 2020, 103692

129) A.M. Remennikov, T.A. Rose, Predicting the effectiveness of blast wall barriers using neural networks, International Journal of Impact Engineering 34(12), 2007, 1907–1923

130) M. Yong, B.G Falzon, L. Iannucci, On the application of genetic algorithms for optimising composites against impact loading. International Journal of Impact Engineering 35(11), 2008, 1293–1302.

131) N. KılıÇ, B. Ekici, S. Hartomacıoğlu, Determination of penetration depth at high velocity impact using finite element method and artificial neural network tools, Defence Technology 11(2), 2015, 110-122

132) C.P. Kohar, L. Greve, T.K. Eller, D.S. Connolly, K. Inal, A machine learning framework for accelerating the design process using CAE simulations: An application to finite element analysis in structural crashworthiness, Computer Methods in Applied Mechanics and Engineering 385, 2021,114008

133) L. Lanzi, C. Bisagni, S. Ricci, Neural network systems to reproduce crash behavior of structural components, Computers & Structures, 82(1), 2004, 93-108

134) E. Sakaridis, N. Karathanasopoulos, D. Mohr, Machine-learning based prediction of crash response of tubular structures, International Journal of Impact Engineering 166, 2022, 104240

135) N. Karathanasopoulos, K. S. Pandya, D. Mohr, Self-piercing riveting process: Prediction of joint characteristics through finite element and neural network modeling, Journal of Advanced Joining Processes 3, 2021, 100040

136) Y. Gao, D. Li, W. Zhang, Z. Guo, C. Yi, Y. Deng, Constitutive modelling of the TiB2-B4C composite by experiments, simulation and neutral network. International Journal of Impact Engineering 132, 2019, 103310

137) B. Jordan, M. B. Gorji, D. Mohr, Neural network model describing the temperature- and rate-dependent stress-strain response of polypropylene, International Journal of Plasticity 135, 2020, 102811

138) A. Zhang, D. Mohr, Using neural networks to represent von Mises plasticity with isotropic hardening, International Journal of Plasticity 132, 2020, 102732

139) L. Greve, B. Schneider, T. Eller, M. Andres, J.-D. Martinez, B. van de Weg, Necking-induced fracture prediction using an artificial neural T network trained on virtual test data, Engineering Fracture Mechanics 219, 2019, 106642

140) X. Li, C.C. Roth, D. Mohr, Machine-learning based temperature- and rate-dependent plasticity model: Application to analysis of fracture experiments on DP steel, International Journal of Plasticity 118, 2019, 320-344

141) A.E. Gongora, S. Mysore, B. Li, W. Shou, W. Matusik, E.F. Morgan, K.A. Brown, E. Whiting, Designing Composites with Target Effective Young's Modulus using Reinforcement Learning. In Proceedings of the 6th Annual ACM Symposium on Computational Fabrication (SCF '21). Association for Computing Machinery, New York, NY, USA, 2021, Article 2, 1–1

142) O. Ibragimova, A. Brahme, W. Muhammad, J. Lévesque, K. Inal, A new ANN based crystal plasticity model for FCC materials and its application to non-monotonic strain paths. International Journal of Plasticity 144, 2021, 103059

143) A. Toghroli, M. Mohammadhassani, M. Suhatril, M. Shariati, Z. Ibrahim, Prediction of shear capacity of channel shear connectors using the ANFIS model, Steel Compos. Struct 17(5), 2014, 623-639

144) M. Shariati, M. Mafipour, P. Mehrabi, A. Bahadori, Y. Zandi, M.N, Salih, H. Nguyen, J.Dou, X. Song, S.P. Ngian, Application of a Hybrid Artificial Neural Network-Particle Swarm Optimization (ANN-PSO) Model in Behavior Prediction of Channel Shear Connectors Embedded in Normal and High-Strength Concrete. Applied Sciences 9(24), 2019, 5534

145) R.S. Yang, C.X. Ding, L.Y. Yang, P. Xu, C. Chen, Hole Defects Affect the Dynamic Fracture Behavior of Nearby Running Cracks, Shock and Vibration 2018(1), 2018, 5894356

146) Y. Wang, R. Yang, G. Zhao, Influence of empty hole on crack running in PMMA plate under dynamic loading, Polymer Testing 58, 2017, 70-85

147) M.F. Basoglu, Z. Zerin, A. Kefal, E. Oterkus, A computational model of peridynamic theory for deflecting behavior of crack propagation with micro-cracks, Computational Materials Science 162, 2019, 33-46

148) N. Kazarinov, Yu. Petrov, A. Utkin, Fracture delay effect: analogy between crack initiation due to short pulse loads and mass-spring system failure, International Journal of Impact Engineering 175, 2023, 104513

149) H. Neuber, Kerbspannunglehre: Grundlagen fur Genaue Spannungsrechnung, Springer-Verlag, Berlin, 1937

150) V.V. Novozhilov, About the necessary and sufficient brittle strength criterion, Prikl. Mat. Mekh. 33(2), 1969, 212-222

151) C. Ma, L.B. Freund, The extent of the stress intensity factor field during crack growth under dynamic loading conditions, ASME J Appl Mech 53, 1986, 303–310

152) A.M. Bragov, Yu.V. Petrov, B.L. Karihaloo, A.Yu. Konstantinov, D.A. Lamzin, A.K. Lomunov, I.V. Smirnov, Dynamic strengths and toughness of an ultra-high performance fibre reinforced concrete, Engineering Fracture Mechanics 110, 2013, 477-488

153) C. Liu, W.G. Knauss, A.J. Rosakis, Loading rates and the dynamic initiation toughness in brittle solids, International Journal of Fracture 90, 1998, 103-118

154) V. Bratov, Y. Petrov, A. Utkin, Transient near tip fields in crack dynamics. Science China Physics, Mechanics & Astronomy 54(7), 2011, 1309-1318

155) X. Yang, Z.-C. Ou, C. Yan, Z. Duan, F. Huang, A Microscopical Model for Incubation Time and Its Associated Dynamic Load-Carrying Capacity, International Journal of Applied Mechanics 14(6), 2022, 2250060

156) N.A. Kazarinov, Y.V. Petrov, A.A. Gruzdkov, On dynamic fracture of one-dimensional elastic chain, Advanced Structured Materials 164, 2022, 303-314

157) B.M. Levitan, V.V. Jikov, Quasiperiodic Functions and Differential Equations, MSU publishing house, Moscow, 1978, 204p. (in Russian)

158) A. Zigmund, Trigonometric Series, Mir, Moscow, 1965, 616p. (in Russian)

159) H. Homma, D.A. Shockey, Y. Murayama, Response of cracks in structural materials to short pulse loads, J. Mech. Phys. Solids 31(3), 1983, 261-279

160) V. Bratov, Y. Petrov, Application of incubation time approach to simulate dynamic crack propagation, Int. J. Fract. 146, 2007, 53-60

161) T. Nakamura, C.F. Shih, L.B. Freund, Computational methods based on an energy integral in dynamic fracture, International Journal of Fracture 27, 1985, 229-243

162) C.F. Shih, B. Moran, T. Nakamura, Energy release rate along a three-dimensional crack front in a thermally stressed body, International Journal of Fracture 30, 1986, 79-102

163) K. Ravi-Chandar, Dynamic fracture, Elsevier, 2004, 264p.

164) Yu.A. Kostandov, A.N. Ryzhakov, S.I. Fedorkin, Failure of solid polymers under pulse tension, Problemy Prochnosti 7, 1992, 18-21

165) I. Smirnov, Y. Sudenkov, Crack Propagation in PMMA Plates under Various Loading Conditions, 3th International Conference on Fracture June 16–21, 2013, Beijing, China

166) T. Masaki, Mechanical Properties of Toughened ZrO2-Y2O3 Ceramics. Journal of American Mechanical Society 69(8), 1986, 638-640

167) A.J.A Winnbust, K. Keiser, A.J. Burggraaf, Mechanical Properties and Fracture Behaviour of ZrO2-Y2O3 Ceramics, Journal of Materials Science 18, 1983, 1958-1966

168) J. Jiusti, E.H. Kammer, L. Neckel, N.J. Lóh, W. Trindade, A.O. Silva, O.R.K. Montedo, A. De Noni Jr., Ballistic performance of Al2O3 mosaic armors with gap-filling materials, Ceramics International 143, 2017, 2697-2704

169) H.C. Bergstrom, C.L. Sollenberger, W. Mitchel, Energy aspects of single particle crushing. Trans AIME 220, 1961, 367–372

170) Yu.V. Petrov, A.A. Gruzdkov, V.A. Bratov, Structural-temporal theory of fracture as a multiscale process, Physical Mesomechanics 15(3-4), 2012, 232-237

171) H. Varela-Rizo, M. Weisenberger, D.R. Bortz, I. Martin-Gullon, Fracture toughness and creep performance of PMMA composites containing micro and nanosized carbon filaments, Composites Science and Technology 70, 2010, 1189–1195

172) D.G. Spear, A.N. Palazotto, R.A. Kemnitz, Modeling and Simulation Techniques Used in High Strain Rate Projectile Impact, Mathematics 9(3), 2021, 274

173) Y. Lecun, L. Bottou, Y. Bengio, P. Haffner, Gradient-based learning applied to document recognition, Proceedings of the IEEE 86(11), 1998, 2278-2324,

174) M. Golberg, H.A. Cho, University of Nevada, Las Vegas, USA, Introduction to Regression Analysis, WIT press, 2010, 452p.

175) D.J. Benson, J. Hallquist, Computation for transient and impact dynamics, Encyclopedia of Vibration (Editors: David J. Ewins, Simon G. Braun, Singiresu S. Rao), 2001, 278–286

176) V. Kumar, K. Ramamurthy, Meshfree and finite element modelling of impact: A comparative study, International Journal of Impact Engineering 90, 2016, 146-153

177) W.Y. Li, C. Zhang, C.J Li, H. Liao. Modeling Aspects of High Velocity Impact of Particles in Cold Spraying by Explicit Finite Element Analysis, J Therm Spray Tech 18, 2009, 921-933

178) https://www.dynasupport.com/howtos/material/negative-volume-in-soft-materials

179) D. Scheffler, J. Zukas, Practical aspects of numerical simulation of dynamic events: material interfaces, International Journal of Impact Engineering 24(8), 2000, 821–842

180) S. Ma, X. Zhang, X.M. Qiu, Comparison study of MPM and SPH in modeling hypervelocity impact problems, International Journal of Impact Engineering 36(2), 2009, 272-282

181) L. Wang, W.M. Coombs, C.E. Augarde, M. Cortis, T.J. Charlton, M.J. Brown, J. Knappett, A. Brennan, C. Davidson, D. Richards, A. Blake, On the use of domain-based material point methods for problems involving large distortion, Computer Methods in Applied Mechanics and Engineering 355, 2019, 1003-1025

182) E. Oterkus, I. Guven, E. Madenci, Impact damage assessment by using peridynamic theory, Cent.Eur.J.Eng 2, 2012, 523–531

183) M.O. Ignatiev, Y.V. Petrov, N.A Kazarinov, Simulation of Dynamic Crack Initiation Based on the Peridynamic Numerical Model and the Incubation Time Criterion, Technical Physics 66(3), 2021, 422-425

184) M.O. Ignatiev, Y.V. Petrov, N.A. Kazarinov, E. Oterkus, Peridynamic formulation of the mean stress and incubation time fracture criteria and its correspondence to the classical Griffith’s approach, Continuum Mechanics and Thermodynamics 35(4), 2023, 1523-1534

185) Y.P. Lian, X. Zhang, Y. Liu, An adaptive finite element material point method and its application in extreme deformation problems, Computer Methods in Applied Mechanics and Engineering 241–244, 2012, 275-285

186) N.A. Kazarinov, Y.V. Petrov, A.V. Cherkasov, Spatial and Temporal Discreetness as a Crucial Property of the Dynamic Fracture Process, Mechanics of Solids 55(5), 2020, 673-678

187) N. Kazarinov, V. Bratov, Y. Petrov, Simulation of dynamic crack propagation under quasistatic loading, Applied Mechanics and Materials 532, 2014, 337-341

188) N.A. Kazarinov, V.A. Bratov, Yu.V. Petrov, G.D. Fedorovsky, Evaluation of fracture incubation time from quasistatic tensile strength experiment, Materials Physics and Mechanics 19(1), 2014, 16-24

189) Y.V. Petrov, A.V Cherkasov, N.A. Kazarinov, Instability of critical characteristics of crack propagation, Acta Mechanica 232(5), 2021,1997-2003

190) N.A. Kazarinov, Y.V. Petrov, V.A. Bratov, V.Yu. Slesarenko, Numerical investigation of stress intensity factor - crack velocity relation for a dynamically propagating crack, Materials Physics and Mechanics 29(1), 2016, 39-42

191) Y. Petrov, N. Kazarinov, Instabilities encountered in the dynamic crack propagation process under impact loading as a natural consequence of the dynamic fracture discreetness, Procedia Structural Integrity 28, 2020, 1975-1980

192) N. Kazarinov, I. Smirnov, Y. Sudenkov, Y. Petrov, V. Slesarenko, Experimental investigation of dynamic crack propagation in PMMA plates, Procedia Structural Integrity 6, 2017, 83-89

193) N.A. Kazarinov, A.D. Evstifeev, Y.V. Petrov, S.A. Atroshenko, R.R. Valiev, The Effect of Grain Refinement on Solid Particle Erosion of Grade 5 Ti Alloy, Journal of Materials Engineering and Performance, 2018, 27(6), 3054-3059

194) Y.V. Petrov, S.A. Atroshenko, N.A. Kazarinov, A.D. Evstifeev, V.Y. Solov'ev, Dynamic fracture of the surface of an aluminum alloy under conditions of high-speed erosion, Physics of the Solid State 59(4), 2017, 661-666

195) N.A. Kazarinov, A.D. Evstifeev, Y.V. Petrov, S.A. Atroshenko, V.A. Lashkov, R.Z. Valiev, A.S. Bondarenko, Surface Roughness Investigation of Ultrafine-Grained Aluminum Alloy Subjected to High-Speed Erosion, Journal of Materials Engineering and Performance 25(9), 2016, 3573-3579

196) A.D. Evstifeev, Y.V. Petrov, N.A. Kazarinov, R.R. Valiev, Strength of the Ti–6Al–4V Titanium Alloy under Conditions of Impact and Short Pulse Loading, Physics of the Solid State 60(12), 2018, 2358-2362

197) A.D. Evstifeev, N.A. Kazarinov, Y.V. Petrov, S.A. Atroshenko, R.R. Valiev, High-rate erosion of Ti–6Al–4V ultrafine-grained titanium alloy obtained via intensive plastic torsional deformation, Physics of the Solid State 59(9), 2017, 1794-1797

198) Y.V. Petrov, A.M. Bragov, N.A. Kazarinov, A.D. Evstifeev, Experimental and numerical analysis of the high-speed deformation and erosion damage of the titanium alloy VT-6, Physics of the Solid State 59(1), 2017, 93-97

199) A. Evstifeev, N. Kazarinov, Y. Petrov, L. Witek, A. Bednarz, Experimental and theoretical analysis of solid particle erosion of a steel compressor blade based on incubation time concept, Engineering Failure Analysis 87, 2018, 15-21

200) V. Slesarenko, N. Kazarinov, S. Rudykh, Distinct failure modes in bio-inspired 3D-printed staggered composites under non-aligned loadings, Smart Materials and Structures 26(3), 2017, 35053

201) R.Z. Valiev, E.A. Prokofiev, N.A. Kazarinov, G.I. Raab, T.B. Minasov, J. Stráský, Developing nanostructured Ti alloys for innovative implantable medical devices, Materials 13(4), 967

202) N. Kazarinov, A. Stotskiy, A. Polyakov, R.Z. Valiev, N. Enikeev, Finite Element Modeling for Virtual Design to Miniaturize Medical Implants Manufactured of Nanostructured Titanium with Enhanced Mechanical Performance, Materials 15(21), 2022, 7417